Using an activator of hERG (RPR-260245) in a model of acquired and inherited Long QT syndrome type 2

by

Valentine Sergeev

B.Sc., Simon Fraser University, 2015

Thesis Submitted in Partial Fulfillment of the
Requirements for the Degree of
Master of Science

in the
Department of Biomedical Physiology and Kinesiology
Faculty of Science

SIMON FRASER UNIVERSITY
Summer 2017

Approval

Name:	**Valentine Sergeev**
Degree:	**Master of Science**
Title:	Using an activator of hERG (RPR-260245) in a model of acquired and inherited Long QT syndrome type 2
Examining Committee:	**Chair:** Damon Poburko Assistant Professor

Glen Tibbits
Senior Supervisor
Professor

Thomas Claydon
Co-Supervisor
Associate Professor

Shubhayan Sanatani
Supervisor
Adjunct Professor

Peter Ruben
External Examiner
Professor
Department of BPK
Simon Fraser University

Date Defended/Approved: July 17th, 2017

Abstract

The human ether-a-go-go related gene (hERG) channel is the molecular correlate of the rapid delayed rectifier current (I_{Kr}); its dysfunction causes Long QT syndrome type II (LQT II). RPR-260245 (RPR) is an activator of hERG that increases hERG current by slowing deactivation. Thus, it represents a potential treatment strategy for LQT. However, only few studies have addressed its impact on cardiac physiology. We used electrophysiology techniques in *Xenopus Laevis* oocytes and optical mapping in induced pluripotent stem cells derived cardiomyocytes (hiPSC-CMs) to test the effects of RPR on hERG and on the cardiac action potential. We show that RPR has little effect on the cardiac AP in WT iPSC-CMs but demonstrate a partial rescue in our model of acquired LQT (aLQT) under dofetilide block and a partial rescue in our model of LQT II. Finally, RPR significantly increases protective hERG current, especially in instances of the R56Q mutation.

Keywords: hERG, LQT II, Genome Editing, Induced Pluripotent stem cells, Cardiac Physiology, Electrophysiology.

Dedication

This thesis is dedicated to K.M., without whom this thesis would not have been possible.

Acknowledgements

First, I would like to thank Sanam Shafaattalab. She taught me many of the cell-culture techniques that I would go on to use in this thesis. She also performed the optical mapping experiments on which I have placed significant weight in this thesis. Without her skill, her hard work and her generosity this thesis would have not been possible. I would also like to thank Marvin Gunawan who, along with Sanam, did a tremendous amount of work to help optimize the genome editing technology that I applied in this thesis. Also thank you to Charlie Stevens who helped me with the initial design of the gRNA and donor template and Nancy helped me clone the gRNA into the pCCC vector. To Kaveh and Alison, thank you for your help with regard to molecular biology technique – you both are truly experts. I want to thank Sabi for being a very reliable friend. He was always willing to cover a day of my cell culture duties when I needed him to. He was also very keen to lend an ear and give constructive criticism when I ran into trouble (scientific and otherwise!).

From the Claydon lab, I would like to thank Christina. She was my first mentor in this lab (in any lab actually) and her absolute insistence on producing the best quality of work has (partially) rubbed off on me. Also, thank you to Patrick and Sam who have always been very approachable and have helped my understanding of hERG biophysics tremendously (as has Christina). And of course, Ji who provided a tremendous amount of technical assistance as well as mentorship.

I would like to thank Dr Shubhayan Sanatani for his role on my supervisory committee. Although my thesis moved quite substantially away from its original direction, Dr Sanatani still provided support and new opportunities that would otherwise have been very difficult to find. I would like to thank my co-supervisor, Dr Tom Claydon. Tom went above and beyond what was required of him. His meticulous nature forced me to consider my own experiments and interpretation more carefully. He leads by example and his kindness is something to emulate. Finally, I would like to thank my senior supervisor, Dr. Glen Tibbits. The opportunities and the resources that he was able to provide speak volumes about his character. As a master's student, I was able to attend two international conferences – one being in Denmark! He is also generous with his time and motivates not by giving deadlines or setting unrealistic expectations, but by bestowing his absolute confidence in his students' abilities. I consider myself very fortunate to have had Glen as my mentor.

Table of Contents

List of Tables

List of Figures

List of Acronyms

SFU	Simon Fraser University
hERG	human ether-a-go-go related gene
TdP	Torsades de Pointes
AP	Action Potential
APD	Action potential duration
MAP	Monophasic action potential
CTD	Calcium transient duration
ARI	Activation-recovery interval
RPR	RPR-260243
PAS	Per-Arnt-Sim (domain)
cNBHD	Cyclic nucleotide-binding homology domain

Chapter 1. Introduction

1.1. Background

The human ether-a-go-go related gene (hERG) codes for Kv11.1, a potassium channel that is expressed in a variety of tissues including smooth muscle (Farrelly et al., 2003) tumour (G. A. M. Smith et al., 2002), neural (Chiesa, Rosati, Arcangeli, Olivotto, & Wanke, 1997), and heart tissue (Curran et al., 1995). The importance of hERG in the myocardium is demonstrated by considering the consequences of its dysfunction. Loss-of-function mutations in hERG cause Long QT syndrome (LQT II), predisposing the myocardium to a lethal form of polymorphic ventricular tachycardia known as Torsades de Pointes which can degenerate into ventricular fibrillation and lead to sudden cardiac death. In this section, I will describe the function of hERG channels as they pertain to the myocardium. I will also describe the mechanisms by which hERG channels can lose their function. Finally, I will outline the role of hERG dysfunction in the pathogenesis of arrhythmia.

1.1.1. hERG function is a result of unique gating characteristics

In the myocardium, hERG is the molecular correlate of the fast component of the delayed rectifier current, I_{Kr} (Sanguinetti, Jiang, Curran, & Keating, 1995). The critical role played by the hERG channel in cardiac rhythm can be attributed to its peculiar gating kinetics. The channels display slow activation and deactivation kinetics yet fast inactivation kinetics. Furthermore, these processes are voltage dependent. Therefore, in response to phase 0 depolarization, channels begin to activate, yet they inactivate rapidly and thus pass little current during phases 1 and 2. As the myocardium begins to repolarize, hERG channels rapidly recover from inactivation, but are slow to close, allowing them a window to pass repolarizing current that drives termination of the cardiac action potential (Fig 1) (Vandenberg et al., 2012). Crucially, the channels exhibit hysteretic behavior where the energetic landscape for deactivation and activation are different. Intuitively, one would expect opening and closing of the channel to be a reversible, symmetrical process, as it is in many other potassium channels. If this were to be true, then the kinetics and the voltage dependence for hERG channel activation and deactivation would be the same. However, in numerous channels, including hERG, this is not the case (Thouta et al., 2017)

Through mechanisms that are not yet fully understood, prolonged depolarization further stabilizes the open state and changes the energetic landscape for deactivation of the channel (Hull, Sokolov, Van Slyke, & Claydon, 2014; Tan, Perry, Ng, Vandenberg, & Hill, 2012). This process, termed relaxation, results in slowed deactivation gating. Interestingly, whereas relaxation in many channels is slow, an apparent energetic separation of activation and deactivation gating can be observed in hERG channels at physiologically relevant durations. As a result, the slowed closing of hERG may leave channels in the open state longer and help to drive the membrane potential towards resting or diastolic values. Consistent with this, evidence shows that hERG channels remain open even after the cell has repolarized back to resting membrane potential (Du et al., 2010; Lu et al., 2001). In these studies, the authors showed that despite being open, no current is conducted since the RMP is close to E_{K^+}; however, the open hERG channels pass a large, transient, repolarizing current in response to a premature depolarization. By these means, it has been suggested that repolarizing current conducted via hERG channel as they close slowly protects against arrhythmia. Consistent with this, an *in silico* action potential modelling study showed that in instances of ischemia-mediated acidosis, acceleration of hERG deactivation not only leads to decreased hERG current but also reduced the amount of transient hERG current that helps to suppress ectopic beats. The authors suggested that these observations may help to explain the large incidence of arrhythmia during ischemic events (Du et al., 2010). Clinically, the importance of slow deactivation is underscored by the discovery that mutations that accelerate deactivation cause loss of function of hERG channels and LQT II (J. Chen, Zou, Splawski, Keating, & Sanguinetti, 1999). In summary, these studies highlight the critical role of hERG channel function in the maintenance of normal rhythm in the myocardium.

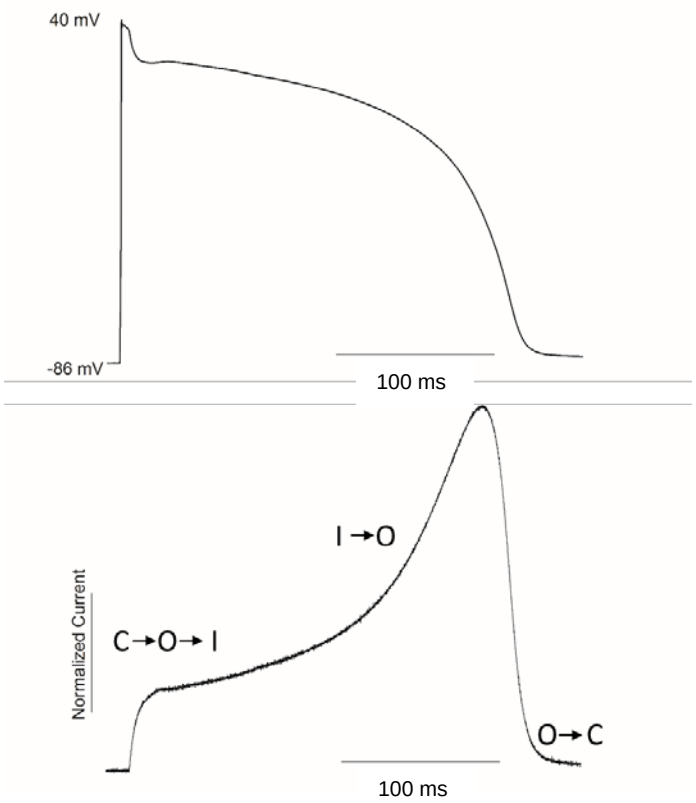

Figure 1: The unique gating gating mechanism of hERG contributes to its function in the cardiac action potential. A current trace (bottom) in response to an action potential waveform (top) in *Xenopus* oocytes. During phase 0, hERG channels open (C → O) but inactivate rapidly (O → I). During phase 3, hERG channels recover from inactivation (I → O) to pass depolarizing current. Deactivation is slow (O → C).

1.1.2. Mechanism of hERG dysfunction

It is generally accepted that hERG dysfunction causes arrhythmia, specifically, Long QT Syndrome Type II. Yet the mechanistic links between hERG dysfunction and arrhythmia are rarely discussed in great detail. Broadly, a loss-of-function in hERG is anything that impairs its ability to conduct repolarizing current in phase 3 of the cardiac action potential. In this section, I will summarize the various mechanisms that cause dysfunction in hERG.

Drug block causes LQT II and is the most common cause of acquired LQT.

I_{Kr} blockade by pharmaceutical agents is the most common cause of acquired LQT syndrome (aLQT). This is a result of a surprisingly high affinity that hERG displays to a wide variety of compounds. Mutagenesis studies have demonstrated that aLQT due to hERG block is conferred largely by the presence of two aromatic residues at the base of the S6 pore helices (Lees-Miller, Duan, Teng, & Duff, 2000). As hERG channels assemble as a tetramer, tyrosine 652 and phenylalanine 656 are suggested to form a pocket rich in π electrons and hydrogen atoms that facilitate the binding of drugs. Mutating either of these residues to small, hydrophobic amino acids (i.e., alanine or valine) increases the IC_{50} of drugs like dofetilide, cisapride, and terfenidine by a factor of 100 for cisapride and terfenidine and 10,000 for dofetilide (Kattman et al., 2011; Mitcheson, Chen, Lin, Culberson, & Sanguinetti, 2000). Unlike most K_v channels, the hERG channel lacks a PVP motif that, in other K_v channels, forms the gate. A lower position of the gate in hERG channels, at position Q664 (Thouta et al., 2014), has been suggested to increase the size of the pore, providing more space for blockers to occupy (Thouta et al., 2014). Very recently, the hERG channel cryo-EM structure was resolved at 3.8 Å; it shows several long and narrow hydrophobic pockets that extend laterally from the central cavity (W. Wang & MacKinnon, 2017). The authors suggest that drugs such as dofetilide can insert a functional group into one of these pockets to form a stable interaction, while the main portion of the molecule rests in the central cavity of the pore and blocks the ion permeation pathway. The authors note that several residues (including Y652 and F656) line these hydrophobic pockets and serve to stabilize interactions. Finally, inactivation may also play an important role in drug block, as inhibitors preferentially bind to the inactivated state, and channels that exhibit reduced inactivation demonstrate reduced affinity to hERG blockers (Ficker, Jarolimek, Kiehn, Baumann, & Brown, 1998). In summary, the most common form of acquired LQT occurs as a result of hERG channel block, which is the result of not only the unique structure of hERG but also its distinctive gating mechanisms.

Congenital LQT II can be caused by three mechanisms.

In a study that screened 44,596 Caucasian neonates for LQT syndrome, it was found that 17 had a QTc of greater than 450 ms (indicating a diagnosis of LQT with a high degree of certainty). The authors reported the prevalence of LQT as 1:2,534 (95% CI: 1:1,583 to 1:4,350) (Schwartz et al., 2009). This is likely an underestimate, as some mutations that cause LQT may present with very low penetrance (i.e., no prolongation of

QTc on ECG) and are unmasked in dramatic fashion under certain conditions (e.g., hypokalemia, QT-prolonging drugs) when the patients develop life-threatening arrhythmia (Priori, Napolitano, & Schwartz, 1999). Loss-of-function mutations in hERG (i.e., LQT type II) account for about 40% of all LQT cases, making hERG dysfunction the second most common cause of congenital LQT (Giudicessi & Ackerman, 2013; Kapa et al., 2009). The mutations that cause LQT II can be classified into 3 categories: (1) those that reduce protein synthesis, (2) those with defective trafficking, and (3) those that alter biophysical properties (either by causing a gating deficiency or altering ion permeation). Of note, a single mutation often presents characteristics of more than one of these categories, with some mutations reinforcing dysfunction through two or more separate mechanisms (e.g., decreased trafficking and decreased conductance), while others show mixed phenotypes (e.g., decreased trafficking, but increased activation). Especially in the latter case, identifying the dominant mechanism is of salient importance, as it can inform treatment decisions. In this section I will outline the three mechanisms by which mutations in hERG may cause a loss of function.

Decreased protein synthesis.

About 25–35% of LQT II-associated mutations are nonsense that result in a premature stop codon (Gong, Zhang, Vincent, Horne, & Zhou, 2007; Vandenberg et al., 2012). In a study that examined two LQT II–causing mutants containing frameshifts resulting in early stop codons, R1014X and W1001X, the Zhou group showed that both mutants are degraded through nonsense-mediated decay (Gong et al., 2007). This finding was crucial, as nonsense-mediated RNA decay is a conserved process that occurs whenever a stop codon occurs at least 50–55 bp upstream of the most distal exon-exon boundary (for review see Chang, Imam, and Wilkinson 2007). Nonsense-mediated mRNA decay also proved to be the mechanism by which another LQT II–causing frameshift mutation, P926AfsX14, showed a loss in hERG function (Zarraga et al., 2011). While not all LQT II–causing premature stop codons have been shown to cause a loss of function through nonsense-mediated RNA decay, the conserved nature of the process would lead to the assumption that most nonsense mutations that result in a frameshift mutation would result in RNA decay. Indeed, Gong et al. estimated that about 90% of early stop codons are candidates to undergo nonsense-mediated RNA decay (Gong et al., 2007). However, nonsense mutations are relatively rare compared to missense mutations, and the

likelihood of missense mutations introducing a stop codon is small. In the next section, I will describe the most common fate of missense mutations, which is decreased trafficking.

Decreased trafficking.

Unlike some genetic diseases in which one mutation is responsible for the majority of the incidence of the disease, e.g., ΔF508 in cystic fibrosis (Bobadilla, Macek, Fine, & Farrell, 2002), mutations that cause a loss of function in hERG channels can appear almost anywhere in the channel (Fig 2). Several studies from the Ackerman group have tried to correlate the location of the mutation within the model structure of hERG with disease risk (Fig 2) (Kapa et al., 2009; Kapplinger et al., 2009). They showed that mutations within the pore were highly likely to be pathogenic (95–100% predictive value), as were mutations in other structural domains, such as the Per-Arnt-Sim (PAS) domain, the PAS-associated C-terminal region, and the cyclic nucleotide-binding homology domain (estimated predictive value around 100%) (Fig 2) (Kapa et al., 2009). In this case, the predictive value refers to the likelihood that a de-novo mutation would be pathogenic. However, establishing valid genotype–phenotype relationships based only on sequencing data is difficult, as numerous mutations outside of these domains also cause LQT II (Fig 2): when accounting for regions outside of the relatively well-described functional domains, the predictive value falls to 26% for de-novo mutations in the N-terminus and 56% for de-novo mutations in the C-terminus (Kapa et al., 2009). For both clinicians and researchers, it is thoroughly unsatisfactory that a novel mutation in the C-terminus, for example, can have a one-in-two chance of being pathogenic, so studying the mechanisms of hERG dysfunction has been a high priority. Most notable, the January group presented several important studies in which they systematically assessed a subset of LQT II–associated missense mutations. In 2006, they screened 36 missense mutations and found 28 mutations were defective in trafficking (Anderson et al., 2006). More recently, a more comprehensive study of 167 LQT II–associated missense mutations showed that 88% demonstrated a defect in trafficking; its conclusion was that trafficking deficiency is the most common cause of congenital LQT (Anderson et al., 2014). The authors noted that mutations in the pore region are most likely trafficking-defective (with mutations in S5 exhibiting the most severe phenotypes), while mutations within the intracellular regions are either trafficking deficient or present with a biophysical defect. It is interesting that the region within the pore that had the highest predictive values for pathogenicity also demonstrated that trafficking impairments were the most common cause of dysfunction.

Furthermore, some mutations showed alterations in more than one mechanism: some acted synergistically to reinforce dysfunctions, while others caused a mixed phenotype (Balijepalli et al., 2012; Kanters et al., 2015). Thus, it is still difficult to predict the mechanism by which any mutation outside the pore may cause a loss of function without more detailed molecular investigation. Further complexity was revealed by the recent observation that pharmacological correction of trafficking-deficient mutations may not always be enough to rescue function, as many of the ‘rescued’ channels still show gating and biophysical dysfunction (M. D. Perry et al., 2016). Thus, while defective trafficking is the most dominant mechanism of hERG dysfunction, congenital LQT II is probably not a “predominantly misfolding disease,” as Anderson and colleagues point out (Anderson et al., 2014).

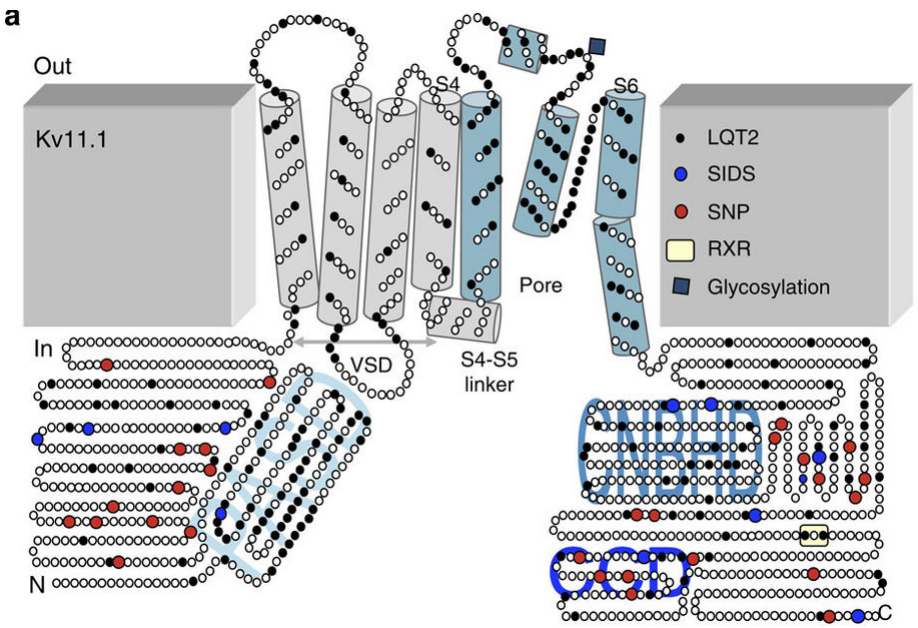

Figure 2: Distribution of disease-causing mutations across the hERG channel. A cartoon representation of the hERG channel, with black circles representing LQT II–associated mutations and blue circles representing mutations associated with sudden infant death syndrome (that were most likely undiagnosed cases of LQT II). Note the high density of disease-causing mutations in the pore region, PAS domain, and cNBHD domain. However, there are still many disease-causing mutations outside of these areas, making it difficult to predict whether novel variants outside of the three domains are pathogenic. Reprinted by permission from Macmillan Publishers Ltd: *Nature Communications.* Anderson, C. L., Kuzmicki, C. E., Childs, R. R., Hintz, C. J., Delisle, B. P., & January, C. T. Large-scale mutational analysis of Kv11.1 reveals molecular insights into type 2 long QT syndrome., 5, 5535. http://doi.org/10.1038/ncomms6535copyright (2014)

From a mechanistic point of view, trafficking defects can be considered synonymous with misfolded proteins. The equivalence between trafficking and folding is a result of a common method used to detect decreased surface expression. As hERG channels undergo several glycosylation steps during maturation, the final hERG channel protein expressed at the membrane represents a fully-glycosylated protein, while immature forms represent a core-glycosylated version. This allows both forms of the hERG protein to be resolved on an SDS-PAGE, and after immunoblotting, the relative amount of surface expression can be inferred from the ratio of the two bands (Z. Zhou, Gong, Epstein, & January, 1998). This assay has proved invaluable in identifying trafficking-deficient mutants. However, the mechanism that underlies the decreased

trafficking to the surface is really misfolded mutants that have been prevented from trafficking through the checkpoint mechanisms within the cell. As Smith and colleagues suggest in their recent review of the pathogenesis of LQT II, hERG channels may be particularly prone to misfolding because of the way the protein is synthesized (Smith et al., 2016). As the secondary structure of hERG already begins to form within the ribosomal subunit, even small missense mutations may disrupt key motifs and have profound consequences on tertiary structure and therefore overall stability (Smith et al., 2016). Regardless of the teleological reasons behind the propensity of hERG channels to misfold, a large body of evidence demonstrates that there are several important checkpoints within the secretory pathway that properly folded hERG proteins must pass before they are inserted into the membrane. If nascent proteins fail to pass these checkpoints, they are retained within the secretory network (more specifically, the endoplasmic reticulum) and are eventually degraded by cytosolic proteasomes modulated through the ER-associated degradation pathway (Gong, Keeney, Molinari, & Zhou, 2005). For example, part of the hERG channel C-terminus interacts with GM130, a Golgi-associated protein that plays a role in trafficking between the ER and Golgi (Roti et al., 2002). The authors suggest that disruption of this interaction due to LQT II–causing mutations in the cNBHD, such as 822M, S818P, and R823W, cause hERG mutants to be retained within the ER (Roti et al., 2002). A corollary to this is the observation that hERG blockers like E-4031 and dofetilide can partially rescue expression (Anderson et al., 2014; Zhou, Gong, & January, 1999), which suggests that they stabilize misfolded channels by directly binding the protein. For example, in the case of N470D, E-4031 reduces the association with the chaperone calnexin and protects against trypsin digestion. Without E-4031 directly associating with $hERG_{N470D}$, calnexin would not dissociate from the mutant (as it would in WT channels) and thereby prevent trafficking. The authors concluded that E-4031 may serve to mask exposed motifs in the mutant that would otherwise be hidden in a properly folded channel (Gong, Jones, & Zhou, 2006). Other chaperones have also been implicated in hERG trafficking through a similar mechanism. Normally, chaperones such as HSP90 and HSP70 help to traffic immature proteins to the Golgi, as they are tightly associated with immature proteins but not mature proteins (Ficker, Dennis, Wang, & Brown, 2003). However, trafficking defective mutants R752W and G601S remain tightly bound to HSP90 and HSP70 (Ficker, Dennis, & Browne, 2003). Taken together, the evidence demonstrates that the retention and selective degradation of misfolded proteins is the likely mechanism

that accounts for decreased surface expression observed in a high fraction of missense mutations.

Biophysical effects.

As alluded to previously, of the mutations that cause congenital LQT II, biophysical perturbations (i.e., gating deficiencies or ion block) represent a minority of the mechanisms responsible for hERG loss of function, constituting 13 out of 167 mutants that Anderson and colleagues screened in their large-scale mutational analysis (Anderson et al., 2014). Nevertheless, many mutations thought to cause trafficking defects have been shown to also affect biophysical properties when rescued pharmacologically (Perry et al., 2016). Thus, understanding the biophysical consequences of mutations is as relevant as ever in the context of the treatment of LQT II.

hERG gating is a complex phenomenon but can most easily be understood as the culmination of three interrelated yet distinct processes: slow activation, rapid inactivation, and slow deactivation. Mutations can affect one or more of these processes to cause dysfunction, but mutations can also render the channel non-conducting because of structural consequences. Here I will provide some examples of mutations that cause a loss of function of hERG channels by affecting these processes, with particular emphasis placed on the mechanistic details regarding deactivation.

hERG channels are selective for potassium, which allows the passage of repolarizing current at physiological potentials (Sanguinetti et al., 1995). Thus, any compromise in the ability of the channel to conduct potassium ions would constitute channel dysfunction. One interesting example is the G628S mutation within the selectivity filter of hERG. This dominant negative mutation associated with LQT II was previously thought to result in channels that were non-conducting; however, upon removal of K^+ from the recording solution, mutant channels were capable of conducting Na^+ with normal biophysical properties (Es-Salah-Lamoureux, Xiong, Goodchild, Ahern, & Fedida, 2011). This example demonstrates that channels may become non-conducting even though they gate, and are trafficked, normally.

Rapid inactivation at positive potentials, as well as recovery from inactivation at negative potentials, imparts inward rectification to hERG channels. These properties contribute to the resurgent hERG channel current conducted in phase 3 of the cardiac AP.

Thus, mutations that enhance inactivation would decrease functional hERG current during the cardiac AP. Indeed, both V630L and A614V mutations show negative shifts in the voltage dependence of steady-state inactivation when co-expressed with WT channels (alone, they are non-conducting) (Tadashi Nakajima et al., 1998). Although Nakajima and colleagues did not directly test the effect of increased inactivation on the cardiac AP, they showed that functional hERG current was decreased, predicting a smaller resurgent current in phase 3, and most likely resulting in a prolonged cardiac AP (Nakajima et al., 1998).

Activation of hERG is much slower than other ion channels that participate in the AP but is still faster than I_{Ks} (Nakagawa et al., 2009). In the time course of the cardiac action potential, activation does not reach a steady-state, making the cell sensitive to small perturbations in the voltage dependence of activation (Thouta et al., 2017). For example, N33T, a mutant that is linked to LQT II, shifts the voltage dependence toward more positive potentials (by 7.6 mV), which reduces channel availability and would decrease functional hERG current. Of note, N33T also accelerates the deactivation kinetics of hERG, demonstrating that these processes are not independent (Chen et al., 1999). As alluded to earlier, deactivation in hERG is particularly slow, representing a hysteresis between activation and deactivation. The importance of this slow deactivation is underscored by the observations that LQT II–associated mutations within the PAS domain slow deactivation (Chen et al., 1999). Of these mutations, R56Q is of particular interest, as its loss of function phenotype is specific to its acceleration of deactivation (Berecki et al., 2005; J. Chen et al., 1999; Q. Liu et al., 2015). Broadly, any mutation that accelerates hERG deactivation decreases hERG current in the latter parts of phase 3, which causes a prolonged APD (Berecki et al., 2005; Liu & Trudeau, 2014). Furthermore, accelerated deactivation also reduces channel availability in phase 4, making the myocardium more susceptible to premature depolarization (Perry et al., 2016). The underlying mechanism responsible for slow deactivation is not fully understood but is distinct from that of activation (Thouta et al., 2017). This clear distinction between deactivation and the other mechanisms, as well as its established clinical significance, makes the mechanism behind slow deactivation important to understand, as treatment therapies may target this mechanism specifically. As this thesis focuses on the physiological role of hERG deactivation, I will take some time to describe what is known with regard to the mechanism of slow deactivation.

There is no complete description of the mechanism underlying slow deactivation. What is clear is that the N-terminus of the hERG channel is intimately involved in the slow deactivation process through physical interaction with the rest of the channel (de la Peña et al., 2011; Gustina & Trudeau, 2009; Ng et al., 2011; J. Wang, Myers, & Robertson, 2000; J. Wang, Trudeau, Zappia, & Robertson, 1998). Wang and colleagues were the first to demonstrate that deleting the N-terminus accelerates deactivation and that the effect is reversed by the addition of an N-terminal peptide (J. Wang et al., 2000). This suggests that the N-terminus is either physically involved in gating or exerts an allosteric effect. Like other members of the EAG sub-family of channels, the N-terminus in hERG contains a PAS domain in the N-terminal region, which spans from amino acids 26 to 135 (Cabral et al., 1998). In other organisms, the PAS domain is a key site of signaling and regulation (Nan et al., 2010). However, no such function has yet to be attributed to the PAS domain in hERG (Morais-Cabral & Robertson, 2015). Instead, the current view is that the N-terminus physically interacts with the core of the channel to modulate gating, and these interactions include the cyclic nucleotide-binding homology domain (cNBHD). This conclusion comes from functional studies, such as Gustina et al. (2009), which showed that the C-terminus was necessary for slow deactivation. In a later study, the same group demonstrated that direct interaction of the PAS domain and the cNBHD is necessary for slow deactivation. They showed that either neutralizing the arginine in position 56 within the PAS domain (as with R56Q) or reversing the charge yielded accelerated deactivation kinetics. Likewise, reversing the charge of Aspartate at position 803 in the cNBHD also accelerated deactivation. However, a double mutation that reversed the charge in both domains (i.e., R56D/D803R) partially restored slow deactivation kinetics. This observation demonstrated that the PAS domain interacts with the cNBHD that includes R56/D803 as a site of interaction (Ng, Phan, Hill, Vandenberg, & Perry, 2014). Structural evidence also supports this view. Structures of the related mEAG1 channel showed that the PAS domain physically interacts with the cNBHD (Haitin, Carlson, & Zagotta, 2013). Moreover, recent cryo-EM structures of hERG and EAG structures show that the N-terminus is involved in complex interactions that modulate the stability of the open state of hERG channels.

A recent study by Perry and colleagues showed that 14/34 pharmacologically corrected trafficking mutants had altered deactivation properties (Perry et al., 2016). The authors showed that accelerated deactivation was a common feature in these rescued mutant channels and that this was associated with a decreased protective current: that is,

a decreased hERG conductance following the completion of the AP (Perry et al., 2016). Thus, if rescue of hERG trafficking is ever to be considered as a viable treatment approach, accelerated deactivation must also be understood and be corrected.

In this section, I have discussed the many mechanisms that can lead to hERG channel dysfunction. Broadly speaking, any perturbation that decreases hERG current can be categorized as a loss of function. In the cardiac action potential, loss of hERG function leads to decreased rate of repolarization, particularly at slower heart rates (Nakagawa et al., 2009; Wilde et al., 1999). In the next section, I will outline some of the mechanisms that link hERG channel dysfunction and decreased repolarization with arrhythmia.

1.1.3. hERG dysfunction can cause arrhythmia

There is nothing inherently arrhythmogenic about loss of function mutations in hERG: a prolonged AP is not necessarily arrhythmogenic. In fact, it can even be protective against arrhythmia (Peter Milberg et al., 2002; Studenik, Zhou, & January, 2001). This is perhaps one of the reasons that, while mutations in hERG may prolong the QT interval, they only predispose to arrhythmia, explaining the relatively low incidence of Torsades de Pointes (TdP) in LQT II patients (Moss et al., 2002). In this section, I will give a brief description of some of the mechanistic links between hERG loss of function and arrhythmia.

Decreased repolarization as a result of hERG dysfunction causes early-after depolarization (EADs) that act as a trigger for arrhythmia.

Even before the Keating group discovered that hERG is the molecular correlate of I_{Kr} (Sanguinetti et al., 1995), there was already evidence that QT-prolonging drugs such as quinidine (later shown to block hERG) caused early-after depolarization (EAD), providing a mechanistic link between QT prolongation and Torsades de Pointes (el-Sherif, 1991). Later, a study on Langendorff-perfused rabbit hearts showed that low extracellular K^+ and E-4031 (which both decrease hERG function) caused EADs in multiple foci, with “a pattern of activation that varied from beat to beat” (Asano, Davidenko, Baxter, Gray, & Jalife, 1997). As the authors concluded, the variability of triggered activity would “set the stage for the initiation of drifting spiral waves with consequent gradual undulation in the QRS configuration typical of TDP” (Asano et al., 1997). Thus, even before it was known

that E-4031 blocked hERG channels, there was already evidence that hERG dysfunction leads to EADs that cause arrhythmia. At the same time, the mechanism of EAD formation was being actively investigated.

Although there was early evidence that EADs were mediated through sarcolemma Ca^{2+} entry (Marban, Robinson, & Wier, 1986), the details of the mechanism only came to light in the latter part of the 1990s. Several studies showed that prolongation of the action potential caused reactivation of L-type Ca^{2+} channel ($CaV_{1.2}$) window currents that triggered EADs (Yan et al., 2001). Furthermore, it was shown that increases in L-type conductance promotes EAD formation (Tanskanen, Greenstein, O'Rourke, & Winslow, 2005). In contrast, blocking L-type Ca^{2+} channels reduced EAD formation in the context of hERG loss of function (P Milberg et al., 2012; Spencer et al., 2014). Thus, the current model of EAD formation is that, during instances of reduced repolarization reserve, L-type Ca^{2+} channels can be reactivated and cause a secondary depolarization (Bers, 2001). These depolarizations serve as triggers for arrhythmia. At the most basic level, EAD formation would simply be caused by a prolongation of the action potential, brought about by decreased repolarization as a result of reduced hERG current. The reality is rarely this simple.

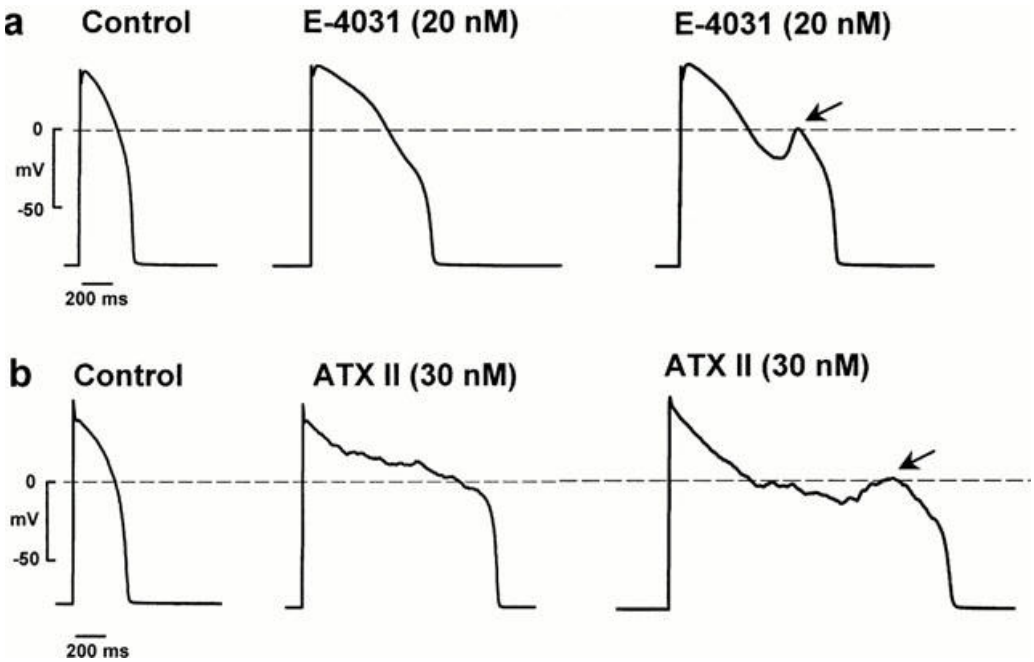

Figure 3: Demonstration of EADs due to prolonged APD in cardiomyocytes. Effects of E-4031 (a hERG blocker) and ATX II (slows I_{Na+} decay by delaying inactivation) on rabbit ventricular action potentials recorded using the perforated patch method. The authors noted that in the case of ATX II, 28% of cells showed EADs, while in the E-4031 model, 84% of cells showed EAD formation. This difference can be attributed to differences in the shape of the AP. Reprinted with permission from John Wiley and Sons. Studenik, C. R., Zhou, Z., & January, C. T. (2001). Differences in action potential and early afterdepolarization properties in LQT II and LQT3 models of long QT syndrome. *Br J Pharmacol*, 132(1), 85–92. http://doi.org/10.1038/sj.bjp.0703770

There is compelling evidence that the extent of APD prolongation is not predictive of EAD formation. Indeed, the morphology of the action potential might be more important in predicting EAD formation. More specifically, triangulation of the AP that is characterized by a shallower phase 3 repolarization caused by a selective prolongation of latter portions of the APD is thought to be most predictive. The evidence for this is compelling. For example, in a study of 702 class III anti-arrhythmic and hERG channel blockers, triangulation of the AP morphology was better correlated with induction of polymorphic ventricular tachycardia compared to other agents that similarly prolonged AP duration (Hondeghem, Carlsson, & Duker, 2001). In fact, prolongation of the APD may actually be anti-arrhythmic, as it increases the effective refractory, which can serve to decrease the substrate for arrhythmia: for example, hERG blockers are used to cardiovert patients in

atrial fibrillation (Camm et al., 2012). One important study on QT-prolonging antibiotics clearly demonstrated the importance of AP morphology on arrhythmogenicity. In a comparison of three antibiotics that all prolonged the QT interval and lengthened monophasic action potentials (MAP) by a similar degree, Milberg and colleagues showed that the antibiotics that were the most likely to induce EAD formation (and be more arrhythmogenic) were the drugs that produced the greatest triangulation of the MAP (Milberg et al., 2002). In fact, erythromycin, which showed the greatest triangulation of the MAP, was the most arrhythmogenic, while azithromycin showed very rapid phase 3 repolarization (thus a smaller degree of triangulation) and demonstrated no EAD formation and no arrhythmia. What's more, azithromycin even supressed induction of TdP brought about by the other two antibiotics tested. The authors concluded that the rate of phase 3 repolarization is crucial, that is, the faster the repolarization, or the more square the AP, the less likely the EAD formation (Milberg et al., 2002). Indeed, this is consistent with the mechanism of reactivation of L-type channels, as a prolonged phase 3 would activate L-type window current to a greater degree and thus lead to more EAD formation. Thus, a loss of function in hERG that leads not only to an increase in APD but perhaps more importantly to a triangulation of the AP may be more likely to cause EADs. These EADs then create ectopic foci within the myocardium that can lead to the formation of arrhythmia. Importantly, simulations showed that arrhythmias caused by EADs occur during normal wave propagation and do not require structural abnormalities, further corroborating the evidence that suggests that EADs alone are sufficient to cause arrhythmia (Vandersickel et al., 2014). I will return to this issue in the following section.

Overall, there is a large body of evidence demonstrating that EADs are intimately involved in the pathogenesis of arrhythmia as a result of hERG dysfunction. This body of evidence also demonstrates that AP prolongation alone does not cause EADs and is not sufficient in linking hERG dysfunction with arrhythmia. Finally, it is also clear that EADs are mediated through a Ca^{2+}-dependent mechanism, suggesting that treatment for LQT II could involve targeting this mechanism rather than hERG channels specifically. However, EADs may not be the only link between hERG dysfunction and arrhythmia. In the next section, I will examine the evidence that suggests that spatial dispersion might also be an important link between hERG dysfunction and arrhythmia.

Spatial dispersion may provide the substrate for arrhythmia but is not necessary in the pathogenesis of arrhythmia.

In 1998, Yan and Antzelevitch first described the cellular basis for the T-wave in the ECG. Building on their previous work that characterized a new type of cell located within the mid-myocardium (Sicouri & Antzelevitch, 1991), they correlated surface ECG and action potentials and showed that these mid-myocardial cells, or m-cells had an action potential that was much longer than either the epicardial or the endocardial cells. They suggested that, unlike the old model, in which epicardial cells repolarize first and endocardial cells last, it is the m-cells that repolarize last, and the sum of the gradients between all three layers produces an upright T-wave (Fig 4a). Crucially, they showed that, upon application of the QT-prolonging drug, dl-Sotalol (a hERG blocker), not only was the onset of repolarization delayed (explaining the lengthened QT interval), but the m-cell duration was also prolonged disproportionately compared to the epicardium (Fig 4b). This increase in dispersion of repolarization across the myocardial wall, they argued, set up large voltage gradients and therefore provided a substrate for arrhythmia (Yan & Antzelevitch, 1998). The current model relates transmural dispersion to enhanced voltage gradients across the wall, and these gradients provide a substrate for arrhythmia while ectopic beats or EADs provide the trigger (Qu & Weiss, 2015). However, the presence of m-cells or more precisely, their contribution to normal cardiac electrophysiology is not without controversy. For example, the Opthof group remains unconvinced to this day, and perhaps for good reasons. Using whole human, pig, and canine hearts, the Opthof group has never detected significant levels of transmural dispersion mediated through m-cells (Opthof et al., 2016). They continue to suggest that EAD formation is the most important factor with regard to arrhythmogenesis in the context of LQT (Opthof et al., 2016).

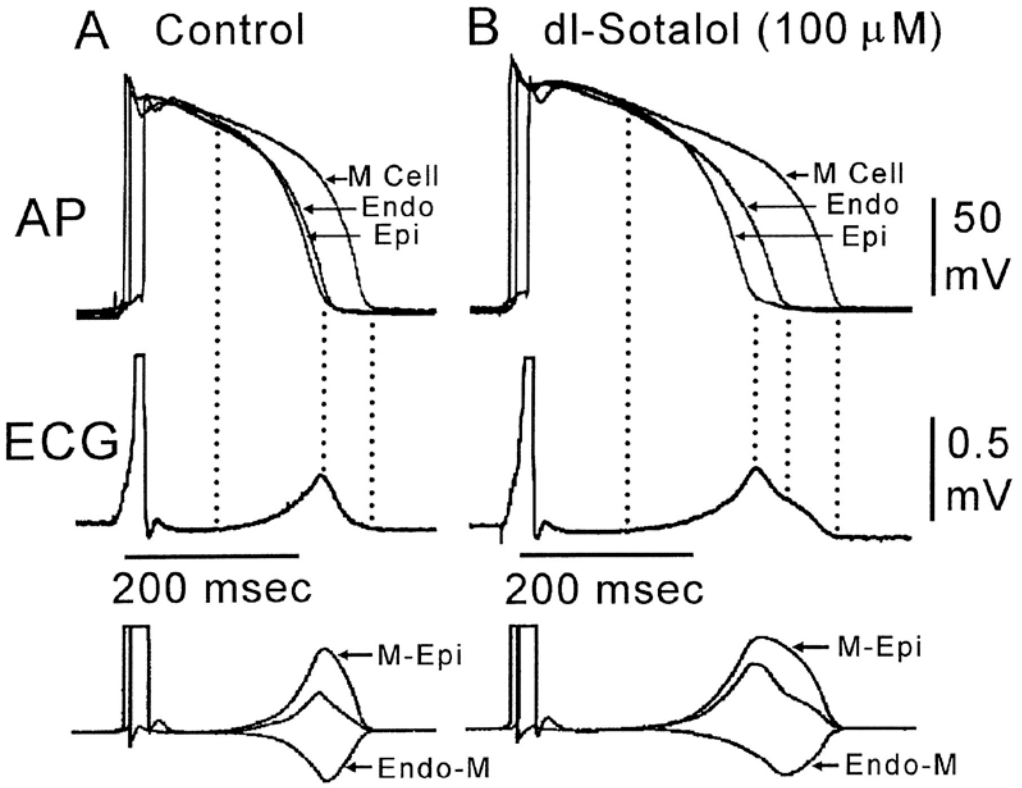

Figure 4: Correlation of T-wave with APD recorded from three layers of a canine left-ventricular wedge. (A) In control conditions, the m-cells show the longest APD; consequently, a transmural voltage difference develops. The sum of two differences (Epi-M and Endo-M) are thought to produce the upward t-wave in the ECG. (B) After 100 μM of dl-Sotalol, a blocker of hERG, the APD of all three layers is prolonged, explaining the long QT interval characteristic of hERG dysfunction. However, as the APD of the m-cells is disproportionately prolonged, a large transmural gradient develops between the m-cells and the other layers. This increase in transmural dispersion is thought to provide a substrate for arrhythmia. However, the importance of m-cells and the role of transmural dispersion in arrhythmogenesis is still controversial. Reprinted by permission from Wolter Kluwer Health. Yan, G.-X., & Antzelevitch, C. (1998). Cellular Basis for the Normal T Wave and the Electrocardiographic Manifestations of the Long-QT Syndrome. Circulation, 98(18). https://doi.org/10.1161/01.CIR.98.18.1928..

An energetic debate emerged with respect to m-cells and the role of spatial dispersion in arrhythmia in 2011 with a series of “Point/Counterpoint” comments in *Heart Rhythm* (Janse, Coronel, & Opthof, 2011a, 2011b; Kohl, Bollensdorff, & Quinn, 2011; Nattel et al., 2011; Wilson, Jennings, & Rosenbaum, 2011a, 2011b). The central criticism of the spatial dispersion model rests in the concept that an excised wedge is not a heart;

therefore, the observation that Yan and Antzelevitch made could not be generalized to the whole human heart, and by extension, transmural dispersions could not be causal in arrhythmia (Janse et al., 2011a). More specifically, Janse and colleagues pointed out that the APD recordings that Yan and Antzelevitch made were from the cut surface of the wedge, and therefore were from electrically uncoupled sites. They then cited their own work, in which they used the rather indirect measure of activation-recovery intervals (by extracellular means) to measure repolarization. In this work, they failed to detect m-cells or any significant dispersion of repolarization across the left ventricle wall (Opthof, Coronel, & Janse, 2009). Finally, they noted that, normally, canine T-waves are discordant from the QRS interval (that is, the T-wave would show a downward deflection in lead II), while they appear to be concordant in the wedge preparation (Janse et al., 2011a). Taken together, these criticisms suggest that isolation of the wedge fundamentally changes the properties of the myocardium to such a degree that wedges would be an invalid model of cardiac electrophysiology (Janse et al., 2011a). Janse et al. (2011a) also noted a functional study that questions the role of transmural dispersion in the pathogenesis of arrhythmia. In this study the authors failed to detect transmural dispersion with dl-sotalol and observed no instances of arrhythmia (Coronel, Wilms-Schopman, Opthof, & Janse, 2009). The authors concluded that even though some spatial dispersion may occur as a result of QT-prolonging drugs, this does not have a significant role to play in the pathogenesis of arrhythmia. Instead, they suggested that arrhythmia in LQT is more likely a result of multiple ectopic foci (Opthofet al., 2009).

In response, Wilson and colleagues note that the extracellular recording methods used may lack the precision to detect m-cells (Wilson et al., 2011a). And while they acknowledge that the differences they observed between the layers of the myocardium within the wedge are most likely not as clear in the myocardium of a whole heart due to some degree of uncoupling in the wedge preparation (Wilson et al., 2011b), they draw attention to Yan and Antzelevitch's correlation between surface measures and the activation-recovery measures that were taken within the deeper layers of the wedge (Yan & Antzelevitch, 1998). Furthermore, they argue that since the ECG recordings from the wedge are strongly correlated with APD measures (Fig 4), the surfaces at which the APD measures were taken must be representative of the entirety of the tissue.

Overall, there is still some debate as to the role of spatial dispersion of repolarization in the context of LQT. Many studies have associated the presence of spatial

dispersion with arrhythmia in the context of QT-prolonging drugs (Fabritz et al., 2003; Milberg et al., 2004), but these studies did not confirm if it was a result of disproportionate prolongation of m-cells or transmural dispersion specifically. Also, in all of these studies, dispersion was associated with EADs, making it difficult to say that dispersion alone is causal. Here, the study that tested three QT-prolonging drugs becomes relevant again (Milberg et al., 2002). Besides demonstrating that the morphology of the AP was a crucial factor in the formation of EADs, they observed that, while all three antibiotics increased dispersion of repolarization, only those that were also associated with EADs led to TdP. Moreover, application of one actually abolished EADs and TdP (Milberg et al., 2002). This work clearly demonstrates that the formation of EADs alone is sufficient to induce arrhythmia and that spatial dispersion may only be a mediating factor.

1.2. RPR activates hERG by slowing deactivation

As acquired Long QT is a serious concern for drug development, significant effort has been diverted towards screening compounds to evaluate their hERG-blocking properties (Vandenberg et al., 2012). As a result, a relatively small number of hERG activators have been fortuitously discovered in the screening of these compounds. hERG activators can be grouped into four categories, based on their mechanisms of action. Type IV activators, such as Mallotoxin, shift the voltage dependence of activation toward negative potentials (Zeng et al., 2006). Type III activators, such as ICA-105574, attenuate inactivation (Garg et al., 2011; Gerlach et al., 2010). Type II activators, such as PD-118057, increase the open probability of channels (Perry, Sachse, Abbruzzese, & Sanguinetti, 2009; Zhou et al., 2005). Of particular interest to us are Type I activators, such as RPR, because they slow deactivation. RPR is a small molecule rich in aromatic rings. Evidence from an alanine scan demonstrates that several residues at the bottom of the S5 segment (Val549, Leu550, Leu553, Phe557) and the bottom of the S6 segment (Asn658, Val659, Ile662, Leu666, or Tyr667) are important RPR binding sites, as mutating any of the residues to alanine reduces the sensitivity of the channel to RPR (Perry et al., 2007). More recently Gardner and colleagues applied a chimera approach that substituted part of the native hERG sequence with the respective sequence from the relatively insensitive mouse ERG channel (rERG). They demonstrated that sequence differences between the two channels in the end of the C-linker and start of the cNBHD in rERG were

largely responsible for the increased sensitivity of hERG to RPR compared to rERG (Gardner & Sanguinetti, 2015).

The effects of RPR have been well characterized in heterologous expression systems. The first report by Kang et al. (2004) demonstrated that RPR profoundly slows the rate of channel deactivation and therefore increases functional current without any corresponding changes in parameters like activation and inactivation. A 2007 study by Perry, Sachse, & Sanguinetti confirmed RPR's effect on deactivation but also noted a small depolarizing shift of inactivation, which by itself would predict an increase in functional current (Perry, Sachse, & Sanguinetti, 2007). Of note, Kang et al. (2004) also demonstrated that RPR had an inhibitory effect on L-type Ca^{2+} channels, particularly at higher concentrations, as they showed a 30% reduction in L-type current in the presence of 30 µM of RPR. However, the effect of RPR on cardiac physiology has only been directly tested in Langendorff-perfused guinea pig hearts and isolated guinea pig myocytes. In these systems, the effects of RPR were not clear. For example, in isolated guinea pig myocytes, 10 µM of RPR was relatively ineffective at shortening the APD. However, in the presence of 10 nM of dofetilide (which prolonged the APD), 10 µM of RPR showed a partial rescue by shortening the APD (Kang et al. 2004). To date, the 2005 study remains the only examination of the effect of RPR in an animal model (Kang et al., 2004).

1.3. Induced pluripotent stem cells offer unique advantages in the study of cardiovascular physiology

In the past decade, there has been a shift toward a more personalized form of medicine that strives to account for individual differences in disease pathogenesis to predict effectiveness of treatment or pharmaceutical therapy. This is often referred to as Precision Medicine. These trends have been especially prevalent in the field of cardiac electrophysiology. With increasing reliance on gene sequencing data, it has become clear that genes alone do not completely predict disease (I. Y. Chen, Matsa, & Wu, 2016). For example, otherwise silent mutations might become pathogenic in the background of gene modifiers (K897T) (Crotti et al., 2005) or specific drug therapies that expose the phenotype (Burridge et al., 2016). For this reason and others, induced pluripotent stem cells have rapidly become a popular model.

In 2006, the Yamanaka group showed that when mouse fibroblasts were transfected with a combination of four transcription factors known to be important in the maintenance of embryonic stem cells, the fibroblasts reverted to a pluripotent state (Takahashi & Yamanaka, 2006). They showed that these induced pluripotent stem cells had the ability to differentiate into all three germ layers. The next year, the Yamanaka group repeated this experiment with human fibroblasts, showing that, like in mice, it was possible to revert human somatic fibroblasts into a pluripotent state (Takahashi et al., 2007). This was a major breakthrough that won Shinya Yamanaka, along with Sir John B. Gurdon, the 2012 Nobel Prize in physiology or medicine. Human induced pluripotent stem cells (hiPSCs) not only overcame the ethical issues surrounding the use of human embryonic stem cells (hESC) but also can be derived directly from patients, preserving their genetic information (Sterneckert, Reinhardt, & Scholer, 2014). In the field of cardiology, direct clinical application of hiPSC-based technology is still some time off, but it holds great promise as the risk of immune rejection may be minimized if patient hiPSC are used to derive heart tissue for implantation. Furthermore, as hiPSCs can be proliferated, they can provide a more robust source of cardiomyocytes for patients (compared to transplants) (Sterneckert, Reinhardt, & Scholer, 2014). For example, one study in monkeys demonstrated that hiPSC-derived cardiomyocytes (hiPSC-CMs) can be implanted into areas that have undergone ischemia in order to improve heart function (Chong et al., 2014). However, significant concerns remain regarding this application, including immune rejection (if patient-matched hiPSCs are not used), the possibility of arrhythmia originating from graft sites, and the possibility of oncogenesis from residual hiPSC-cells within the implantation site (Masoudpour & Laflamme, 2017). Despite these limitations in the clinical setting, researchers have successfully applied hiPSC-CMs in the research setting, successfully modeling several disease states.

hiPSC-CMs provide distinct advantages over other models.

Traditionally, the field of cardiac electrophysiology has relied on a combination of heterologous expression systems and animal models to study the pathogenesis of arrhythmia. This is in part a result of the difficulty in obtaining human cardiac tissue, as biopsies are cumbersome, painful and often provide insufficient numbers of cells. This is one of the reasons why heterologous expression systems, such as mammalian and human immortalized cell lines (e.g., Chinese hamster ovary (CHO), human embryonic kidney (HEK), and *Xenopus laevis* oocytes) have been popular models of cardiac

electrophysiology (Berjukow et al., 1996; Masu et al., 1987). All these expression systems share the common property of having relatively few endogenous ion channels expressed at the membrane. Therefore, once they are transfected with a gene coding for an ion channel of interest, these cells express membrane currents that can be studied in relative isolation. However, what one gains in specificity, one loses in generalizability. Because these ion channels are studied in isolation, or at best with a few accessory proteins co-transfected, many of the native interactions, such as post-translational modification that may be important in disease-causing mutations, may be missed if there is no prior evidence of these interactions (Choe et al., 2006). Furthermore, as the ion channels are not in their native gene context (they are grossly overexpressed), important dose-dependent relationships (i.e., haploinsufficiency) or important stoichiometric consequences (i.e., β-unit assembly) may be obscured. Other, more subtle regulation, such as changes in potentially important gene regulatory networks that can affect the function of cardiac ion channels, may also be missed (Nadadur et al., 2016). In the worst case, expression systems may give completely erroneous results that do not translate into physiology (Nakajima et al., 1999; Nakajima et al., 1998).

On the other hand, animal models, and in particular mouse models, provide physiological context for researchers who seek to understand the pathogenesis of arrhythmia, especially if combined with transgenic technologies. Indeed, proteins other than ion channels that cause arrhythmia, such as the Ca^{2+} sensitizing Troponin T mutations, can be studied in these systems (Baudenbacher et al., 2008). These proteins, along with other ion channels, can be studied in their native contexts, and the effects of their dysfunction can be observed at the cellular (T. Powell & Twist, 1976), tissue (Goshima & Tonomura, 1969) and organ (Zimmer, 1998) level. Furthermore, genetic diseases may be studied in a physiological context by exploiting mouse transgene technologies (Baudenbacher et al., 2008). However, while many biological processes are remarkably conserved across species, concrete differences between human and animal physiology limit the generalizability of the conclusions gleaned from experiments in animal models. For example, a normal heart rate for a mouse might be upwards of 500 bpm (Watanabe et al., 2011), compared with a human heart rate of 70 bpm. Some of these differences are particularly important in the context of arrhythmia—how can you study a tachyarrhythmia in a model with a heart rate of 500 bpm? Furthermore, APD and AP morphology can differ as a result of changes in gene or protein expression. For example,

in the context of hERG, it has been shown that I_{Kr} expression is not detected in adult mouse myocytes (Wang, Feng, Kondo, Sheldon, & Duff, 1996), making mouse models poor for studying hERG dysfunction (and negating the benefits achieved from transgene technologies). Models with larger animals like sheep or pigs are attractive alternatives as their cardiac physiology is closer to that of humans; however, for many applications, they are prohibitively expensive and require specialized infrastructure (A. C. Powell et al., 1992). Still, differences in protein expression (levels) or specific sequences of proteins (evolutionary divergence) also make translational research in larger animal models difficult.

Induced pluripotent stem cell derived cardiomyocytes offer an attractive model for the study of human cardiac electrophysiology. In contrast to heterologous expression systems, hiPSCs can be differentiated into functional cardiomyocytes with all the major currents that would be seen in a cardiac cell (Liu, Laksman, & Backx, 2016). Furthermore, they can be differentiated as a monolayer (Lian et al., 2013) and studied at the tissue level; alternatively, they may be dissociated into single cells and studied at the single-cell level (Caspi et al., 2009). Unlike heterologous expression systems, hiPSC-CMs demonstrate appropriate responses to β-adrenergic agonists (e.g., isoproterenol) and M_2 muscarinic receptors (Liu et al., 2016), suggesting that second messenger systems' function in hiPSC-CMs is similar to that in native CMs. As hiPSCs can be proliferated, they offer a realistic alternative to relatively scarce human cardiomyocytes obtained from patients or cadavers. In contrast to animal models, hiPSCs are human cells that express a similar proteome compared to adult cardiomyocytes, although some aspects of their gene expression appear to be closer to the fetal gene program (Yang, Pabon, & Murry, 2014). Furthermore, they exhibit physiological parameters, such as heart rate, that are closer to those of human cardiomyocytes (Hoekstra, Mummery, Wilde, Bezzina, & Verkerk, 2012). Finally, unlike animal models, in which transgene technologies are expensive, it is realistic and relatively simple (though not always easy) to perform precise genome editing in hiPSCs (Ran et al., 2013).

hiPSCs are amenable to genome editing. Mutant hiPSCs can then be differentiated into cardiomyocytes to model genetic disease.

The ability to precisely modify the genome of hiPSCs has only emerged with the recent rapid advance of genome editing technologies such as TALENs and CRISPR-Cas9 (Gaj, Gersbach, & Barbas, 2013). In the CRISPR-Cas9 system (Clustered, Short

Interspaced Palindromic Repeats), a target-specific sequence RNA (red in Fig. 2) and an invariable target-independent activating RNA (black in Fig. 2) associate with Cas-9 to guide its endonuclease activity to introduce specific double stranded breaks within the genome (Jinek et al., 2012). These breaks are either repaired through the error-prone mechanism of non-homologous end joining (NHEJ) (Bibikova, Golic, Golic, & Carroll, 2002), leading to targeted disruptions of a gene, or through the high-fidelity repair mechanism of homology-directed repair (HDR). By introducing an exogenous donor template, the HDR mechanism can be co-opted to induce specific point mutations or small insertions within genes (Chen et al., 2011). Genome-edited hiPSCs can then be differentiated into cardiomyocytes, in which the consequences of either a large gene disruption (i.e., knock out) or targeted point mutations can be studied. Genome editing technologies, combined with the relative ease by which hiPSCs can be obtained from patients harboring a novel variant, can facilitate the creation of monogenic controls. That is, a point mutation can be introduced to revert a patient allele back to WT to study the consequence of the original mutation in the patient's genetic background.

An example of the power of hiPSC-CMs to model electrical diseases of the heart.

A remarkable study from the Conklin group (in collaboration with others) aptly demonstrates the advantages of hiPSC-CMs (Spencer et al., 2014). In this study, they used hiPSCs derived from skin fibroblasts of patients with a LQT II mutation in hERG (A422T) that causes a loss of function through decreased trafficking to the membrane. By simultaneously recording membrane voltage (via whole cell patch) and calcium transients using a Ca^{2+}-sensitive dye, Fluo-4, in a cluster of beating CMs, the authors showed that prolongation of the action potential was associated with prolongation of the Ca^{2+} transient. Furthermore, they demonstrated that the prolongation of the APD and the calcium transient were associated with the formation of EADs. In addition, the authors demonstrated the mechanistic link between prolonged APD, Ca^{2+}, and EADs. They demonstrated that application of nifidipine, a blocker of the L-type Ca^{2+} channel, abolished EADs in the LQT II hiPSC-CMs. A similar abolition of EADs was also observed with cyclopiazonic, a blocker of the sarcolemmal Ca^{2+} ATPase (SERCA), while caffeine (an RyR2 agonist) exacerbated EADs. These findings demonstrated that EADs are mediated in part through sarcolemmal Ca^{2+} release and suggested that a pharmacological approach to treating LQT may involve targeting Ca^{2+} rather than hERG channels (Spencer et al., 2014). Thus, this study successfully used patient-derived cells to demonstrate a disease-

causing mechanism, to test various pharmacological approaches to reverse the phenotype, and to reveal an important mechanistic insight regarding the interplay between voltage and calcium dynamics in disease states. A study like this would not be possible without the use of hiPSC-CMs, and as such it provides an excellent example of their research value and future potential.

The application of hiPSC-CMs to basic research is still challenging.

Nevertheless, there are still numerous challenges and drawbacks with regard to hiPSC-CMs as models of disease or drug interaction. Many of these challenges are functions of the developmental immaturity of hiPSC-CMs. First, there are some significant morphological and functional differences between hiPSC-CMs and human adult cardiomyocytes. In fact, it has been shown that the phenotype of hiPSC-CMs is closer to fetal-like cardiomyocytes than adult. In terms of morphology, hiPSC-CMs are smaller, with an underdeveloped T-tubule structure and disorganized contractile filaments (Karakikes et al., 2015; Sun et al., 2012). Also, there is a decreased expression of some key Ca^{2+}-handling proteins, most notably, the ryanodine receptor) RyR2 and the Ca_V-beta auxiliary unity 1 (Cavβ1) (Satin et al., 2008). As a result, hiPSC-CMs demonstrate altered Ca^{2+}-handling properties, such as a slower time to peak (in the calcium transient) and reduced calcium-induced calcium release (Hwang et al., 2015) in comparison to adult CMs. Furthermore, hiPSC-CMs show decreased functional expression of some key cardiac currents, most notably I_{k1} (Bosman et al., 2013). Thus, the maximum diastolic potential is relatively depolarized in hiPSC-CMs. This can lead to pre-inactivation of $Na_v1.5$ channels and may explain the slowed phase 0 upstroke observed in hiPSC-CMs and, consequently, the slowed conduction velocity across hiPSC-CM monolayers (Liu, Laksman, & Backx, 2016). Finally, as there are many differentiation techniques, it has been argued that there is considerable variability between, and even within, different laboratories also limiting the wide application of hiPSC-CMs as models of disease. While this may imply a limitation to the wider application of hiPSC-CMs as models of disease, the observation in a recent study that hiPSC-CMs from three different laboratories using different differentiation techniques produces similar Ca^{2+}-handling phenotypes (Hwang et al., 2015) provides cause for optimism.

Despite these challenges, hiPSC-CMs have been successfully applied to model LQT II syndrome using patient-derived hiPSC-CMs, demonstrating their suitability as a

model system for congenital and acquired LQT II (Terrenoire et al., 2012; Itzhaki et al., 2011; Lahti et al., 2012; Spencer et al., 2014; Terrenoire et al., 2013). One possible reason for the particular success related to modeling LQT II is that hERG is robustly expressed in hiPSC-CMs. Several studies have shown that both hERG1a and hERG1b transcripts are robustly expressed within 50 days of differentiation (Caspi et al., 2009; Mehta et al., 2011; Otsuji et al., 2010). Data from our group agree with these findings (Shafaattalab et al., 2016). Many of the same studies have also shown functional I_{Kr} current in hiPSC-CMs by blocking with hERG specific blockers like dofetilide and E-4031 (Caspi et al., 2009; Mehta et al., 2011; Otsuji et al., 2010).

In summary, hiPSCs offer unique advantages in the study of cardiac arrhythmia and despite their limitations, they are well suited for modelling LQT II.

1.4. Rational and Objectives

Objective 1: To assess the physiological consequences of accelerated and slowed deactivation of hERG channels

The effect of R56Q has been relatively well-studied in heterologous expression systems. This particular mutation was first described by the Sanguinetti group as one of eight mutations in the PAS domain found to cause LQT II in patients (Chen et al., 1999). When expressed in *Xenopus* oocytes, R56Q had the most significant effect. Furthermore, the R56Q mutation shifted the voltage dependence of inactivation by 49 mV, which by itself, would predict a gain in function (Chen et al., 1999). In 2005, Berecki et al., (2005) tested the role of the R56Q mutation in a more physiological context using the 'dynamic action potential clamp' to demonstrate the effect of the R56Q mutation on hERG current and the APD. They showed that when they replaced the native I_{Kr} in rabbit myocytes with a scaled I_{Kr} current from hERG-expressing HEK 293 cells (either expressing R56Q or WT hERG channels), R56Q caused a prolongation of the APD_{90} by about 80 ms at 1 Hz. The authors also showed, paradoxically, that the hERG resurgent current was larger than $I_{hERG\text{-}WT}$ but it had an accelerated rate of decay. Interestingly, no differences were seen in APD at higher pacing frequencies. A more recent study, using both hiPSC-CMs and HEK 293 cells infected with an adenoviral vector either coding for hERG WT or hERG R56Q (Liu and Trudeau, 2015), tested whether or not an exogenously expressed N-terminal segment could rescue the hERG dysfunction in R56Q cells. Like Berecki et al. (2005), they observed that under voltage clamp, resurgent hERG current in R56Q cells was also larger

than in WT, and similarly, the decay was faster in HEK 293 cells. (Liu and Trudeau, 2015). Nevertheless, they showed a larger effect of R56Q on APD of hiPSC-CMs, compared to Berecki et al.'s (2005) study, as the mean APD_{90} was prolonged from about 175 ms in WT hiPSC-CMs to about 300 ms in R56Q hiPSC-CMs.

Thus, we wanted to know if the same effect of R56Q was present in a more physiologically relevant model; that is, in hiPSC-CMs monolayers that express endogenous hERG (as opposed to overexpression through viral vectors). As discussed earlier, the effect of RPR has only been characterized once in an animal model (Kang et al., 2004) and has never been tested in human cardiomyocytes. Furthermore, the effect of RPR in a model of acquired arrhythmia has, to our knowledge, never been tested at any level. Therefore, we wanted to test the effect of RPR in human hiPSC-CMs carrying a mutation that causes LQT II. As RPR slows deactivation, we were particularly interested in whether or not RPR could rescue dysfunction caused specifically by an acceleration of deactivation (as in the R56Q mutation). Finally, the combination of two opposing conditions (i.e., RPR and R56Q) gives us an excellent opportunity to explore the physiological consequences of modulating rates of hERG deactivation.

We answered these questions by studying the effects of the R56Q mutation and the application of RPR in two systems. We first evaluated the effects of both R56Q and RPR on fundamental biophysical parameters, such as voltage dependence of activation, deactivation, and inactivation; and the effect of R56Q on the time course of deactivation. To better approximate the physiological effects of both R56Q and RPR, we measured resurgent current in response to a ventricular-like action potential clamp. Finally, we assessed the effect of R56Q and RPR on the hERG protective current using a premature stimulation protocol. We then moved into a more physiologically relevant system. We applied genome editing techniques to introduce the R56Q mutation into hiPSC cells and differentiated them into auto-rhythmic cardiomyocyte monolayers. To measure the effects of the R56Q mutation and RPR, we applied optical mapping techniques to R56Q and WT monolayers in the presence or absence of RPR and tracked voltage and calcium transients across a population of cells.

Objective 2: To assess the effect of RPR in a model of acquired LQT II

The acquired form of LQT is the most common form of the syndrome and hERG block is the most common cause of aLQT. This is primarily a result of the surprisingly high

affinity that hERG displays for a wide range of drugs (see Section 1.1.2). As a result, many clinically useful drugs have either been withdrawn from the market or have never made it to clinical trials. Thus, pharmacologically rescuing the phenotype of aLQT represents tremendous potential. In light of the particular importance of slow deactivation of hERG function, targeting this mechanism is an attractive approach. Nevertheless, the impact of RPR has never been tested in human cardiomyocytes. Furthermore, only one study has reported the effect of RPR in the context of drug block, and it was in a guinea pig heart (Kang et al., 2004). Thus, we wanted to test the effect of RPR in a human model of aLQT resulting from hERG block. To test this, we applied optical mapping techniques to hiPSC-CMs with RPR, in both the absence and presence of dofetilide.

Chapter 2. Methods

2.1. Two electrode Voltage Clamp

2.1.1. Molecular Biology

WT or mutant hERG1a open reading frame (cDNA) sequence was inserted into pBluescript II SK (+) 3.0 kb plasmid (PBKS) within Hind III and Xho I restriction sites. Bacterial cells were transformed with the vector to amplify and purify the cDNA constructs. Plasmid cDNA was extracted using a spin column extraction kit (Qiagen). To engineer the R56Q mutation into the hERG1a transcript, site directed mutagenesis was conducted via two step overlap extension PCR with primers synthesized by Sigma Genosys. A second round of amplification and extraction was undertaken in order to generate workable amounts of mutant cDNA. To validate the site directed mutagenesis, clones were sequenced by Sanger sequencing (Genewiz). To synthesize cRNA for oocyte injection, WT or R56Q cDNA was linearized with Xba 1 endonuclease, which cuts downstream of the 3' end of the hERG gene and cRNA was transcribed using the mMessage mMachine T7 Ultra cRNA transcription kit (Ambion, Austin, TX) that utilized the T7 promotor region in PBSK.

2.1.2. Oocyte preparation and injection

African clawed frogs (*Xenopus laevis*) oocytes were isolated using terminal surgical procedures in accordance with the policies outlined by the Simon Fraser University Animal Care Committee and the Canadian Council of Animal Care. The follicular layer was removed via collagenase treatment. (0.25 mg/mL collagenase type 1A in $MgOR_2$ solution: 96 mM NaCl, 2 mM KCl, 20 mM MgCl2, and 5 mM HEPES for 45 minutes). Stage V and VI oocytes were then manually defolliculated. Oocytes were injected with 50 nL cRNA solution of varying concentration in calcium-free $MgOR_2$ solution. The oocytes were then incubated in SOS+ media (96 mM NaCl, 2 mM KCl, 1.8 mM $CaCl_2$, 1 mM $MgCl_2$, 5 mM HEPES, 5% horse serum, 2.5 mM sodium pyruvate, and 100 mg/L gentamicin sulfate, pH 7.4) at 19 °C for 1 – 2 days.

2.1.3. Electrophysiology

Whole cell membrane currents were recorded from oocytes expressing WT or R56Q mutant hERG1a using two-electrode voltage clamp.

Equipment

Currents were recorded using an Axocalmp 900A amplifier (Axon Instruments) with a Digidata 1440 A/D interface and pClamp 10 software (Axon Instruments, Foster City, CA). All experiments were performed in ND96 solution (in mM: 96 NaCl, 3 KCl, 1 $MgCl_2$, 0.5 $CaCl_2$, and 5 HEPES, pH 7.4). Microelectrodes had a resistance of 0.2–2.0 MΩ when filled with 3 M KCl. Signals were acquired at a sampling rate of 10 kHz with a 4 kHz low-pass filter. Experiments were performed at room temperature.

Protocols and analysis

Conductance–voltage relationships were constructed for both activation and deactivation using protocols with physiological durations. To measure the voltage dependence of activation, channels were activated (conditioning pulse) from a holding potential of -80 mV mV to voltages between -80 mV and 60 mV for 250 ms, and then repolarized to -60 mV (test pulse). Tail currents were normalized to the maximum value recorded and plotted against the membrane potential of the conditioning pulse. The conductance–voltage relationship was then fit with a single Boltzmann function:

$$(1)\ G_{conditioning} = \frac{1}{1 + e^{\frac{V_{1/2} - V_{conditioning}}{k}}}$$

where $G_{conditioning}$ is the relative conductance normalized to maximum conductance (G/Gmax), $V_{1/2}$ is the voltage at which half maximal conductance was recorded, $V_{conditioning}$ is the conditioning voltage and k is the slope factor. To measure the voltage dependence of deactivation, channels were activated from a holding potential of -80mV to +20 mV for 250 ms followed by 750 ms deactivation steps (conditioning) to potentials ranging from -120 mV to +20, before a final (test) step to -60 mV. To measure the voltage dependence of deactivation, normalized tail current amplitudes during the test pulse were plotted against the membrane of the potential and then fit with a single Boltzmann function (1).

To measure the time course of deactivation, we used a similar protocol as presented in Fig 7a (inset) but extended the deactivating (i.e., conditioning) pulse to 4 s in order to record near-complete deactivation. We also increased the time and potential of the activating pulse to +60 mV over 500 ms. Deactivating current was fitted with a double exponential function:

$$(2)\ I_t = A_1 e^{\frac{-t}{\tau_{slow}}} + A_2 e^{\frac{-t}{\tau_{fast}}} + C$$

where I_t is the current at time t, A1 is the amplitude of slow tau, τ_{slow} , A2 is the amplitude of fast tau, τ_{fast}, and C is a constant. As the hERG activator compound, RPR, imparts complex deactivation kinetics we did could not fit deactivation current recorded in the presence of RPR as done previously (Perry et al., 2007).

To measure inactivation, we employed the rectification method as previously described (Sanguinetti et al., 1995). Channels were activated from a holding potential of -80mV to +20 mV for 250 ms followed by deactivation steps to potentials (V_{test}) ranging from -120 mV to +20. Peak currents in the second pulse were plotted against membrane potential to generate fully activated current-voltage (I-V) relationships. The rectification factor was derived from the deviation of the I-V relationship from linearity:

$$(3)\ R = \frac{I}{G \cdot n\left(V_{test} - E_{K+}\right)}$$

where R is the rectification factor, I is the fully activated current, G is the slope conductance (i.e., linearity) calculated from the fully activated I-V relationship using the only currents at the three most negative potentials, n is the activation factor (that is 1 as our channels are fully activated), V_{test} is the deactivation step at which I is measured, and E_{K+} is the measured reversal potential for K^+.

Voltage ramp protocols that mimic a ventricular action potential, with or without premature stimulations, were adapted from (Perry et al., 2016). The membrane was depolarized to +30 mV for 500 ms followed by a repolarization ramp to -80 mV over 220 ms. Premature stimulations to 0 mV were applied at 20 ms intervals during, or after the ramp protocol. To account for variable expression between cells, currents were normalized to the slope conductance recorded in each cell (Perry et al., 2016), which was

calculated by fitting the peak tail current-voltage relationship with a linear function over a range of 3-4 strongly hyperpolarized potentials where inactivation is negligible and channels produce a current that increases linearly with increasing driving force (voltage).

Statistics

We employed a two-way split-plot ANOVA to measure the difference between the $V_{1/2\ of}$ activation and deactivation within WT and R56Q cells (paired) and between WT and R56Q (main plot). We conducted the same analysis for slope factor. To test the effect of RPR on the $V_{1/2}$ of activation, $V_{1/2}$ of deactivation and $V_{1/2}$ of inactivation, we employed a two-way split-plot ANOVA with WT and R56Q as the main plot and the drug (paired) as the subplot. We conducted the same analysis for slope factor as well as for maximum peak protective current. In this thesis, means and standard error (SE) are reported as: mean (SE).

2.2. Genome editing of induced Pluripotent Stem Cells

2.2.1. Culturing hiPSCs

We obtained hiPSCs from a commercial source (colony #: iPS IMR90-1, WiCell). We used Matrigel (Corning) as a plating matrix (basement membrane). Before cells were plated, 1 mg of Matrigel was rapidly mixed with 12 ml of cold DMEM/F12 media (Millipore Sigma). 1 ml of the mixture was applied to one well of a 6 well plate (Sarstedt). Plates were gently rocked to facilitate even distribution. To allow the matrix sufficient time to polymerize, plates were incubated at room temperature for 1 hr before use; plates were either used for cell culture right away or an additional 1 ml of DMEM/F12 was added to each well and the plate was stored in the incubator (37°C, 5% CO_2). Coated plates older than 1 week were not used.

To thaw hiPSCs, the cell-containing cryotubes (Sarstedt) were taken out of the liquid nitrogen freezer (-150°C), and quickly thawed in a water bath (room temperature) until only a small frozen pellet remained. Using a P1000 pipette, the thawed cells were transferred into a 50 ml centrifuge tube (Falcon, Fisher Scientific) containing 7 mL mTeSR media (StemCell Technologies) at room temperature. The 50 ml centrifuge tube was then centrifuged at 300 g for 5 min to allow removal of the freezing media from the cell suspension. The media was aspirated, taking care to keep the cell pellet intact. 2 mL of

fresh complete mTeSR supplemented with 10 μM of Y-27632, a Rho Kinase inhibitor (ROCK) to promote cell attachment and increase viability (StemCell Technologies) was added and gently mixed. At this point, the DMEM/F12 was aspirated from the Matrigel plates and 2 ml of cells was added (one cryotube into each well of a 6-well plate). The cells were then transferred to the incubator (37°C, 5% CO_2).

During culture of hiPSCs, mTeSR was replaced daily (2 ml). Cells were passaged every 3 to 4 days or once they reached ~70% confluency. To passage hiPSCs, the cells were washed with 1 mL of EDTA-Varsene (Lonza). An additional 1 mL of EDTA-Varsene was then added and the plates were incubated at room temperature for 8 min. To lift cells, EDTA-Varsene was first gently aspirated and 1 ml of mTeSR was added. The cells were lifted from the plate by repeating pipetting with a P1000 pipette (7 to 10 times), taking care not to break aggregates. Immediately following this, 1/12 to 1/20 of the total suspension was transferred to another Matrigel coated plate, containing 2 ml TeSR supplemented with 10 μM ROCK. The plate was gently rocked to ensure an even distribution of cells. This procedure was repeated for all confluent wells. The newly passaged plates were then incubated overnight (37°C, 5% CO_2). The next day, and each day thereafter, 2 mL of mTeSR was replaced (without ROCK).

2.2.2. Design of the vector to facilitate homology-directed repair

To introduce the R56Q mutation into hiPSCs, we adapted the protocol developed by the Zhang group in the Broad Institute of Massachusetts Institute of Technology (MIT) (Ran et al., 2013). First, we designed an asymmetric single stranded oligonucleotide donor that is homologous to the region around R56 but contains the G > A transition that is seen in R56Q LQT II patients (Moss et al., 2002), as well as a silent G > A transition in the 3rd base the Glu58 codon to knock-out the PAM site and prevent continuous cutting (Fig 5a). Furthermore, we designed the donor to be asymmetrical with respect to the predicted cut site in order to increase the probability of integration (Richardson et al., 2016) (Fig B1). Next, we designed the guide RNA (gRNA) specific to the genomic region around R56 using the Genetic Perturbation Platform from the Broad Institute (Cambridge, MA) (Doench et al., 2016). We ordered the guide sequence and the ssODN from IDT (IDT) Two synthetic oligonucleotides were ordered from IDT and annealed to create the double-stranded 20 bp guide sequence using a thermocycler (C1000 Thermo Cycler, BioRad) with the following cycling parameter: Initial denaturation: 95°C, 5 min; annealing: 95°C-

85°C in 5s, 85°C-25°C in 10 min; hold: 4°C. The guide sequence was then cloned into the pCCC vector, generously provided by Dr. Francis Lynn. The pCCC vector is based on the pc458 vector (Addgene; plasmid 48138) where the CBH promoter was exchanged for a full-length CAGGS promoter to maximize expression in hESCs and hiPSCs (Krentz and Lynn, 2014). The vector contains two promotor sites: the first is U6, an RNA polymerase III site that facilitates the expression of the gRNA, while second is a modified CAG promoter (CMV enhancer/chicken beta-actin promoter/rabbit beta-globin splice acceptor), an RNA polymerase II site that facilitates expression of both the CAS9 and eGFP proteins (Fig 5a).

The guide sequence was cloned into the vector as outlined in Ran et al, 2013. The pCCC vector was digested with Invitrogen™ Anza™ 4 BpiI, targeting the BBSI site (1 ug of pCCC plasmid, 2 µl of 10x buffer, 1 µl enzyme and water to 20 µl). Digested plasmids were purified using ethanol precipitation and silica columns (GeneJet, Thermofisher Scientific). Digested vectors were then combined with 20 bp guide sequence and ligated using T4 ligase (Thermofisher) (50:250 ng vector to insert, 2 µl buffer, 1 µl enzyme and water to 20 µl). The ligation reaction was allowed to proceed at 16°C overnight. The next day, competent DH5-α *E. Coli* cells were transformed with the ligated mix using the calcium chloride method. To do this, 10 µl of ligated reaction mixture was added under a high concentration of $CaCl_2$ and the cells were placed at 42 °C for 45 sec followed by 2 min of recovery in ice. 100 µl Luria-Bertani (LB) broth was then into the cell mixture and placed the cells at 37 °C for 1 h. The entire mixture of cells was pated onto 30 cm petri dishes coated with agar and supplemented with 100 ug/ml ampicillin, and plates were incubated at 37°C for 16 h. The next day, we selected 10 colonies, placing each colony into 5 ml of LB supplemented with 1 mM final concentration of ampicillin in a separate aerated capped test tube (Sarstedt). The test tubes were then placed into a shaking incubator (37 °C) at 200 rpm overnight. The next day, 500 µl of the cell-rich broth out of each test tube was combined with 500 µl glycerol (80% - 100%) and frozen at -70°C. The rest of the suspension was used for DNA extraction using the QIAprep Spin Miniprep Kit (Qiagen). Briefly, this method employs a strong ionic detergent (SDS) to solubilize cell membranes in the presence of RNAase and EDTA. The solution is then neutralized with acetic acid and the DNA is precipitated with ethanol/high salt mixture using silica columns to collect the DNA. Finally, the DNA is eluted in water or elution buffer (Qiagen). The

purified plasmid DNA was sequenced to confirm a successful insertion of the guide sequence into the vector using Sanger sequencing (Genewiz).

2.2.3. Transfection of hiPSCs and Fluorescence activated cell sorting

Using Lipofectamine 3000 (Thermofisher), we transfected hiPSCs in a 12 well plate (Sarstedt) with 500 ng of pCCC-R56Q and 10 picomols of ssODN (Fig 5a). Since the pCCC vector contains GFP as a transcriptional reporter, we isolated GFP^+, single cell hiPSCs using Fluorescence-Activated Cell Sorting (FACS) into 6 well plates at limiting dilution (500 cells/well). We used the BD Jazz (BD Sciences, Singapore) for FACS (GFP 488 nm laser and 530/30 mm band pass filter). We used sorting medium to improve cell viability (5 μM ROCK, 1 μM CHIR99021, 0.4 μM PD0325901 and 2 μM SB 431542) as per Valamehr et al., (2012) (Fig 5b). To allow the cells time to properly adhere, we did not change media for 4 days after sorting. As the viability of cells was very low after FACS, only 12-30 colonies appeared on each plate after 7 days. Using mechanical methods, we isolated single hiPSC colonies into individual wells of a 96-well plate (SigmaAldrich) containing 70 μl mTeSR. We replaced this media every day. Once the cells were confluent, we used a 12-channel pipette to passage the cells (at 1/12) into a second 96-well plate (Fig 5c). We waited 24 hours for the cells in the first plate to re-adhere and used that plate for DNA extraction.

2.2.4. Genotyping

To genotype cells, we designed a protocol that was suitable for use in a 96 well format. To extract DNA, we washed the cells with 100 μl PBS and then added 100 μl of direct lysis buffer (Viagen Biotech) diluted 1:1 with water and supplemented with 50 μl/ml of Proteinase K (1mg/ml) (Viagen Biotech). We then incubated the plate on a shaking platform at 55°C for 4 h. After allowing the lysates to cool, we transferred the contents into a sealed 96-well PCR plate (BioRad) and placed it into a thermal cycler set at 85 °C for 45 min in order to deactivate the Proteinase K enzyme.

To increase the yield and the specificity of the PCR product, we applied a nested PCR approach. In this approach, the first amplification is a standard PCR reaction. For this we used 2 μl of crude lysate in a 25 μl total volume for each well (per 1 reaction in μl: 11.5 water, 2.5 10x buffer, 0.25 forward primer (at 10 μM), 0.25 reverse primer (at 10 μM),

2.5 MgCl, 5 Q solution (Qiagen), 0.5 dNTP (at 10 μM) and 0.5 μl Taq enzyme (ABM)). The primers were designed using Primer-BLAST (Ye et al., 2012). We ordered the primers as synthetic oligonucleotides from IDT (Springfield, IL). Cycling parameters are as follows: Initial denaturation: 95°C, 5 min; annealing: 57°C, 30s; extension: 70°C, 60s; denaturation: 95°C, for 34 cycles; final extension: 70°C, 10 min; hold: 4°C. The second step in the nested PCR approach employs primer-pairs specific to the amplicon from the first reaction. In this second step, we used double the recipe from the first reaction (i.e., 50 μl reaction total) with 2 μl of PCR product from the first reaction. Before sequencing the amplified DNA, we purified the PCR product using ethanol/high salt precipitation and silica columns (GeneJet PCR Purification Kit, Thermofisher Scientific). We sequenced all the colonies using Sanger sequencing (Genewiz). All the colonies that were positive for the mutation, as well as 5 WT colonies, were expanded into 6-well plates.

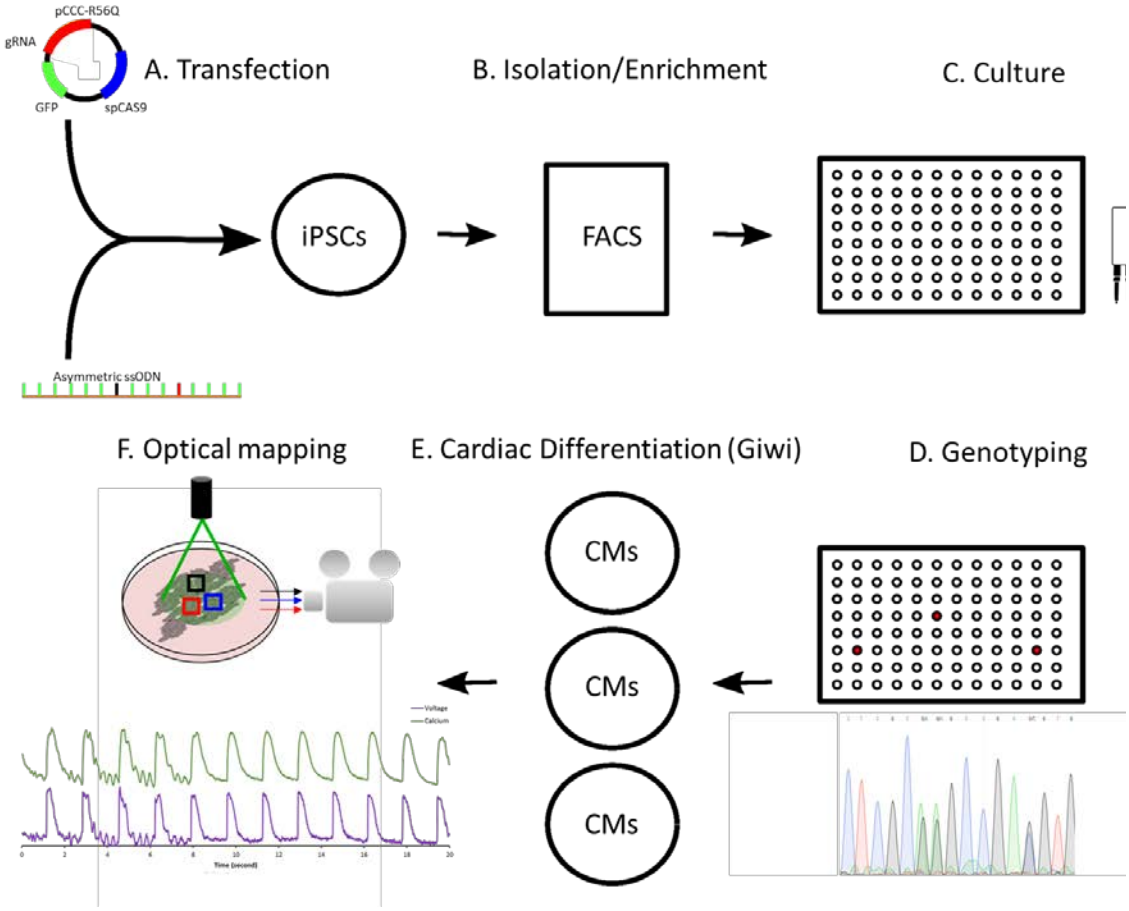

Figure 5: hiPSC-CMs genome editing workflow. A) hiPSC were transfected with plamids containing coding regions for the gRNA, eGFP and CAS9; and a donor template. (B) Transfected cells were then isolated using FACS and left to grow into colonies. C) Monogenic colonies were separated into 96 well format and D) genotyped using standard PCR and Sanger sequencing. E) Cells containing mutations, as well as some WT cells, were differentiated into cardiomyocytes monolayers. F) Opitcal mapping techniques were used to track voltage and calcium transients from regions of interest.

2.3. Differentiation and culturing of Cardiomyocytes

To differentiate hiPSCs into cardiomyocytes, we employed the protocol developed by Lian et al. (Giwi) using an early activation of Wnt signaling in an insulin free B27/RPMI medium to induce mesoderm formation followed by a subsequent inhibition of Wnt signaling to induce cardiac specification (Fig. 6). (Lian et al., 2013). We plated hiPSCs into 35 mm dishes (Sarstedt) at a density of between 0.75 and 1.5 million cells. After 3-5 days

(until 95-100% confluent), we began differentiation (day 0) by adding CHIR99021, an inhibitor of GSK3, to a final concentration of 12 µM in 2 ml of RPMI media supplemented with B27 without insulin (RPMI/B27-). After 24 hours, we replaced the media with RPMI/B27-. Crucially, we did not change the media for the next 72 hours. This allows secreted growth factors (including Activin A and BMP4) to accumulate in the media. To induce cardiac specification, we added IWP-4, and inhibitor of Wnt signaling. Using a P1000 pipette, we aspirated 1 ml of conditioned media out of each well of cells and combined it with 1 ml of fresh RPMI and B27-. To this mixed media, we added IWP-4 to a final concentration of 5 µM. On day 5, we replaced the media with 2 ml of RPMI B27-. On day 7, we replaced the media with RPMI supplemented with complete B27. This media was replaced every 2 days thereafter. After monolayers began spontaneously contracting (between day 10 and 12), we replaced the media every 3 days.

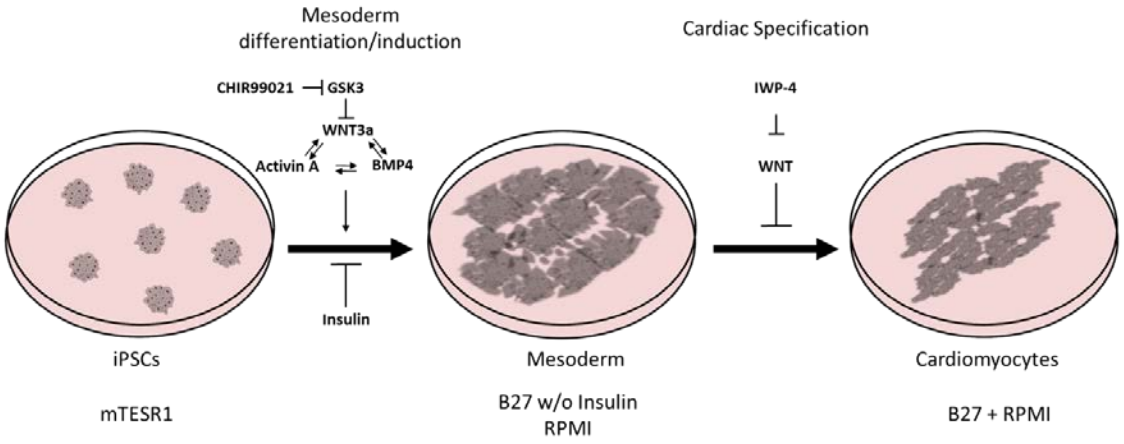

Figure 6: Differentiation of hiPSCs into auto-rhythmic monolayers through biphasic modulation of Wnt signaling. To induce mesoderm differentiation, GSK3 signaling is inhibited. This increases Wnt3a signaling along with Activin A and BMP4. As insulin inhibits this process, it is left out of the B27 growth supplement that is added to the RPMI media To induce cardiac specification, Wnt signaling is inhibited by IWP-4.

2.4. Optical mapping of hiPSC-CMs

Consistent with the appearance of robust hERG current, we waited until at least day 50 and then used optical mapping methods to observe voltage and calcium transients across monolayers of CMs. To monitor voltage, we loaded the cells with the potentiometric dye, RH-237. To monitor calcium transients, we loaded the cells with Rhod-2-AM. Both dyes were co-excited with light at 532 nm wavelength: Rhod-2 emission was monitored between 565 nm and 600 nm while RH-237 was monitored at >710nm (LP) (Lin et al., 2015). Signals were acquired using a Hamamatsu ORCA Flash 4 digital CMOS camera at 37°C, with processing using an in-house custom software run on IDL. Blebbistatin, an inhibitor of Myosin II ATPase, was applied to arrest contraction in hiPSC-CMs.

After a baseline recording, we either added RPR to a concentration of 10 or 30 µM (control) or 100 nM dofetilide (a model of acquired LQT II). In the case of our model of

acquired arrhythmia, after 30 min, we added RPR to a concentration of 10 µM, and then after 30 more minutes, we added more RPR to a final concentration of 30 µM. In each condition, we attempted to electrically stimulate the cells to 70 bpm but this was not always successful. In the case of our model of inherited arrhythmia (R56Q genome edited hiPSC-CMs) we added RPR to a final concentration of 10 µM. After 20 – 30 min, we added more RPR to a final concentration of 30 µM. To minimize photo-bleaching of the dyes, we performed recordings in 20 sec increments. In order to account for variability between individual action potential and calcium transients, all signals from a recording increment are averaged to give aggregate voltage and calcium signals

Chapter 3. Results

3.1. Biophysical assessment of hERG WT, R56Q in the absence and presence of RPR.

3.1.1. R56Q accelerates deactivation

To test the biophysical effects of the R56Q hERG channel mutation, we recorded membrane currents from *Xenopus* oocytes injected with WT or R56Q mutant hERG1a cRNA. Voltage protocols used to record deactivation and activation, along with example current traces are displayed in Fig. 7a and 7b. Qualitatively, we observed that R56Q accelerated the time course of deactivation. This is especially evident in the test pulse of each protocol. By fitting each current decay with a double exponential function (see Methods), we quantified the time course of deactivation for WT and R56Q across a range of voltages. An example of such a fit at a single voltage is presented in Fig 1c (-110 mV test pulse). In Fig 7d, mean τ_{fast} values derived from such fits are plotted against voltages ranging from -110 mV to -40 mV for R56Q (red) and WT (black). As hERG deactivation kinetics are best fit with a double exponential function (Vandenberg et al., 2012), we calculated time constants from each term of our double exponential fit (i.e., τ_{fast} and τ_{slow}). In Fig 7d, we have plotted only the τ_{fast} as the relative contribution of τ_{fast} to deactivation kinetics is relatively larger in R56Q channels (Appendix B). Here, we observed that R56Q greatly reduced the fast rate constant of deactivation across all tested voltages (Fig 7D). However, while the magnitude of individual rate constants give mechanistic insight, physiological time course of deactivation is best approximated with a weighted average ($\tau_{weighted}$) of both τ_{fast} and τ_{slow} (see methods). Using this measure, we also observed a large acceleration of mean time course of deactivation for R56Q compared to WT across all tested voltages (Fig 7e).

The voltage dependence of activation and deactivation of WT and R56Q channels are plotted in Fig 7f. At physiological durations, the slow opening and closing kinetics of hERG channels means that they do not reach steady-state activation, or deactivation. Therefore, we hypothesized that changes in the kinetics of deactivation observed in Fig 1a-e would have a profound effect of the voltage dependence of deactivation. Indeed, we found strong evidence that in R56Q channels, the mean voltage dependence of

deactivation was shifted towards more depolarized potentials by 30 (1.9) mV compared to WT ($p<0.0001$) (Fig 1f). We also found strong evidence that the mean slope factor of the voltage dependence of deactivation in R56Q was 2.1 (0.5) mV smaller than WT (indicating a greater voltage sensitivity) ($p=0.003$) (Fig 7f). Importantly, we found no evidence that there was a difference between the mean voltage dependence of activation for R56Q compared to WT ($p=0.78$) (Table 1), nor was there a difference in mean slope factor for the voltage dependence of activation and deactivation (Table A1) ($p=0.99$).

Table 1: Effect of accelerated deactivation on the mean conductance-voltage relationships for activation and deactivation of WT and R56Q hERG channels at physiological durations

Protocol	Genotype	n	Mean (mV)	SD (mV)	SE (mV)	95% CI – lcl,ucl (mV)
Activation	R56Q	6	-8.4	2.8	1.1	-11.3, -5.4
	WT	5	-6.6	2.2	1.0	-9.4, -3.9
Deactivation	R56Q	6	-34.4	2.2	0.9	-36.7, -32.2
	WT	5	-64.7	4.8	2.6	-70.6, -58.6

CI: Confidence Interval; lcl: lower confidence interval; ucl: upper confidence interval

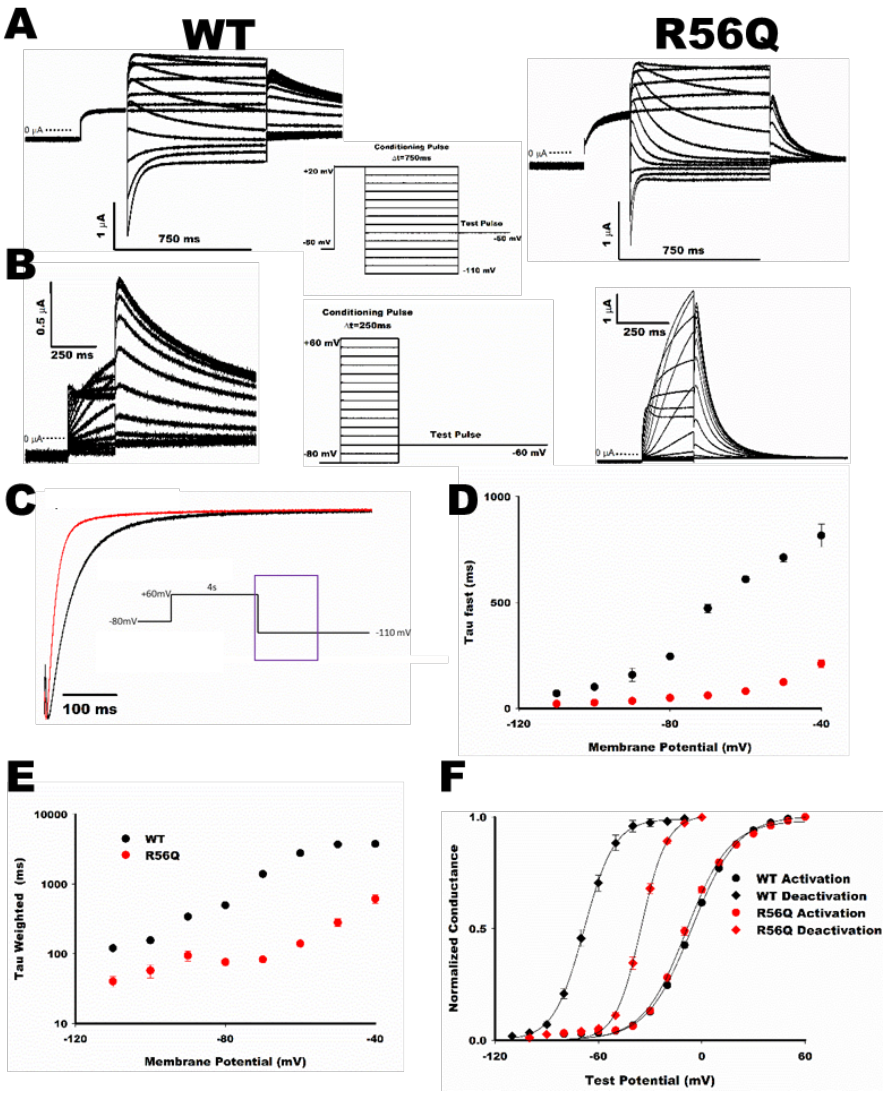

Figure 7: R56Q causes a loss of function due to accelerated deactivation. Sample deactivation **(A)** and activation **(B)** current traces recorded from R56Q (right) and WT (left) channels. **C)** Normalized sample current traces at -110 mV after a 4 s activating pulse at 60 mV demonstrates the acceleration in deactivation in R56Q constructs (red trace) compared to WT constructs (black). **D)** τ_{fast} values plotted against voltage show a significant acceleration in deactivation in R56Q channels (red) compared to WT (black). **E)** Weighted τ_{fast} plotted against voltage approximate the actual time course of deactivation **F)** Conductance–voltage relationships in R56Q (red) and WT (black) channels for activation (circles) and deactivation (diamonds) protocols respectively. Note that there is no difference in the voltage dependence of activation (circles) between R56Q and WT, while R56Q (red diamonds) exhibits a large depolarizing shift in the voltage dependence of deactivation compared to WT (black diamonds).

3.1.2. RPR slows deactivation to a similar degree in both WT and R56Q

To test the effect of RPR had on the conductance-voltage (GV) relationship, we perfused 10 μM RPR onto oocytes expressing WT or R56Q channels and applied the same activation and deactivation protocols as in Fig 7 (Figs 8 and 9). Sample WT deactivation current traces in the absence and presence of RPR are shown in Fig 8a. Sample deactivation current traces for R56Q are shown in Fig 9a. The effect of RPR on the mean conductance–voltage relationships for activation and deactivation are shown in Fig 8b and 8c for WT and in Fig 9b and 9c for R56Q. We did not find evidence of an effect of 10 μM RPR on the mean voltage dependence of activation in WT cells (p=0.68) (Fig 8b). Similarly, we did not find evidence of an effect of 10 μM RPR on the mean voltage dependence of activation in R56Q (p=0.23) (Fig 9b). Values are presented in Table A2. We also did not observe any evidence of an effect of RPR on the slope factor of activation in either WT (p=0.88) or R56Q (p=0.37) channels. Taken together, these data indicate that RPR had no observable effect on the conductance–voltage relationship of activation in hERG WT or R56Q channels at physiological durations.

In the case of the voltage dependence of deactivation Boltzmann fits suggested an apparent shift in mean $V_{1/2}$ towards more hyperpolarized potentials in WT by 7.1 (1.4) mV (p=0.008) (Fig 8c). However, the fit was poor as there was a large conductance at negative potentials, suggesting incomplete channel closure. Therefore, we observed a relatively larger hyperpolarizing shift in the mean conductance–voltage relationship at more negative potentials (-60 mV to -110 mV) (Fig 8c). We observed a similar trend in R56Q as 10 μM RPR increased the conductance at more negative potentials. Similarly, the fit of the GV relationship was also poor. Therefore, we did not find evidence that 10 μM RPR shifted the mean $V_{1/2}$ of deactivation towards more hyperpolarized (p=0.14) (Fig 9c). Values are presented in Table A3.

In addition, we sought to test the effect of 10 μM RPR on steady-state inactivation. To do this, we calculated the deviation from linearity of fully activated current voltage relationships (Fig 8d inset and Fig 9d inset) (see methods). Values are presented in Table A4. We found no evidence that the mean GV relationship of steady-state inactivation was affected by the R56Q mutation (F=1.45; p=0.27). We also found no evidence that RPR shifted the mean GV relationship of activation, either in WT channels or in R56Q channels

(F=1.92; p=0.22). There was also no evidence of an interaction between R56Q and 10 µM RPR on the mean steady-state inactivation (F=1.3; p=0.3).

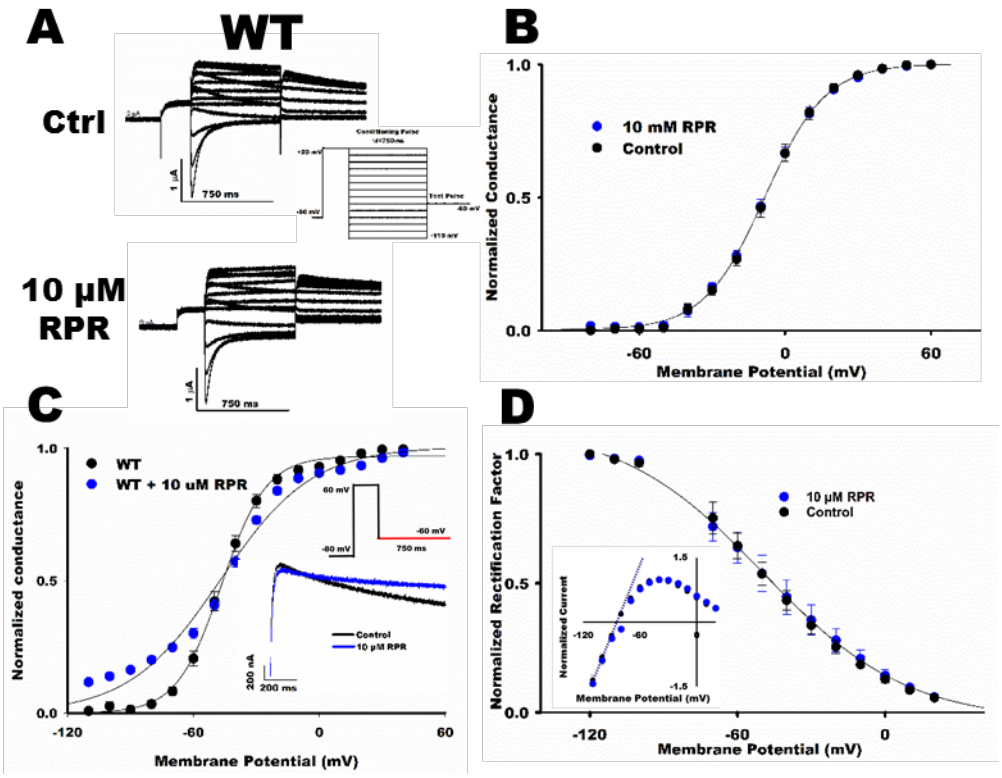

Figure 8 RPR slows deactivation in WT hERG channels. A) Sample traces of deactivation in WT channels **B)** WT voltage dependence of activation (GV) in the presence (blue) and absence (black) of RPR shows no effect of RPR on the conductance–voltage relationship of activation. **C)** RPR (blue) had an apparent effect on the GV of deactivation in WT cells, with the largest effect seen at voltages between -60 mV and -110 mV. Note the poor fit in the presence of RPR. Inset shows differences in kinetics after application of 10 µM RPR in the same cell **D)** RPR has no effect of the voltage dependence of steady-state inactivation. Inset shows deviation from linearity used to calculate steady-state inactivation.

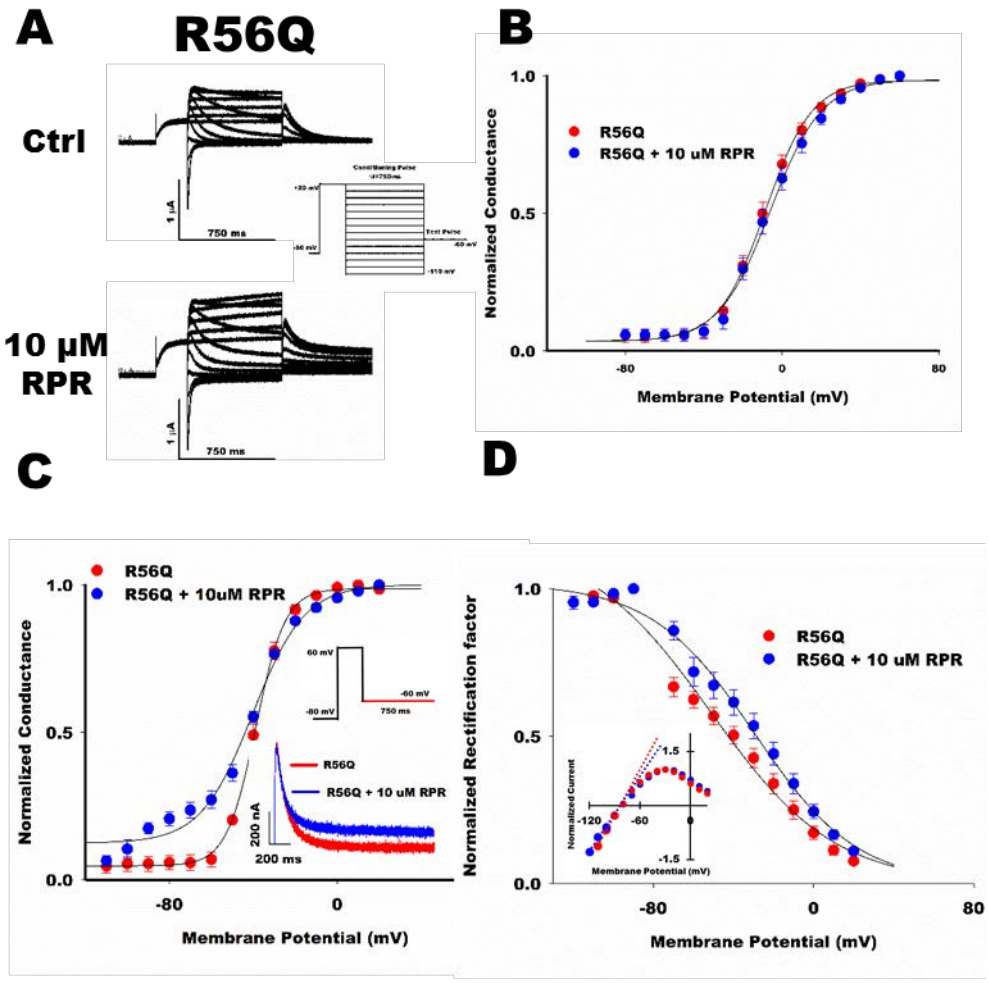

Figure 9: The effect of RPR on R56Q is similar to that on WT channels. A) Sample traces of deactivation in R56Q channels. **B)** R56Q voltage dependence of activation (GV) in the presence (blue) and absence (red) of RPR shows no effect of RPR on the conductance–voltage relationship of activation. **C)** RPR (blue) had an apparent effect on the GV of deactivation in R56Q cells, with the largest effect seen at voltages between -60 mV and -110 mV. Note the poor fit in the presence of RPR. Inset shows differences in kinetics after application of 10 µM RPR in the same cell **D)** RPR has no effect of the voltage dependence of steady-state inactivation. Inset shows deviation from linearity used to calculate steady-state inactivation

3.1.3. R56Q increases resurgent current. RPR also increases resurgent current but only in WT channels

Figure 10a (inset) demonstrates the voltage protocol adapted from Perry et al. (2016) designed to simulate a ventricular action potential and its corresponding sample WT hERG current (Fig 10a). By taking the integral of the resurgent current, we can approximate the amount of charge moved during phase 3. By normalizing to the slope conductance measured in each oocyte, we can account for differential expression levels and compare the total charge moved between WT and R56Q channels (Fig 10b). Mean normalized integrals of resurgent current are plotted for WT (blue) and R56Q channels, in the presence and absence of 10 μM RPR. We found evidence that in the control solution (ND96), R56Q channels moved a mean of 1420 (405) μC more charge than WT channels ($p=0.027$). We also found evidence that in WT channels, 10 μM of RPR increased the mean amount of charge moved by 723 (207) μC ($p=0.039$) but not in R56Q channels ($p= 0.89$). Together, these data show that R56Q increases resurgent current in *Xenopus* oocytes in response to a ventricular ramp protocol. Additionally, 10 μM RPR increases resurgent current in WT but not R56 channels.

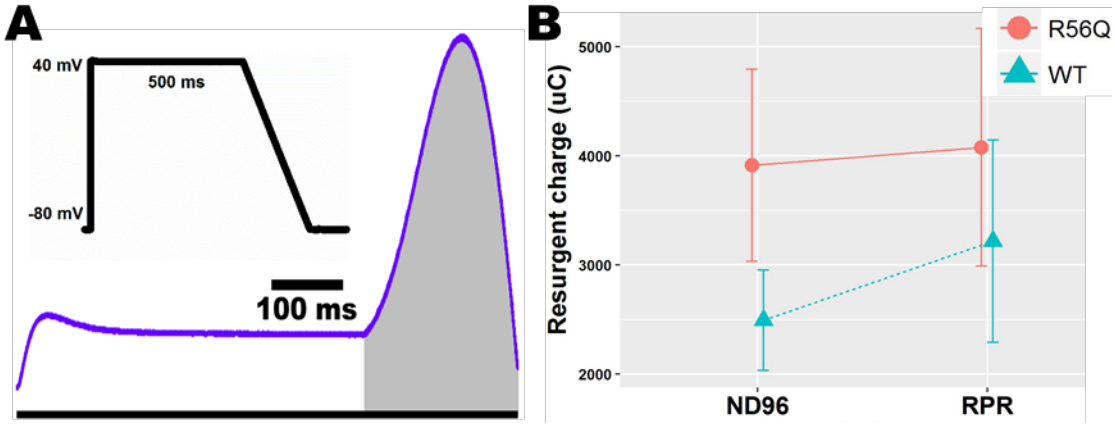

Figure 10: Mean integrals of currents is response to action potential clamp. A) An example of ionic current elicited in response to a ramp protocol designed to simulate the ventricular action potential. The shaded region represents the total amount of charge moved during phase 3. **B)** Profile plot for the integral of WT ionic current (blue) and R56Q (red) with and without RPR show no differences in mean integrals between any of the groups

3.1.4. R56Q decreases protective hERG current and 10 μM RPR partially rescues this effect

To test the effect of R56Q on the protective current carried by hERG in the early refractory period of the action potential, we employed the premature stimulation protocol outlined in Figure 11a (inset). An example of the current elicited in response to one sweep is pictured in Fig 5a. This current is in response to a simulated premature stimulation to 0 mV introduced at the termination of the ramp phase. Other premature stimulations were applied at different coupling durations, such that they either interrupted the ramp phase or closely followed it. From Fig 11a, it is clear that hERG channels pass a robust, large transient repolarizing current in response to premature stimulations applied early in the refractory period. Figure 11b shows how we accounted for any capacitive current. We fit each transient current to a single exponential function and extrapolated back to the start of the corresponding premature stimulation. From these fits, we measured the peak current, which represents the peak protective current (PPC) at that coupling duration. Figure 11c shows example protective current traces recorded during the premature stimulation protocol shown in panel A in both WT and R56Q mutant channels, in the

absence and presence of RPR. The protective current elicited from R56Q channels shown in Figure 5d (top) demonstrates a sharp decline in protective current near the end of the ramp phase and an almost complete abolition following the ramp. Interestingly, 10 µM RPR partially restored the loss of this protective current. Mean PPC is plotted for WT (Fig 11e) and R56Q (Fig 11f) against the coupling interval. To quantify the effect sizes, we chose to compare the magnitude of the PPC at the coupling interval at which the PPC was the largest for WT (Fig 11 E and F, arrow). We called this maximum peak protective current (PPC_{max}). We reasoned that the coupling interval at which the PPC_{max} reaches its maximum magnitude in WT cells is also the interval at which hERG channels offer the greatest protection against premature beats. Mean PPC_{max} is plotted in Fig 12 for WT (blue) and R56Q (Red) channels, in the presence and absence of 10 µM RPR. We found strong evidence that the R56Q construct decreased mean PPC_{max} by 49 (4.1) µA ($p<0.001$). We also found evidence that 10 µM RPR partially rescued R56Q protective current as it increased mean PPC_{max} by 13 (3.1) µA ($p=0.01$). However, we found only weak evidence that 10 µM RPR increased mean PPC_{max} in WT channels, as mean PPC_{max} was increased by 9 (3.0) µA ($p=0.06$) in the presence of 10 µM RPR (Fig 12). These data show that R56Q profoundly decreases peak protective hERG current (Fig 12) and that 10 µM RPR partially rescues the current loss. Interestingly, the effect of RPR on maximum peak protective current was much greater in R56Q channels than in WT channels (Fig 12).

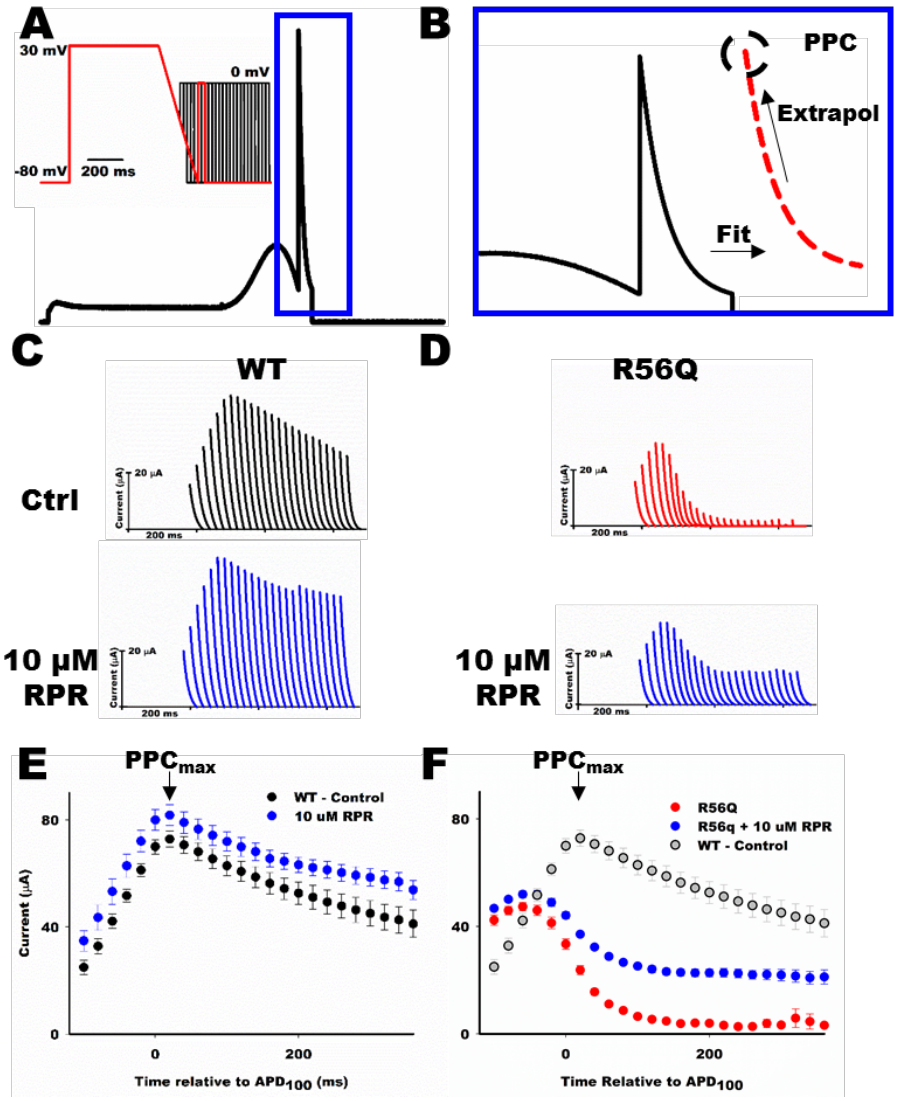

Figure 11: R56Q decreases protective current and RPR demonstrates a partial rescue. A) Example of one sweep of a premature stimulation protocol with the corresponding voltage command (active voltage sweep in red). **B)** To account for capacitance, the current decay was fitted with a single exponential. This function was extrapolated back to the start of the premature stimulations. This value was taken as a measure of peak protective current (PPC) **C)** Transient currents (in response to a premature stimulation) are plotted for WT cells to illustrate how the peak protective current is enhanced by RPR (blue) compared to WT (black). **D)** R56Q current transients (red) plotted without RPR (top) and with the addition of 10 µM RPR (bottom, blue). **E)** Peak protective current for WT cells in control conditions in the absence (black) and presence (blue) 10 µM RPR is plotted against coupling interval where 0 represents the end of the AP ramp. **F)** R56Q peak protective currents plotted (red) against coupling interval and with the addition of 10 µM RPR (Red). WT control PPC is also plotted for reference (gray).

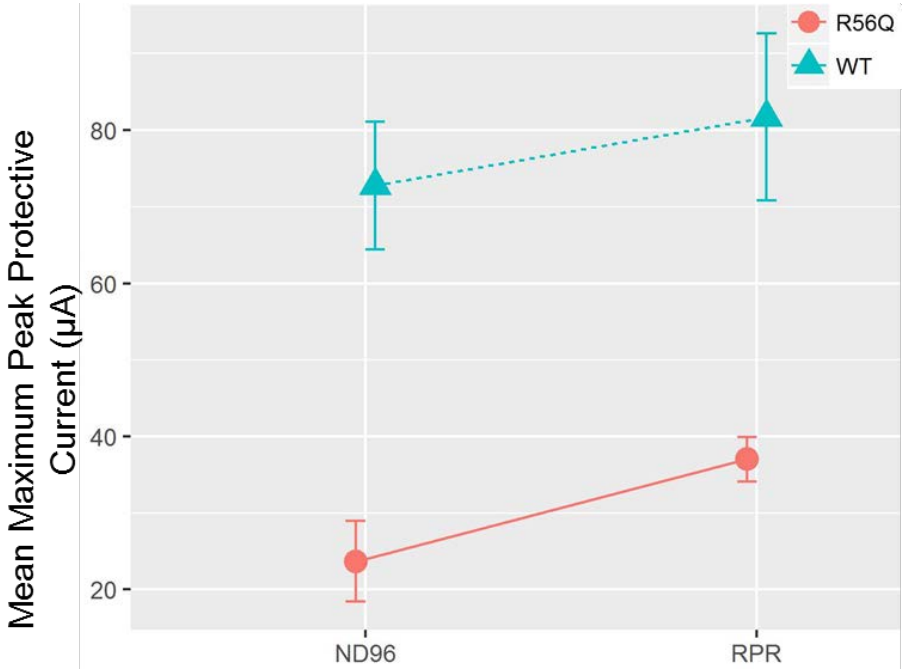

Figure 12: Profile plot of mean PPC_{max} Mean peak protective currents plotted at the coupling interval at which WT reached its maximum (APD_{100} + 20 ms) for R56Q channels (red) in the presence and absence of RPR and for WT channels (blue) in the presence and absence of RPR .

3.2. Physiological experiments

Next, we wanted to employ a more physiologically relevant model. We differentiated genome edited R56Q hiPSCs, as well as WT hiPSCs, into monolayers of cardiomyocytes. Our hiPSC-CMs began contracting spontaneously within 10-12 days post differentiation. The beating rates were lower than human hearts (20-40 bpm) and varied between colonies (data not shown). As it has been shown that it takes about 40-50 days for levels of I_{Kr} expression to reach meaningful levels (see section 1.3), we only conducted experiments in hiPSC-CMs that were 50 days or older. We used optical mapping techniques to simultaneously track voltage and calcium transients from regions of interest (ROIs - containing several thousand cells). Here, we present our results from our model of inherited LQT II due to accelerated deactivation and results from our model of acquired LQT II due to drug block.

3.2.1. In a model of acquired LQT II RPR partially rescues hERG loss of function

To better test the effect of RPR on cardiac physiology, we performed optical mapping experiments on monolayers of hiPSC-CMs with and without RPR. Furthermore, to test whether RPR could rescue prolonged APD as a result drug block, we also performed experiments in the presence of 100 nM dofetilide. In Fig 13a, sample simultaneous recordings of voltage and calcium transients are shown. To minimize photo-bleaching of the dyes, we performed recording in 20 sec increments. In order to account for variability between individual action potential and calcium transients, all signals from a recording increment were averaged to give aggregate voltage and calcium signals. In WT cells alone, we observed that neither 10 µM RPR (Fig 13b, left) nor 30 µM RPR (data not shown) had an observable effect on AP duration (APD_{80} = 550 ms) or AP morphology. The same trends were observed in the calcium transient (Fig 13c). When we applied 100 nM dofetilide, we observed a significant prolongation of the APD_{80} by 315 ms, as well as significant triangulation of the AP morphology (Fig 13b, right). After subsequent application of 10 µM RPR, we observed a slight shortening of the APD in earlier durations (APD_{50} to APD_{70}), but no shortening of the APD at later durations (APD_{80}-APD_{100}) (Fig 13b, right). Also, we observed no change in the AP morphology after the application of 10 µM RPR. In the calcium signal, we also observed a prolongation of the calcium transient duration (CTD) with the application of dofetilide, consistent with predictions. However, contrary to our hypothesis, 10 µM RPR further prolonged the CTD in earlier durations (APD_{20} to APD_{70}) (Fig 13c, right). In summary, 10 µM RPR did not have a meaningful effect either in control conditions, or following dofetilide block.

Next, we tried a higher concentration of RPR (30 µM) following dofetilide block (Fig 14). Again, we observed that dofetilide significantly prolonged the APD (APD_{80} control = 580 ms; APD_{80} 100 nM dofetilide = 980 ms) and introduced some triangulation (Fig 14a). When we applied 30 µM RPR, we observed that the APD across the entire length of the repolarization phase shortened (APD_{80} decreased by 150 ms). The averaged calcium transient largely mirrored this trend but to a lesser degree in terms of transient duration. However, we saw a slight slowing of the upstroke (Fig 14b).

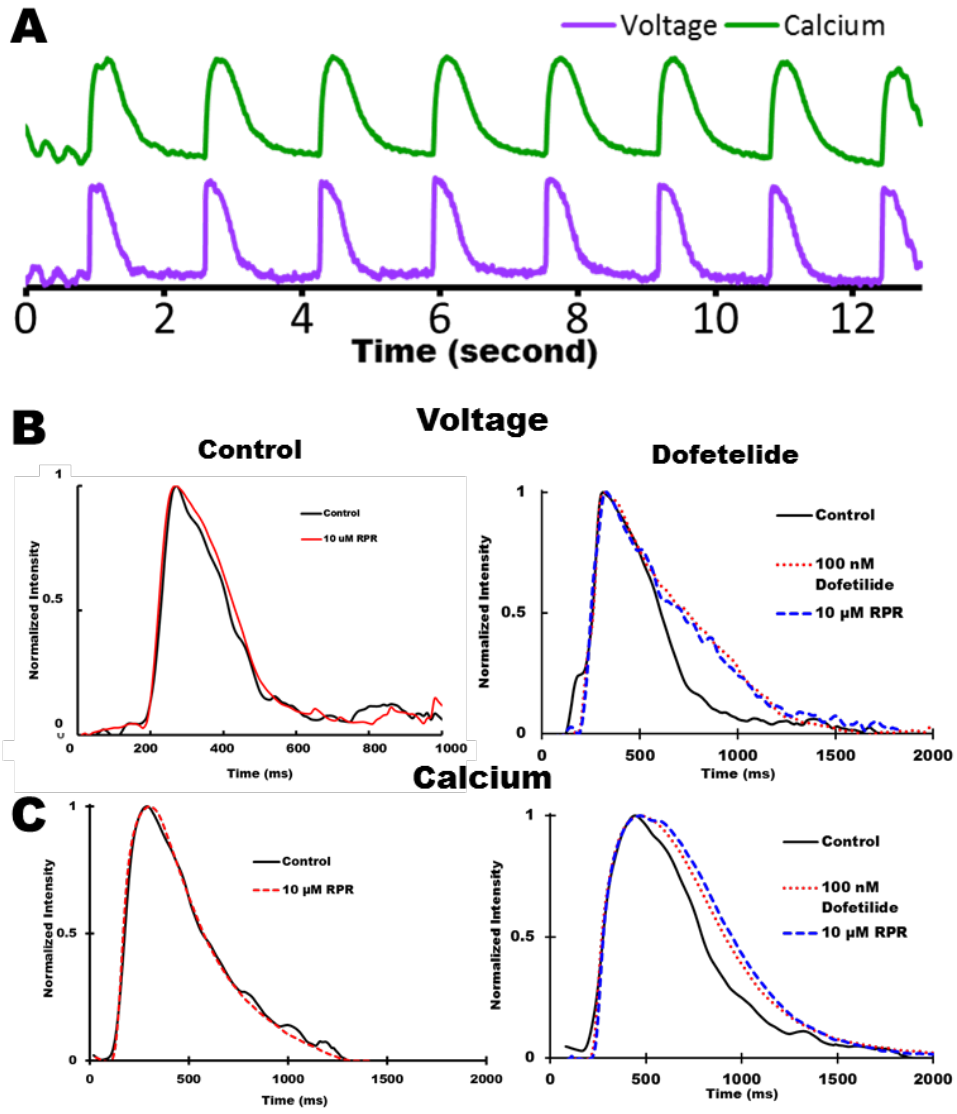

Figure 13: The effects of RPR under dofetilide block. A) Representative V_m and Ca^{2+} signals following a region of interest in hIPSC-CM monolayer **B)** Cumulative averages of action potentials constructed from a 20 s recording. Left, 10 µM RPR in the absence dofetilide. Right, 10 µM RPR in the presence of dofetilide. **C)** Cumulative averages of calcium transients. Same conditions as voltage.

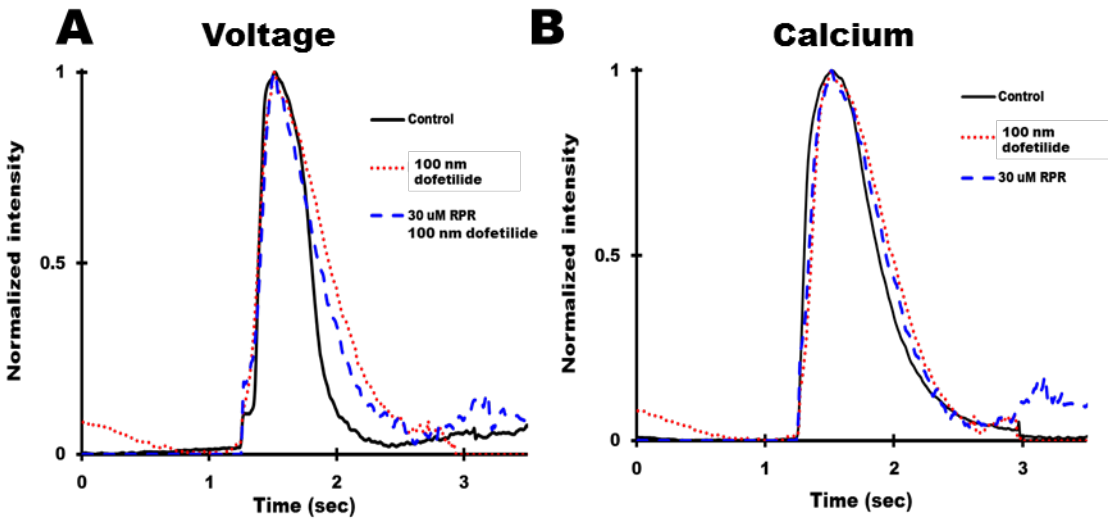

Figure 14: At a higher concentration, RPR partially rescues prolonged APD caused by dofetilide. Effect of 30 μM RPR on cumulative averages of action potentials **(A)** and calcium transients **(B)** following the application of dofetilide in WT monolayers.

3.2.2. In a model of inherited arrhythmia, RPR significantly reduces APD.

Genome editing a homozygous R56Q mutation in hiPSC-CMs

To understand the physiological role of fast deactivation, we wanted to express R56Q channels in their native physiological environment and avoid the potentially confounding influence overexpression. To this end, we performed genome editing in hiPSCs, using CRISPR-CAS9, in hiPSCs to introduce the R56Q mutation in hERG. Because the endonuclease activity of CAS9 requires a conserved sequence of three nucleotides (NGG) adjacent to the guide sequence (known as the protospacer adjacent motif, or PAM; Fig 15 and Fig B1, yellow), we also introduced a silent mutation in E58 (Fig 15). This was crucial in order to prevent CAS9 from re-binding to successfully modified sequences. We successfully introduced a G > A missense mutation in the hERG gene in hiPSCs in a homozygous manner (Fig 15). The predicted effect on the protein sequence is the mutation of the basic Arg56 residue to the polar glutamine residue. We also introduced a silent G > A mutation at position E58.

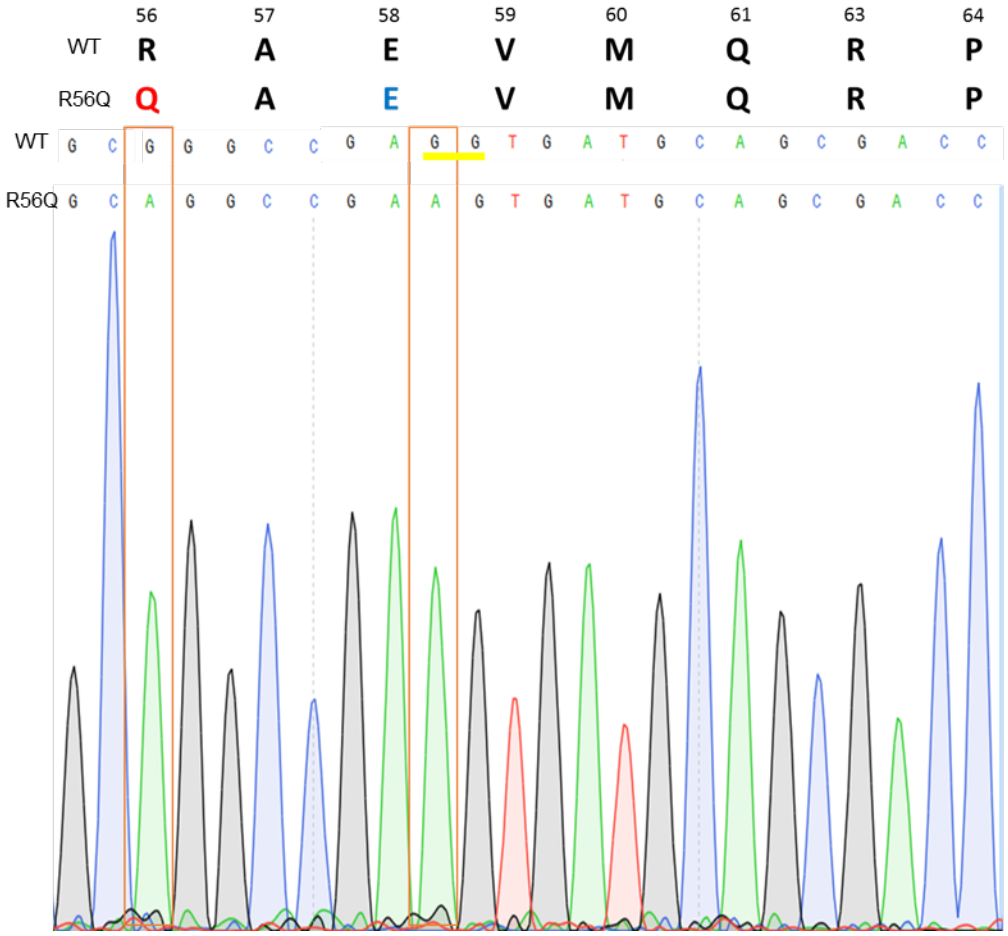

Figure 15: Sequencing data show successful genome edit of R56Q. Sanger sequencing demonstrates the presence of the R56Q homozygous mutations (G > A) as well as a silent mutation at E58 (G > A) engineered to disrupt the PAM sequence (yellow). The presence of two peaks (orange boxes) would represent a heterozygous mutation, while a respective single peak represents a homozygous mutation

Optical mapping of the hiPSC-CMs harboring the R56Q mutation shows that RPR shortens the APD.

Using the same approach as in our model of acquired arrhythmia, we investigated the effect of 10 µM and 30 µM RPR on a hiPSC-CM monolayer carrying the homozygous R56Q mutation. In control conditions, the APD_{80} of hiPSC-CMs $R56Q^{+/+}$ was 640 ms (Fig 16a), which was longer than that recorded from WT hiPSC-CMs, consistent with the effects of a loss of function of hERG channels. Following application of 10 µM RPR, the APD_{80} of hiPSC-CMs $R56Q^{+/+}$ was unexpectedly prolonged by 310 ms (Fig 16a). However, application of 30 µM RPR, significantly shortened the APD of these cells by 200 ms (Fig 16a). These effects were largely mirrored in the calcium signal. The CTD_{80} of hiPSC-CMs $R56Q^{+/+}$ was prolonged from 870 ms in control conditions to 1051 ms with 10 µM RPR. With 30 µM RPR, the CTD_{80} of these cells slightly shortened to 970 ms. We also observed a slight slowing of the upstroke with both concentrations of RPR hiPSC-CMs $R56Q^{+/+}$ (Fig 16b).

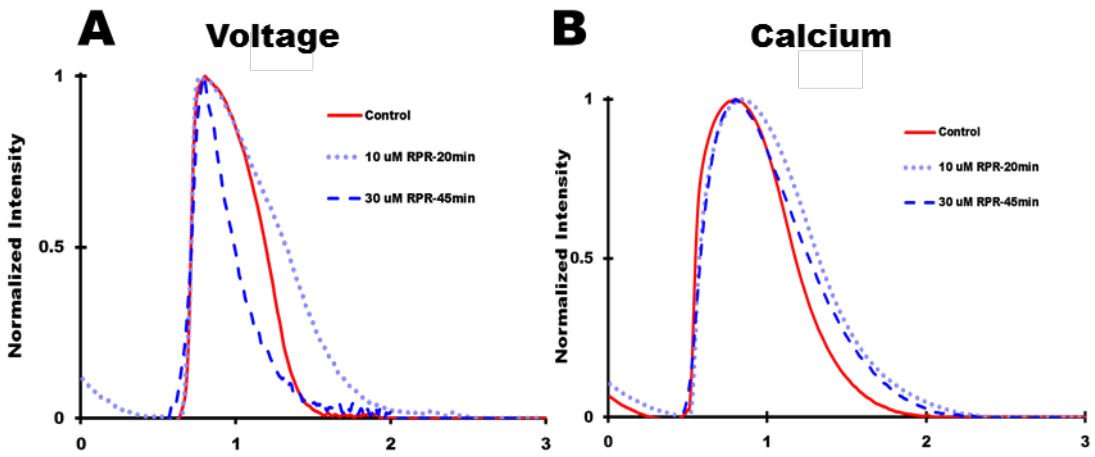

Figure 16: Optical mapping of R56Q hiPSC-CMs. Effect of 10 µM RPR (light blue dots) and 30 µM RPR (dark blue dash) on cumulative averages of action potentials **(A)** and calcium transients **(B)** in monolayers of hiPSC-CM $R56Q^{+/+}$.

Chapter 4. Discussion

4.1.1. Biophysical characterization of the effects of the R56Q mutation and RPR

R56Q accelerates deactivation while RPR slows deactivation. Neither R56Q nor RPR affect activation.

We showed that R56Q increases the rate of deactivation (Fig 7 C-D). As the deactivation kinetics of hERG are best fit with a double exponential function (Vandenberg, 2012), two (or more) separate mechanisms have been proposed to underlie the deactivation (Thouta et al., 2016). Interestingly, the contribution of τ_{fast} to the deactivation kinetics was relatively larger in R56Q channels compared to WT (Appendix: Fig B2a). As evidenced by the differences in mean τ_{fast} values between R56Q and WT channels (Fig 7d), R56Q profoundly accelerates deactivation in hERG (note the logarithmic scale). Interestingly, the R56Q mutation accelerates deactivation in a similar manner as does deleting the entire EAG domain (Thouta et al., 2016). In fact, mutations across the channel, such as the cNBHD (Gustina et al., 2011) can accelerate deactivation. Furthermore, co-expressing WT channels with R56Q does not slow deactivation. This suggests that mutations that accelerate deactivation are concerted, rather than additive. That is, it seems unlikely that each PAS domain is slightly slowing deactivation; instead slow deactivation requires full functional interactions between a full complement of PAS domains and the core of the channel. This idea was first developed by Tseng's group and it led them to suggest that a 'master' switch regulated slow deactivation (Liu, Zhang, Jiang, & Tseng, 2003). This idea is attractive and it further supports the notion that slow deactivation is a unique mechanism that may be a potential target for therapy.

We also assessed the effect of R56Q on the voltage-conductance (GV) relationships of activation and deactivation at physiological durations. We showed that, in R56Q channels, the voltage dependence of deactivation was profoundly affected, since we observed a 30 (1.9) mV shift in the mean $V_{1/2}$ of deactivation towards more depolarized potentials in R56Q channels ($p<0.0001$) (Fig 5f). We also showed that R56Q mutants had an increased voltage sensitivity during deactivation, compared to activation or WT deactivation (2.1 (0.5); $p=0.003$). As our group has shown previously, the conductance-voltage relationships of hERG at steady-state require test pulses greater than 15 s (Thouta

et al., 2016). Thus, since we constructed our GV relationships at physiological durations (i.e., non-steady-state), the $V_{1/2}$ of deactivation is directly affected by the kinetics of deactivation. Because R56Q channels deactivate much faster than WT channels, a greater proportion of the R56Q channels close compared to WT at a given time (Fig 7a). Therefore, when the test pulse is sufficiently short, the magnitude of tail currents for R56Q channels are much smaller with respect to deactivating voltages compared to WT channels, resulting in a right-ward shift of the voltage-conductance relationship. Indeed, if measured at the steady-state, the magnitude of this difference would be greatly reduced. Our group has shown that in hERG channels with a truncated N-terminus (Δ2-135 hERG accelerates deactivation to a similar degree as R56Q), the difference in $V_{1/2}$ for deactivation between WT and Δ2-135 channels at steady state is half of what it would be at physiological durations (Thouta et al., 2016). Thus, the large shift in the $V_{1/2}$ of deactivation can partly be explained by the accelerated deactivation kinetics of R56Q. The same line of reasoning can also explain the increased voltage sensitivity of the GV relationship of deactivation in hERG channels. In the same study, our group also showed that the voltage sensitivity increases with longer deactivating durations (and activating durations) (Thouta et al., 2016).

In contrast, the voltage dependence of activation was not affected by the R56Q mutation (Fig 5f). This is consistent with the two most recent studies that characterized R56Q (Berecki et al., 2005; Liu and Trudeau, 2015). Berecki et al. (2005) also noted a significant increase in the rate of activation in R56Q channels at 36°C but not at 23°C, again predicting a gain of function. This latter point is relevant as it demonstrates the importance of recording hERG current at physiological temperatures, and therefore represents one limitation of using *Xenopus* oocytes as a heterologous expression system (we recorded current at room temperature as their membranes degrade rapidly at higher temperatures) (Stuhmer & Parekh, 1995). Taken together, these results confirm that accelerated deactivation is the mechanism by which R56Q causes dysfunction in hERG.

As RPR introduces complex deactivation kinetics in hERG, it is not feasible to fit current decay with a double exponential function as in WT channels under control conditions (Perry et al., 2007). Instead, to test the effect of RPR, we constructed GV relationships in the presence and absence of 10 μM RPR. We reasoned that, at physiological durations, slowed deactivation would increase the tail currents (in the same way that R56Q decreases tail currents) and shift the GV relationship towards more

hyperpolarized potentials. In fact, for both WT (Fig 8c) and R56Q (Fig 9c) channels, we observed an increase in conductance with 10 µM RPR and the effect was particularly evident at more negative potentials. In WT channels, 10 µM RPR completely prevented their closing during the 750 ms deactivating pulse, even at very negative potentials (Fig 8c). Similarly, R56Q channels only closed completely at -110 mV. This suggests that RPR has a relatively small effect at more positive potentials where little deactivation occurs but it is effective at slowing the closure channels at more negative potentials. As a result of this inconsistent effect, the GV relationships of deactivation for WT and R56Q were not easily fitted with a Boltzmann, which explains our inability to show evidence for a mean shift in the $V_{1/2}$ of deactivation for R56Q channels (Fig 9c; Table A3). In fact, it is apparent that in the presence of RPR, the GV of deactivation no longer represents a sigmoidal relationship. We conclude that our calculated $V_{1/2}$ values are therefore most likely an underestimation of the effect of RPR in the conductance-voltage relationship.

We did not observe an effect of 10 µM RPR on the voltage dependence of activation, in either WT channels (p=0.67), or R56Q (p=0.23) (Fig 8b and Fig 9b; Table A2). This is consistent with some of the reported results from Kang et al. (2004) and Perry et al. (2007), at 10 µM. However, the latter group also tested 30 µM RPR and observed a 5.2 (0.8) mV shift towards more hyperpolarized potentials and a slight slowing of activation.

The effect of R56Q and RPR on inactivation in *Xenopus* oocytes

The R56Q mutation has been reported to shift the voltage dependence of steady-state inactivation towards more depolarized potentials, predicting a gain of function (Berecki et al., 2005; Chen et al., 1999; Liu and Trudeau, 2015). We did not find evidence that the mean $V_{1/2}$ of steady-state inactivation in R56Q differed from WT (p=0.96). In contrast, some mixed results have been reported with regards to the effect of RPR on steady-state inactivation. Perry et al. (2007) reported that 10 µM RPR caused a depolarizing shift in the steady-state inactivation, while Kang et al. (2004) found no effect. We did not find any evidence that 10 µM RPR shifted the mean $V_{1/2}$ of steady-state inactivation towards more depolarized potentials in WT channels p=0.99), nor in R56Q channels (p=0.27).

One possible reason for the difference in reports regarding steady-state inactivation is that several protocols can be used to measure steady-state inactivation. For

example, Kang et al. (2004) used a double-pulse protocol where channels were inactivated at +60 mV and then the potentials were stepped from -110 mV to +40 mV to measure the recovery from inactivation. One issue with this method is that, at more negative potentials, where deactivation is fastest (Fig 7e), some channels have already closed by the time they are fully recovered (Vandenberg et al., 2012). Therefore, this method underestimates the extent of recovery from inactivation at more negative potentials. On the other hand, Perry et al. (2007) used the rectification method (as did we) where the current-voltage relationship for a double-pulse protocol is used to calculate the deviation from linearity as channels inactivate (Fig 8d inset and Fig 9d inset). Another method, termed 'the extrapolation method' uses the same principle as the rectification method, except the current at each voltage is fitted with a double exponential function and extrapolated back to the start of the second pulse. This is done to account for some deactivation that, at more negative potentials, has already taken place by the time channels fully recover (Vandenberg, 2012). These differences can be particularly important in cases that perturb the deactivation kinetics, as is the case with R56Q and RPR. One problem with both 'rectification' methods is that the linear fit that is used to calculate the deviation from linearity (or rectification) is derived by fitting only 3 or 4 values towards more hyperpolarized potentials. Consequently, even the presence of small endogenous currents may introduce large errors in the rectification factor (Table A4).

Limitations: *Xenopus* oocytes as a non-mammalian heterologous expression system

There are several well-known limitations associated with using Xenopus oocytes. First, as they are a heterologous expression system, the limitations that I associated with heterologous expression systems in general (section 1.3) are still applicable. Namely, hERG is grossly over-expressed without its native subunits, splice variants or post-translational modification that are known to affect its function (Choe et al., 2006; Stuhmer & Parekh, 1995). Also as a growing body of evidence is showing, dysregulation in complex gene-regulatory networks specific to cardiac cells can influence and/or cause cardiac arrhythmia (Nadadur et al., 2016). These interactions are impossible to account for within a single celled, non-mammalian heterologous expression system. Furthermore, as it has been shown that trafficking-defective hERG mutants can be rescued by expression at lower temperatures, and considering that we incubated our oocytes at 19° C, our TEVC experiments cannot account for differences in trafficking between WT and R56Q channels

(Zhou et al., 1999). Indeed, if R56Q was a trafficking-deficient mutation, our biophysical assessment would be of limited value as we cannot control expression levels. However, current density measurements by Berrecki et al. (2005) provide good evidence that R56Q is expressed on the membrane to a similar degree as WT channels. In the context of drug studies, the application of oocytes is limited as the large size of their yolk sac necessitates a much higher concentration of drugs to achieve the same effect seen in mammalian cells: for example, the inhibitory effect of methanesulfonanilides on hERG channels was initially missed as these studies used small concentrations of these drugs (Sanguinetti et al., 1995). Another limitation of using oocytes as an expression system that the composition of the oocyte membrane is different than that of mammalian cells (Kleckner & Dingledine, 1998). This might important in the context of hERG studies as there is evidence that components of the membrane (such the phospholipid, phosphatidyl 4,5 bisphosphate) can directly modulate hERG function in the context of adrenergic stimulation (Bian, Cui & McDonald, 2001). Finally, as cardiac arrhythmia reflects a multi-cellular event, extrapolating conclusions from experiments of one type of channel, expressed in a single cell is difficult, particularly if a drug, like RPR, has multiple targets (Kang et al., 2004). Nevertheless, the large size of oocytes, their ability to express a large amount of exogenous protein and the relative absence of endogenous currents, make them a powerful tool for electrophysiological assessment. Furthermore, voltage clamp experiments with hERG-expressing oocytes, provide robust and reproducible data relatively quickly as they can be impaled with large, low resistance recording micropipettes that provide good voltage control (Wagner & Bröer, 2000; Stuhmer & Parekh, 1995). Thus, the TEVC technique in Xenopus oocytes provides an excellent opportunity to study the biophysical effects of R56Q and RPR in hERG in isolation. Finally, when TECV is paired with an additional physiological assessment of hERG function (in our case iPSC-CMs), many of these limitations are minimized and conclusions gleaned from experiments in one system can be tested in the other.

4.1.2. The role of hERG deactivation kinetics in determining APD

Although we did not detect a depolarized shift in the steady-state inactivation of R56Q channels, the presence of this effect would explain our observation of the seemingly paradoxical increase in mean resurgent current in R56Q channels compared to WT channels (Fig 10). Nevertheless, in our hiPSC-CMs R56Q$^{+/+}$, we observed slight

prolongation in the APD compared to WT (Fig 13b and Fig 16a). Indeed, both of these seemingly contradictory observations are consistent with published findings. Although neither Berrecki et al. (2005) nor Liu and Trudeau (2015) quantified the total charge moved by hERG channels during phase 3, their current traces imply that R56Q represents a larger amount of charge moved compared to WT. Also, both studies noted an acceleration in the decay of R56Q resurgent current late in phase 3, though under voltage clamp (i.e., when both AP protocols used to test WT and R56Q channels are identical), these differences are slight. Of course, as membrane potential and membrane currents represent an interdependent feedback system, testing both WT and R56Q channels under the same AP protocol is a slight simplification. Using the dynamic action potential technique (without voltage clamp), Berrecki et al. (2005) showed a prolongation of APD_{90} by about 50 ms at 1 Hz pacing rate in R56Q channels. In any case, these differences were only detected at slower rates (e.g., 0.5 and 1 Hz). One reason for is that at slower heart rates, the AP is prolonged compared to higher heart rates, when APD is shortened to facilitate faster contractions without tetany (Wu & Patwardhan, 2004). With a longer APD (and thus longer phase 3), more R56Q channels close (relative to WT channels), which can be a reinforcing effect: as R56Q channels close, repolarization is further prolonged, allowing even more channels to close. Thus, mutations in hERG may cause dysfunction by accelerating deactivation only by prolonging the APD when it is already relatively long (i.e., at slower heart rates). This suggests that mutations that accelerate deactivation would likely cause arrhythmia at slower heart rates. Although little clinical data is available with respect to mutations that specifically accelerate deactivation, this is consistent with the clinical data regarding LQT II pathogenesis in general. Indeed, the incidence of arrhythmia in LQT II patients has been observed to be higher when the heart rate rapidly accelerates from a slow initial rate. For example, during sudden auditory stimulus when a patient's heart rate rapidly increases from rest (like during a morning alarm for example), LQT II patients are more likely to develop arrhythmia than LQT I patients (Wilde et al., 1999). This is because at slower heart rates, I_{Kr} is the main repolarizing current, while I_{Ks} becomes relatively more important for cardiac repolarization at faster rates (Nakagawa et al., 2009). Furthermore, as heart rate increases, the magnitude of depolarizing currents (such as L-type) increases faster than what can be compensated by I_{Ks} (Liu et al., 2012). In the case of the rapidly deactivating mutants, this may represent a perfect storm. As the APD might already be prolonged at low heart rates, a sudden increase in depolarizing currents without a corresponding increase in I_{Ks} would only prolong the APD further, giving even more time

for mutant channels to deactivate further. This agrees with our observations that the integral of the resurgent current is increased in R56Q channels under voltage clamp, while the APD of hiPSC-CMs R56Q$^{+/+}$ is prolonged. This model may also explain the incidence of arrhythmia associated with mutations in the N-terminus (many of which accelerate deactivation) even though the resurgent current appears to be little affected (Moss et al., 2002).

This line of reasoning can be used to explain our observation that RPR shortens the action potential in monolayers with prolonged APD due to dofetilide block. When we applied either 10 µM RPR (Fig 13b, right) or 30 µM RPR to WT hiPSC-CM monolayers, we did not observe any change in the APD. However, when we applied 30 µM RPR in the presence of 100 nM dofetilide, we observed a significant shortening of the APD (Fig 14a). In contrast to the action of the R56Q mutation, RPR slows hERG channel deactivation. Thus, by the same principle, we suggest that if the cardiac action potential is first prolonged as a result of dofetilide block, more current is passed with RPR as it has more time to increase current; and therefore, the action potential is shortened.

In summary, we have shown that accelerated deactivation prolongs the APD, while slowed deactivation shortens the APD. We note that, in the case of hiPSC-CMs R56Q$^{+/+}$, this prolongation is quite modest, but may become more important during periods of low repolarization reserve. In the case of RPR, the effect was only seen at the highest concentrations (30 µM) and only in instances of prolonged APD (dofetilide).

4.1.3. Mode of action of RPR in a model of acquired LQT II

Although we suggest that the effect of RPR is only apparent under dofetilide block when the APD is prolonged, we cannot exclude two other scenarios in which RPR may shorten APD in the presence of dofetilide; namely, that RPR is an allosteric activator that displaces dofetilide by causing a conformational change in hERG, or secondly, that the shortening of the APD is a product of RPR inhibition of L-type Ca^{2+} channels. With respect to the first scenario, LUF7346 and ML-T531 have both been shown to be allosteric activators in hERG as they shorten the APD in both models of acquired and inherited LQT II (Sala et al., 2016). Like RPR, both ML-T531 and LUF7346 also slow deactivation and decrease inactivation (depolarizing shift in steady-state inactivation) (Sala et al., 2016; Zhang et al., 2012). Using a radiological binding assay, these compounds were

demonstrated to be negative allosteric regulators of dofetilide; that is, they cause a conformational change in hERG that decreases the binding affinity of dofetilide. Both LUF7346 and ML-T531 were shown to increase the dissociation of dofetilide from hERG, but with a different stoichiometry than expected if they competed for the same binding site as dofetilide (Yu et al., 2016). It is interesting that both of these allosteric inhibitors of dofetilide shift the voltage dependence of inactivation towards more depolarized potentials (as does RPR). One interesting connection that the authors did not discuss is the correlation between inactivation and dofetilide block. Blockers (like dofetilide) have been shown to preferentially bind to the inactivated state of the hERG channel since mutations that decrease inactivation (e.g., S620T) also decrease the sensitivity of hERG to blockers (Lees-Miller et al., 2000). Therefore, we suggest that these drugs may reduce dofetilide block through their effect on inactivation. As RPR shares many functional similarities with these allosteric activators (i.e., slowed deactivation and decreased inactivation), we propose that RPR may also be an allosteric activator. This would explain its ability to shorten the APD in the presence of dofetilide, but not in control conditions (Fig 13b and Fig 14a).

Finally, because we observed the shortening of APD at 30 μM RPR, a concentration that has been shown to block L-type Ca^{2+} channels $Ca_V1.2$ by about 30% at 0 mV (Kang et al., 2004), we cannot rule out that inhibition of the L-type current is the mechanism by which RPR shortens the APD in the presence of dofetilide. This is consistent with our observation that the calcium transient duration (CTD) is also shortened after the addition of 30 μM RPR in the presence of dofetilide (Fig 14b). It is also interesting that we did not observe an effect of 30 μM RPR in isolation. This suggests that L-type Ca^{2+} channels are somehow more sensitive to block by RPR during longer durations. Of note, the off-target effect of RPR on L-type might prove anti-arrhythmic since blocking L-type Ca^{+} has been shown to reduce the incidence of EADs caused by hERG dysfunction (Spencer et al., 2014).

In summary, the mechanism by which RPR shortens the APD in the presence of dofetilide is not clear. Nevertheless, the partial rescue of hiPSC-CMs under dofetilide block is promising since many potentially useful drugs never make it past phase II clinical trials due to their propensity to block hERG. Thus, RPR has the potential to act as a therapeutic treatment for aLQT.

4.1.4. Genome-edited hiPSC-CMs as a model of inherited arrhythmia due to accelerated deactivation

Genome editing of homozygous R56Q

To create a more translatable model to describe the pathogenicity of fast deactivation, we wanted to express the R56Q mutation in functional cardiomyocytes that could be studied at the tissue level. We also wanted to express the mutation in a human cardiomyocyte native genetic environment to avoid confounding factors associated with overexpression. To do this, we performed genome editing using CRISPR-Cas9 (Fig B1). When we designed, our genome editing strategy, our primary consideration was to maximize the rate of the high-fidelity mechanism of homology-directed repair (HDR) required for the introduction of the point mutations. This was mainly in response to reports demonstrating the rate of HDR to be as low as 1% in hiPSCs, partly because of the low transfection rates (Miyaoka et al., 2014). To improve this, we enriched the number of transfected cells, by employing FACS that selected only GFP^+ cells (and therefore, expressing CAS-9). Furthermore, we used a single-stranded, asymmetric oligonucleotide template (with respect to the cut site) as it has been shown to increase HDR rates four-fold (Fig B1) (Richardson, Ray, DeWitt, Curie, & Corn, 2016). As a testament to our efforts, we noted a much higher rate of HDR compared to previous studies. We obtained 3 homozygous R56Q colonies. The presence of only homozygous colonies was surprising, since we expected the chances of homozygous mutations to be much lower than heterozygous mutations. One possible reason for this is that we placed the cut site of the CRISPR in close proximity to our intended mutation site (again, to maximize HDR). While this approach indeed increases HDR, it also increases the chance of homozygous mutations (Paquet et al., 2016). This may explain our surprisingly high rate of HDR and homozygous mutants.

RPR in a model of inherited arrhythmia due to fast deactivation

While we were able to obtain beating cells from each of the mutated colonies, we were only able to perform successful optical mapping experiments on one hiPSC-CM $R56Q^{+/+}$ colony. Thus, we do not have a measure of variability between colonies. This is unfortunate as the variability between hiPSC-CMs colonies (both intra- and inter-laboratory) is well documented and represents a general limitation of hiPSC-CMs in the study of cardiac disease (Hwang et al., 2015). In the context of our results, our inability to

attain a measure of variability represents a clear limitation of our study and tempers our conclusions. Therefore, to make stronger conclusions, we would require more data. There is, however, one caveat. Unlike in single cell studies, we employed optical mapping techniques that track voltage and calcium signals from regions of interest (Fig 5f, coloured boxes). Thus, the voltage signals and calcium signals acquired from these regions are already averages of several thousand cardiomyocytes. Nevertheless, we cannot account for differences between colonies that might have been introduced through the genome editing process (e.g., off-target mutations). While further study is needed to explore this more fully, the data from our current experiments provides some novel insight into the mechanism of inherited arrhythmia caused by accelerated deactivation of hERG channels.

Consistent with our hypothesis, we observed a prolongation of the APD by 100 ms in our R56Q$^{+/+}$ monolayer compared to WT monolayers. The magnitude of this effect is consistent with published results (Berecki et al., 2005; Liu and Trudeau, 2016). Contrary to our hypothesis, 10 µM RPR prolonged both the APD and CTD (Fig 16), which is difficult to explain. It also reflects the challenge in interpreting a measure (namely, APD) that is dependent on many interrelated currents and other factors. For example, one consequence of the relative immaturity of hiPSC-CMs is that their expression of I_{K1} current is reduced and so the maximum diastolic potential (MDP) is depolarized. As a result, the MDP in hiPSC-CMs is highly dependent on I_{Kr} (Doss et al., 2012). Therefore, the addition of 10 µM RPR may increase the diastolic hERG current and cause a more hyperpolarized MDP. This suggestion is consistent with the effects of LUF7346, an allosteric activator of hERG, which has a similar effect to RPR, and which has been shown to hyperpolarize the MDP (Sala et al., 2016). The effects of changing MDP is difficult to predict, especially in optical mapping experiments where we can only indirectly infer such changes. For example, one of the consequences of a more hyperpolarized MDP in hiPSC-CMs is an increase in I_{CaL} and I_{Na} as a result of reduced inactivation (Liu, Laksman and Bakx, 2016). Whether or not increased I_{Na} is the cause of the prolongation under 10 µM RPR (we saw no such effect in WT) is difficult to say, though this example illustrates one limitation of our optical mapping approach. Using our potentiometric dye, RH-237, we can only measure relative changes in membrane potential. Furthermore, as voltage-sensitive dyes exhibit their own activation kinetics, fluorescence measurements are too slow to measure upstroke velocity of the action potential. As a result, complex changes affecting multiple

parameters (e.g. RMP, upstroke velocity, maximum depolarizing potential and APD) are difficult to resolve.

In contrast to the effects of 10 µM RPR on hiPSC-CMs R56Q$^{+/+}$ monolayers, 30 µM of RPR shortened the APD_{80} of R56Q$^{+/+}$ monolayers by 200 ms, representing an almost complete rescue (Fig 16a). Nevertheless, 30 µM only partially shortened the CTD compared to 10 µM and the CTD was still prolonged relative to the control. Again, a number of mechanisms could explain the shortening. First, since the APD of R56Q cells is prolonged as a result of accelerated deactivation, RPR may reverse this effect by slowing deactivation, thereby restoring normal APD. Although we did not test 30 µM RPR in oocytes, we found that 10 µM RPR did not fully rescue R56Q channels (as measured by GV relationships) in oocytes. Therefore, we suggest that 30 µM RPR probably does not fully revert accelerated in deactivation seen in R56Q channels (Fig7f and Fig 9c). Second, as 30 µM RPR has been shown to decrease the L-type Ca^{2+} current (Kang et al., 2004), this decrease may lead to a shorter APD. Finally, as both R56Q and RPR have been shown to decrease inactivation, these effects may be additive so that the decreased inactivation leads to an increased resurgent current to the extent that the APD is shortened. This is consistent with our observation that both the R56Q mutation and 10 µM RPR increased the resurgent current compared to WT (Fig 10b). Because we only tested 10 µM RPR, we expect these effects to be even larger at 30 µM. We conclude that a combination of all three mechanisms may cause the rescue of the APD in our model of inherited arrhythmia as a result of accelerated deactivation.

4.1.5. Emerging role of hERG channels in providing a protective current: Future directions

As noted earlier, R56Q caused only a slight prolongation of the APD (Fig 16), which is consistent with published findings (Berecki et al., 2005; Liu and Trudeau, 2016). By comparison, dofetilide prolonged APD_{80} by 340 ms in WT hiPSC-CMs. Thus, it is difficult to reconcile that these two effects: both the R56Q mutation and dofetilide cause arrhythmia, yet the magnitudes of their respective effects on APD are very different.

In stark contrast to the relatively small effects we have described, the effect of R56Q on protective current is profound. For example, in contrast to a prolongation of 20% or 30% in the APD_{80} of our R56Q monolayers (Fig 16a), or the R56Q rabbit myocytes of

Berecki et al. (2005), the reduction in PPC_{max} is close to 70% (Fig 11f; Fig 12). Furthermore, within 100 ms after the termination of the action potential ramp, R56Q channels show an almost complete abolishment of the protective current (Fig 11f). In light of these differences in the effect sizes, we propose that loss of protective current is an important mechanism by which R56Q causes a loss of function.

The importance of the hERG protective current has been proposed several times. For example, Perry et al. (2016) recently demonstrated that almost half of their trafficking-rescued mutants showed decreased levels of protective current (Perry et al., 2016). Furthermore, Du et al. (2010) used *in silico* AP modeling to show that acidosis accelerates deactivation, with a decrease in protective current increasing the susceptibility of model cells to premature stimulation (Du et al., 2010). Indeed, the timing of the maximal protective hERG current (i.e., 20 ms after termination of the AP) makes it uniquely suited to suppress EADs. As described in Section 1.1.3, EADs provide the mechanistic link between hERG dysfunction and arrhythmia. Therefore, an acceleration in deactivation (or any loss of function mutations) might represent a double hit: increased propensity for EAD formation without the dampening effect of the protective current.

To date, all of the descriptions regarding the peak (including ours) have only shown that it is affected, but to our knowledge, no-one has yet to establish a definite link between loss of protective current and arrhythmia. Therefore, we suggest that our model of LQT II is uniquely suited to test this hypothesis since the effect on APD is small and the effect on the protective current is large. The hypothesis can be tested by applying an S1-S2 stimulation paradigm (as we mimicked with the premature stimulation protocol in oocytes) to R56Q hiPSC-CM monolayers to determine the effect of accelerated/slowed deactivation on the effective refractory period (ERP) (Strobel et al., 1990). We suppose that R56Q decreases the ERP and then decreases the protective current, which would be present despite the expected increases in ERP that are normally associated with prolonged APD (Morgan, Cunningham, & Rowland, 1990). Furthermore, an S1-S2 stimulation protocol would also allow us to observe the effect of accelerated/slowed deactivation on the restitution of the action potential (Wu and Patwardhan, 2004). This would allow us to test whether or not R56Q prolongs the APD to a greater degree during the transition from slow to fast heart rates (as we suggested in Section 4.1.2). If this is the case, we would expect a shallower relationship between the diastolic interval and APD at longer diastolic

intervals. Interestingly, a shallower relationship between APD and diastolic intervals has been suggested to be arrhythmogenic (Franz, 2003).

Finally, it would be interesting to test the mechanism by which RPR partially rescues acquired arrhythmia. If we draw parallels between RPR and LUF7346 (see Section 4.1.3), RPR may be a negative allosteric modulator of dofetilide block. Although a radiological binding assay would give the strongest evidence (based on rates of dissociation), a good starting point would be to test whether or not RPR decreases the IC_{50} of dofetilide in a heterologous expression system. If an effect can be demonstrated, it would suggest inhibition. It would also be interesting to see the effect of RPR at a saturating concentration of dofetilide. If the rescue of acquired LQT by RPR primarily involves the activation of functional hERG channels (as opposed to blocked), then we would not expect to see an increase in current. If, however, RPR is in fact an inhibitor (allosteric or otherwise), we would expect to see an increase in the hERG current under saturating concentrations of RPR. Finally, it would be interesting to test whether or not allosteric activators of hERG (e.g., LUF7346) inhibit dofetilide binding through their action on inactivation (Section 4.1.3).

References

Anderson, C. L., Delisle, B. P., Anson, B. D., Kilby, J. A., Will, M. L., Tester, D. J., … January, C. T. (2006). Most LQT2 Mutations Reduce Kv11.1 (hERG) Current by a Class 2 (Trafficking-Deficient) Mechanism. *Circulation*, *113*(3). Retrieved from http://circ.ahajournals.org/content/113/3/365.long

Anderson, C. L., Kuzmicki, C. E., Childs, R. R., Hintz, C. J., Delisle, B. P., & January, C. T. (2014). Large-scale mutational analysis of Kv11.1 reveals molecular insights into type 2 long QT syndrome. *Nature Communications*, *5*, 5535. http://doi.org/10.1038/ncomms6535

Asano, Y., Davidenko, J. M., Baxter, W. T., Gray, R. A., & Jalife, J. (1997). Optical Mapping of Drug-Induced Polymorphic Arrhythmias and Torsade de Pointes in the Isolated Rabbit Heart. *Journal of the American College of Cardiology*, *29*(4), 831–842. http://doi.org/10.1016/S0735-1097(96)00588-8

Balijepalli, S. Y., Lim, E., Concannon, S. P., Chew, C. L., Holzem, K. E., Tester, D. J., … January, C. T. (2012). Mechanism of Loss of Kv11.1 K+ Current in Mutant T421M-Kv11.1–Expressing Rat Ventricular MyocytesClinical Perspective. *Circulation*, *126*(24). Retrieved from http://circ.ahajournals.org/content/126/24/2809

Baudenbacher, F., Schober, T., Pinto, J. R., Sidorov, V. Y., Hilliard, F., Solaro, R. J., … Knollmann, B. C. (2008). Myofilament Ca2+ sensitization causes susceptibility to cardiac arrhythmia in mice. *The Journal of Clinical Investigation*, *118*(12), 3893–903. http://doi.org/10.1172/JCI36642

Berecki, G., Zegers, J. G., Verkerk, A. O., Bhuiyan, Z. A., de Jonge, B., Veldkamp, M. W., … January, C. T. (2005). HERG channel (dys)function revealed by dynamic action potential clamp technique. *Biophysical Journal*, *88*(1), 566–78. http://doi.org/10.1529/biophysj.104.047290

Berjukow, S., Doring, F., Froschmayr, M., Grabner, M., Glossmann, H., & Hering, S. (1996). Endogenous calcium channels in human embryonic kidney (HEK293) cells. *British Journal of Pharmacology*, *118*(3), 748–754. http://doi.org/10.1111/j.1476-5381.1996.tb15463.x

Bian, J., Cui, J., & McDonald, T. V. (2001). HERG K(+) channel activity is regulated by changes in phosphatidyl inositol 4,5-bisphosphate. Circulation Research, 89(12), 1168–76. Retrieved from http://www.ncbi.nlm.nih.gov/pubmed/11739282

Bibikova, M., Golic, M., Golic, K. G., & Carroll, D. (2002). Targeted chromosomal cleavage and mutagenesis in Drosophila using zinc-finger nucleases. *Genetics*, *161*(3), 1169–75. Retrieved from http://www.ncbi.nlm.nih.gov/pubmed/12136019

Bobadilla, J. L., Macek, M., Fine, J. P., & Farrell, P. M. (2002). Cystic fibrosis: A worldwide analysis ofCFTR mutations: correlation with incidence data and application to screening. *Human Mutation*, *19*(6), 575–606. http://doi.org/10.1002/humu.10041

Bosman, A., Sartiani, L., Spinelli, V., Del Lungo, M., Stillitano, F., Nosi, D., … Jaconi, M. (2013). Molecular and Functional Evidence of HCN4 and Caveolin-3 Interaction During Cardiomyocyte Differentiation from Human Embryonic Stem Cells. *Stem Cells and Development*, *22*(11), 1717–1727. http://doi.org/10.1089/scd.2012.0247

Burridge, P. W., Li, Y. F., Matsa, E., Wu, H., Ong, S.-G., Sharma, A., … Wu, J. C. (2016). Human induced pluripotent stem cell-derived cardiomyocytes recapitulate the predilection of breast cancer patients to doxorubicin-induced cardiotoxicity. *Nat Med*, *22*(5), 547–556. Retrieved from http://dx.doi.org/10.1038/nm.4087

Cabral, J. H. M., Lee, A., Cohen, S. L., Chait, B. T., Li, M., & Mackinnon, R. (1998). Crystal Structure and Functional Analysis of the HERG Potassium Channel N Terminus: A Eukaryotic PAS Domain. *Cell*, *95*(5), 649–655. http://doi.org/10.1016/S0092-8674(00)81635-9

Caspi, O., Itzhaki, I., Kehat, I., Gepstein, A., Arbel, G., Huber, I., … Gepstein, L. (2009). In vitro electrophysiological drug testing using human embryonic stem cell derived cardiomyocytes. *Stem Cells and Development*, *18*(1), 161–172. http://doi.org/10.1089/scd.2007.0280

Cecile Terrenoire, Kai Wang, Kelvin W. Chan Tung, Wendy K. Chung, R. H. P., Jonathan T. Lu, Jyh-Chang Jean, … and Robert S. Kass. (2012). Induced pluripotent stem cells used to reveal drug actions in a long QT syndrome family with complex genetics. *The Journal of General Physiology*, *141*(1), 61–72.

Chang, Y.-F., Imam, J. S., & Wilkinson, M. F. (2007). The Nonsense-Mediated Decay RNA Surveillance Pathway. *Annual Review of Biochemistry*, *76*(1), 51–74. http://doi.org/10.1146/annurev.biochem.76.050106.093909

Chen, F., Pruett-Miller, S. M., Huang, Y., Gjoka, M., Duda, K., Taunton, J., … Davis, G. D. (2011). High-frequency genome editing using ssDNA oligonucleotides with zinc-finger nucleases. *Nature Methods*, *8*(9), 753–755. http://doi.org/10.1038/nmeth.1653

Chen, I. Y., Matsa, E., & Wu, J. C. (2016). Induced pluripotent stem cells: at the heart of cardiovascular precision medicine. *Nat Rev Cardiol*, *13*(6), 333–349. Retrieved from http://dx.doi.org/10.1038/nrcardio.2016.36

Chen, J., Zou, A., Splawski, I., Keating, M. T., & Sanguinetti, M. C. (1999). Long QT Syndrome-associated Mutations in the Per-Arnt-Sim (PAS) Domain of HERG Potassium Channels Accelerate Channel Deactivation. *Journal of Biological Chemistry*, *274*(15), 10113–10118. http://doi.org/10.1074/jbc.274.15.10113

Chiesa, N., Rosati, B., Arcangeli, A., Olivotto, M., & Wanke, E. (1997). A Novel Role for HERG K $^{+}$ Channels: Spike-Frequency Adaptation. *The Journal of Physiology*, *501*(2), 313–318. http://doi.org/10.1111/j.1469-7793.1997.313bn.x

Choe, C. U., Schulze-Bahr, E., Neu, A., Xu, J., Zhu, Z. I., Sauter, K., … Isbrandt, D. (2006). C-terminal HERG (LQT2) mutations disrupt IKr channel regulation through 14-3-3ε *Human Molecular Genetics*, *15*(19), 2888–2902. http://doi.org/10.1093/hmg/ddl230

Chong, J. J. H., Yang, X., Don, C. W., Minami, E., Liu, Y.-W., Weyers, J. J., … Murry, C. E. (2014). Human embryonic-stem-cell-derived cardiomyocytes regenerate non-human primate hearts. *Nature*, *510*(7504), 273–277. http://doi.org/10.1038/nature13233

Coronel, R., Wilms-Schopman, F. J. G., Opthof, T., & Janse, M. J. (2009). Dispersion of repolarization and arrhythmogenesis. *Heart Rhythm*, *6*(4), 537–543. http://doi.org/10.1016/j.hrthm.2009.01.013

Crotti, L., Lundquist, A. L., Insolia, R., Pedrazzini, M., Ferrandi, C., De Ferrari, G. M., … Schwartz, P. J. (2005). KCNH2-K897T Is a Genetic Modifier of Latent Congenital Long-QT Syndrome. *Circulation*, *112*(9). Retrieved from http://circ.ahajournals.org/content/112/9/1251.short

Curran, M. E., Splawski, I., Timothy, K. W., Vincent, G. M., Green, E. D., & Keating, M. T. (1995). A molecular basis for cardiac arrhythmia: HERG mutations cause long QT syndrome. *Cell*, *80*(5), 795–803. Retrieved from http://www.ncbi.nlm.nih.gov/pubmed/7889573

de la Peña, P., Alonso-Ron, C., Machín, A., Fernández-Trillo, J., Carretero, L., Domínguez, P., & Barros, F. (2011). Demonstration of physical proximity between the N terminus and the S4-S5 linker of the human ether-a-go-go-related gene (hERG) potassium channel. *The Journal of Biological Chemistry*, *286*(21), 19065–75. http://doi.org/10.1074/jbc.M111.238899

Doench, J. G., Fusi, N., Sullender, M., Hegde, M., Vaimberg, E. W., Donovan, K. F., … Root, D. E. (2016). Optimized sgRNA design to maximize activity and minimize off-target effects of CRISPR-Cas9. *Nature Biotechnology*, *34*(2), 184–191. http://doi.org/10.1038/nbt.3437

Doss, M. X., Di Diego, J. M., Goodrow, R. J., Wu, Y., Cordeiro, J. M., Nesterenko, V. V., … Antzelevitch, C. (2012). Maximum Diastolic Potential of Human Induced Pluripotent Stem Cell-Derived Cardiomyocytes Depends Critically on IKr. *PLoS ONE*, *7*(7), e40288. http://doi.org/10.1371/journal.pone.0040288

Du, C. Y., Adeniran, I., Cheng, H., Zhang, Y. H., El Harchi, A., McPate, M. J., … Hancox, J. C. (2010). Acidosis Impairs the Protective Role of hERG K+ Channels Against Premature Stimulation. *Journal of Cardiovascular Electrophysiology*, *21*(10), 1160–1169. http://doi.org/10.1111/j.1540-8167.2010.01772.x

Duygu, B., Poels, E. M., & Costa Martins, P. A. da. (2013). Genetics and epigenetics of arrhythmia and heart failure. *Frontiers in Genetics*, *4*, 219. http://doi.org/10.3389/fgene.2013.00219

el-Sherif, N. (1991). Early afterdepolarizations and arrhythmogenesis. Experimental and clinical aspects. *Archives Des Maladies Du Coeur et Des Vaisseaux*, *84*(2), 227–34. Retrieved from http://www.ncbi.nlm.nih.gov/pubmed/1708655

Es-Salah-Lamoureux, Z., Xiong, P. Y., Goodchild, S. J., Ahern, C. A., & Fedida, D. (2011). Blockade of permeation by potassium but normal gating of the G628S nonconducting hERG channel mutant. *Biophysical Journal*, *101*(3), 662–70. http://doi.org/10.1016/j.bpj.2011.06.028

Fabritz, L., Kirchhof, P., Franz, M. R., Eckardt, L., Mannig, G., Milberg, P., … Haverkamp, W. (2003). Prolonged action potential durations, increased dispersion of repolarization, and polymorphic ventricular tachycardia in a mouse model of proarrhythmia. *Basic Research in Cardiology*, *98*(1), 25–32. http://doi.org/10.1007/s00395-003-0386-y

Farrelly, A. M., Ro, S., Callaghan, B. P., Khoyi, M. A., Fleming, N., Horowitz, B., … Keef, K. D. (2003). Expression and function of KCNH2 (HERG) in the human jejunum. *American Journal of Physiology - Gastrointestinal and Liver Physiology*, *284*(6), G883–G895. http://doi.org/10.1152/ajpgi.00394.2002

Ficker, E., Dennis, A. T., Wang, L., & Brown, A. M. (2003). Role of the Cytosolic Chaperones Hsp70 and Hsp90 in Maturation of the Cardiac Potassium Channel hERG. *Circulation Research*, *92*(12). Retrieved from http://circres.ahajournals.org/content/92/12/e87.long

Ficker, E., Jarolimek, W., Kiehn, J., Baumann, A., & Brown, A. M. (1998). Molecular Determinants of Dofetilide Block of HERG K+ Channels. *Circulation Research*, *82*(3). Retrieved from http://circres.ahajournals.org/content/82/3/386?ijkey=768607c7a32637156042f96d143331cd99b52d71&keytype2=tf_ipsecsha

Franz, M. R. (2003). The Electrical Restitution Curve Revisited:. Steep or Flat Slope- Which is Better? *Journal of Cardiovascular Electrophysiology*, *14*(s10), S140–S147. http://doi.org/10.1046/j.1540.8167.90303.x

Gaj, T., Gersbach, C. A., & Barbas, C. F. (2013). ZFN, TALEN, and CRISPR/Cas-based methods for genome engineering. *Trends in Biotechnology*, *31*(7), 397–405. http://doi.org/10.1016/j.tibtech.2013.04.004

Gardner, A., & Sanguinetti, M. C. (2015). C-Linker Accounts for Differential Sensitivity of ERG1 and ERG2 K+ Channels to RPR260243-Induced Slow Deactivation. *Molecular Pharmacology*, *88*(1), 19–28. http://doi.org/10.1124/mol.115.098384

Giudicessi, J. R., & Ackerman, M. J. (2013). Genotype- and Phenotype-Guided Management of Congenital Long QT Syndrome. *Current Problems in Cardiology*, *38*(10), 417–455. http://doi.org/10.1016/j.cpcardiol.2013.08.001

Gong, Q., Jones, M. A., & Zhou, Z. (2006). Mechanisms of pharmacological rescue of trafficking-defective hERG mutant channels in human long QT syndrome. *The Journal of Biological Chemistry*, *281*(7), 4069–74. http://doi.org/10.1074/jbc.M511765200

Gong, Q., Keeney, D. R., Molinari, M., & Zhou, Z. (2005). Degradation of trafficking-defective long QT syndrome type II mutant channels by the ubiquitin-proteasome pathway. *The Journal of Biological Chemistry*, *280*(19), 19419–25. http://doi.org/10.1074/jbc.M502327200

Gong, Q., Zhang, L., Vincent, G. M., Horne, B. D., & Zhou, Z. (2007). Nonsense Mutations in hERG Cause a Decrease in Mutant mRNA Transcripts by Nonsense-Mediated mRNA Decay in Human Long-QT Syndrome. *Circulation*, *116*(1). Retrieved from http://circ.ahajournals.org/content/116/1/17.long

Goshima, K., & Tonomura, Y. (1969). Synchronized beating of embryonic mouse myocardial cells mediated by FL cells in monolayer culture. *Experimental Cell Research*, *56*(2–3), 387–392. http://doi.org/10.1016/0014-4827(69)90029-9

Gustina, A. S., & Trudeau, M. C. (2009). A recombinant N-terminal domain fully restores deactivation gating in N-truncated and long QT syndrome mutant hERG potassium channels. *Proceedings of the National Academy of Sciences*, *106*(31), 13082–13087. http://doi.org/10.1073/pnas.0900180106

Haitin, Y., Carlson, A. E., & Zagotta, W. N. (2013). The structural mechanism of KCNH-channel regulation by the eag domain. *Nature*, *501*(7467), 444–8. http://doi.org/10.1038/nature12487

Hoekstra, M., Mummery, C. L., Wilde, A. A. M., Bezzina, C. R., & Verkerk, A. O. (2012). Induced pluripotent stem cell derived cardiomyocytes as models for cardiac arrhythmias. *Frontiers in Physiology*, *3*, 346. http://doi.org/10.3389/fphys.2012.00346

Hondeghem, L. M., Carlsson, L., & Duker, G. (2001). Instability and Triangulation of the Action Potential Predict Serious Proarrhythmia, but Action Potential Duration Prolongation Is Antiarrhythmic. *Circulation*, *103*(15). Retrieved from http://circ.ahajournals.org/content/103/15/2004.short

Hull, C. M., Sokolov, S., Van Slyke, A. C., & Claydon, T. W. (2014). Regional flexibility in the S4–S5 linker regulates hERG channel closed-state stabilization. *Pflügers Archiv - European Journal of Physiology*, *466*(10), 1911–1919. http://doi.org/10.1007/s00424-013-1431-9

Hwang, H. S., Kryshtal, D. O., Feaster, T. K., Sánchez-Freire, V., Zhang, J., Kamp, T. J., … Knollmann, B. C. (2015). Comparable calcium handling of human iPSC-derived cardiomyocytes generated by multiple laboratories. *Journal of Molecular and Cellular Cardiology*, *85*, 79–88. http://doi.org/10.1016/j.yjmcc.2015.05.003

Itzhaki, I., Maizels, L., Huber, I., Zwi-Dantsis, L., Caspi, O., Winterstern, A., … Gepstein, L. (2011). Modelling the long QT syndrome with induced pluripotent stem cells. *Nature*, *471*(7337), 225–229. http://doi.org/10.1038/nature09747

Janse, M. J., Coronel, R., & Opthof, T. (2011a). Counterpoint: M cells do not have a functional role in the ventricular myocardium of the intact heart. *Heart Rhythm*, *8*(6), 934–937. http://doi.org/10.1016/j.hrthm.2010.10.048

Janse, M. J., Coronel, R., & Opthof, T. (2011b). Rebuttal to M cells are present in the ventricular myocardium. *Heart Rhythm*, *8*(7), 1100. http://doi.org/10.1016/j.hrthm.2011.04.028

Jinek, M., Chylinski, K., Fonfara, I., Hauer, M., Doudna, J. A., Charpentier, E., … Modrich, P. (2012). A programmable dual-RNA-guided DNA endonuclease in adaptive bacterial immunity. *Science (New York, N.Y.)*, *337*(6096), 816–21. http://doi.org/10.1126/science.1225829

John Camm, A., Lip, G. Y. H., De Caterina, R., Savelieva, I., Atar, D., Hohnloser, S. H., … Verheugt, F. W. A. (2012). 2012 focused update of the ESC Guidelines for the management of atrial fibrillation. *European Heart Journal*, *33*(21), 2719–2747. http://doi.org/10.1093/eurheartj/ehs253

Kang, J., Chen, X.-L., Wang, H., Ji, J., Cheng, H., Incardona, J., … Rampe, D. (2004). Discovery of a Small Molecule Activator of the Human Ether-a-go-go-Related Gene (HERG) Cardiac K+ Channel. *Molecular Pharmacology*, *67*(3), 827–836. http://doi.org/10.1124/mol.104.006577

Kanters, J. K., Skibsbye, L., Hedley, P. L., Dembic, M., Liang, B., Hagen, C. M., … Jespersen, T. (2015). Combined gating and trafficking defect in Kv11.1 manifests as a malignant long QT syndrome phenotype in a large Danish p.F29L founder family. *Scandinavian Journal of Clinical and Laboratory Investigation*, *75*(8), 699–709. http://doi.org/10.3109/00365513.2015.1091090

Kapa, S., Tester, D. J., Salisbury, B. A., Harris-Kerr, C., Pungliya, M. S., Alders, M., … Ackerman, M. J. (2009). Genetic Testing for Long-QT Syndrome. *Circulation*, *120*(18). Retrieved from http://circ.ahajournals.org/content/120/18/1752.long

Kapplinger, J. D., Tester, D. J., Salisbury, B. A., Carr, J. L., Harris-Kerr, C., Pollevick, G. D., … Ackerman, M. J. (2009). Spectrum and prevalence of mutations from the first 2,500 consecutive unrelated patients referred for the FAMILION? long QT syndrome genetic test. *Heart Rhythm*, *6*(9), 1297–1303. http://doi.org/10.1016/j.hrthm.2009.05.021

Karakikes, I., Stillitano, F., Nonnenmacher, M., Tzimas, C., Sanoudou, D., Termglinchan, V., … Frohman, M. A. (2015). Correction of human phospholamban R14del mutation associated with cardiomyopathy using targeted nucleases and combination therapy. *Nature Communications*, *6*, 6955. http://doi.org/10.1038/ncomms7955

Kattman, S. J., Witty, A. D., Gagliardi, M., Dubois, N. C., Niapour, M., Hotta, A., … Keller, G. (2011). Stage-Specific Optimization of Activin/Nodal and BMP Signaling Promotes Cardiac Differentiation of Mouse and Human Pluripotent Stem Cell Lines. *Cell Stem Cell*, *8*(2), 228–240. http://doi.org/10.1016/j.stem.2010.12.008

Kleckner, N. W., & Dingledine, R. (1988). Requirement for Glycine in Activation of NMDA-Receptors Expressed in Xenopus Oocytes. Source: Science, New Series Annu. Rev. Biochem. Annu. Rev. Biophys. Biophys. Chem.J. Biol. Chem.J. Gen. Physiol. J. Biol. Chem. Biochim. Biophys. Acta FEBS Lett.J. Gen. Physiol. J. Biol. Chem, 241(6694), 835–837. Retrieved from http://www.jstor.org/stable/1702020

Kohl, P., Bollensdorff, C., & Quinn, T. A. (2011). Resolving the M-cell debate: mechanics matters. *Heart Rhythm*, *8*(11), e1; author reply e2. http://doi.org/10.1016/j.hrthm.2011.08.025

Lahti, A. L., Kujala, V. J., Chapman, H., Koivisto, A.-P., Pekkanen-Mattila, M., Kerkelä, E., … Aalto-Setälä, K. (2012). Model for long QT syndrome type 2 using human iPS cells demonstrates arrhythmogenic characteristics in cell culture. *Disease Models & Mechanisms*, *5*(2).

Lees-Miller, J. P., Duan, Y., Teng, G. Q., & Duff, H. J. (2000). Molecular Determinant of High-Affinity Dofetilide Binding toHERG1 Expressed in Xenopus Oocytes: Involvement of S6 Sites. *Molecular Pharmacology*, *57*(2). Retrieved from http://molpharm.aspetjournals.org/content/57/2/367

Lian, X., Zhang, J., Azarin, S. M., Zhu, K., Hazeltine, L. B., Bao, X., … Palecek, S. P. (2013). Directed cardiomyocyte differentiation from human pluripotent stem cells by modulating Wnt/β-catenin signaling under fully defined conditions. *Nature Protocols*, *8*, 162–75. http://doi.org/10.1038/nprot.2012.150

Lin, E., Craig, C., Lamothe, M., Sarunic, M. V, Beg, M. F., & Tibbits, G. F. (2015). Construction and use of a zebrafish heart voltage and calcium optical mapping system, with integrated electrocardiogram and programmable electrical stimulation. *American Journal of Physiology - Regulatory, Integrative and Comparative Physiology*.

Liu, J., Laksman, Z., & Backx, P. H. (2016). The electrophysiological development of cardiomyocytes. *Advanced Drug Delivery Reviews*, *96*, 253–273. http://doi.org/10.1016/j.addr.2015.12.023

Liu, J., Zhang, M., Jiang, M., & Tseng, G.-N. (2003). Negative charges in the transmembrane domains of the HERG K channel are involved in the activation- and deactivation-gating processes. *The Journal of General Physiology*, *121*(6), 599–614. http://doi.org/10.1085/jgp.200308788

Liu, Q., Trudeau, M. C., Fiene, S., Anson, B., Thomson, J., & Kamp, T. (2015). Eag Domains Regulate LQT Mutant hERG Channels in Human Induced Pluripotent Stem Cell-Derived Cardiomyocytes. *PLOS ONE*, *10*(4), e0123951. http://doi.org/10.1371/journal.pone.0123951

Lu, Y., Mahaut-Smith, M. P., Varghese, A., Huang, C. L., Kemp, P. R., & Vandenberg, J. I. (2001). Effects of premature stimulation on HERG K(+) channels. *The Journal of Physiology*, *537*(Pt 3), 843–51. http://doi.org/10.1111/j.1469-7793.2001.00843.x

Marban, E., Robinson, S. W., & Wier, W. G. (1986). Mechanisms of arrhythmogenic delayed and early afterdepolarizations in ferret ventricular muscle. *Journal of Clinical Investigation*, *78*(5), 1185–1192. http://doi.org/10.1172/JCI112701

Masoudpour, H., & Laflamme, M. (2017). Cardiac repair with pluripotent stem cell-derived cardiomyocytes: proof-of-concept but new challenges. *The Journal of Thoracic and Cardiovascular Surgery*. http://doi.org/10.1016/j.jtcvs.2017.05.088

Masu, Y., Nakayama, K., Tamaki, H., Harada, Y., Kuno, M., & Nakanishi, S. (1987). cDNA eloping of bovine substance-K receptor through oocyte expression system. *Nature*, *329*(6142), 836–838. http://doi.org/10.1038/329836a0

Mehta, A., Chung, Y. Y., Ng, A., Iskandar, F., Atan, S., Wei, H., … Shim, W. (2011). Pharmacological response of human cardiomyocytes derived from virus-free induced pluripotent stem cells. *Cardiovascular Research*. http://doi.org/10.1093/cvr/cvr132

Milberg, P., Eckardt, L., Urgen, H., Biertz, J., Ramtin, S., Reinsch, N., … Haverkamp, W. (2002). Divergent Proarrhythmic Potential of Macrolide Antibiotics Despite Similar QT Prolongation : Fast Phase 3 Repolarization Prevents Early Afterdepolarizations and Torsade de Pointes. *Journal of Pharmacology and Experimental Therapeutics*, *303*(1), 218–225. http://doi.org/10.1124/jpet.102.037911.they

Milberg, P., Fink, M., Pott, C., Frommeyer, G., Biertz, J., Osada, N., … Eckardt, L. (2012). Blockade of ICa suppresses early afterdepolarizations and reduces transmural dispersion of repolarization in a whole heart model of chronic heart failure. *British Journal of Pharmacology*, *166*(2), 557–568. http://doi.org/10.1111/j.1476-5381.2011.01721.x

Milberg, P., Ramtin, S., Mönnig, G., Osada, N., Wasmer, K., Breithardt, G., … Eckardt, L. (2004). Comparison of the in vitro electrophysiologic and proarrhythmic effects of amiodarone and sotalol in a rabbit model of acute atrioventricular block. *Journal of Cardiovascular Pharmacology*, *44*(3), 278–286. http://doi.org/10.1097/01.fjc.0000129581.81508.78

Mitcheson, J. S., Chen, J., Lin, M., Culberson, C., & Sanguinetti, M. C. (2000). A structural basis for drug-induced long QT syndrome. *Proceedings of the National Academy of Sciences of the United States of America*, *97*(22), 12329–33. http://doi.org/10.1073/pnas.210244497

Miyaoka, Y., Chan, A. H., Judge, L. M., Yoo, J., Huang, M., Nguyen, T. D., … Conklin, B. R. (2014). Isolation of single-base genome-edited human iPS cells without antibiotic selection. *Nature Methods*, *11*(3), 291–3. http://doi.org/10.1038/nmeth.2840

Morais-Cabral, J. H., & Robertson, G. A. (2015). The enigmatic cytoplasmic regions of KCNH channels. *Journal of Molecular Biology*, *427*(1), 67–76. http://doi.org/10.1016/j.jmb.2014.08.008

Morgan, J. M., Cunningham, A. D., & Rowland, E. (1990). Relationship of the effective refractory period and monophasic action potential duration after a step increase in pacing frequency. *Pacing and Clinical Electrophysiology : PACE*, *13*(8), 1002–8. Retrieved from http://www.ncbi.nlm.nih.gov/pubmed/1697947

Moss, A. J., Zareba, W., Kaufman, E. S., Gartman, E., Peterson, D. R., Benhorin, J., … Wang, Z. (2002). Increased risk of arrhythmic events in long-QT syndrome with mutations in the pore region of the human ether-a-go-go-related gene potassium channel. *Circulation*, *105*(7), 794–9. Retrieved from http://www.ncbi.nlm.nih.gov/pubmed/11854117

Nadadur, R. D., Broman, M. T., Boukens, B., Mazurek, S. R., Yang, X., van den Boogaard, M., … Moskowitz, I. P. (2016). Pitx2 modulates a Tbx5-dependent gene regulatory network to maintain atrial rhythm. *Science Translational Medicine*, *8*(354). Retrieved from http://stm.sciencemag.org/content/8/354/354ra115.full

Nakagawa, M., Sekine, Y., Ono, M., Taniguchi, Y., Takahashi, N., Yonemochi, H., & Saikawa, T. (2009). Gender Differences in the Effect of Auditory Stimuli on Ventricular Repolarization in Healthy Subjects. *Journal of Cardiovascular Electrophysiology*, *20*(6), 653–657. http://doi.org/10.1111/j.1540-8167.2008.01401.x

Nakajima, T., Furukawa, T., Tanaka, T., Katayama, Y., Nagai, R., Nakamura, Y., & Hiraoka, M. (1998). Novel Mechanism of HERG Current Suppression in LQT2. *Circulation Research*, *83*(4). Retrieved from http://circres.ahajournals.org/content/83/4/415.long

Nakajima, T., Furukawa, T., Hirano, Y., Tanaka, T., Sakurada, H., Takahashi, T., … Hiraoka, M. (1999). Voltage-shift of the current activation in HERG S4 mutation (R534C) in LQT2. Cardiovascular Research, 44(2), 283–293. http://doi.org/10.1016/S0008-6363(99)00195-9

Nan, B., Liu, X., Zhou, Y., Liu, J., Zhang, L., Wen, J., … Wang, Y.-P. (2010). From signal perception to signal transduction: ligand-induced dimeric switch of DctB sensory domain in solution. *Molecular Microbiology*, *75*(6), 1484–1494. http://doi.org/10.1111/j.1365-2958.2010.07069.x

Nattel, S., Antzelevitch, C., Noble, D., Lin, H., Wang, Z., & Nattel, S. (2011). Resolving the M-cell debate: Why and how. *Heart Rhythm*, *8*(8), 1293–1295. http://doi.org/10.1016/j.hrthm.2011.06.002

Ng, C. A., Hunter, M. J., Perry, M. D., Mobli, M., Ke, Y., Kuchel, P. W., … Moffat, K. (2011). The N–Terminal Tail of hERG Contains an Amphipathic α–Helix That Regulates Channel Deactivation. *PLoS ONE*, *6*(1), e16191. http://doi.org/10.1371/journal.pone.0016191

Ng, C. A., Phan, K., Hill, A. P., Vandenberg, J. I., & Perry, M. D. (2014). Multiple interactions between cytoplasmic domains regulate slow deactivation of Kv11.1 channels. *The Journal of Biological Chemistry*, *289*(37), 25822–32. http://doi.org/10.1074/jbc.M114.558379

Opthof, T., Coronel, R., & Janse, M. J. (2009). Is there a significant transmural gradient in repolarization time in the intact heart? Response to Opthof et al. *Circulation: Arrhythmia and Electrophysiology*, *2*(1). Retrieved from http://circep.ahajournals.org/content/2/1/89

Opthof, T., Janse, M. J., Meijborg, V. M. F., Cinca, J., Rosen, M. R., & Coronel, R. (2016). Dispersion in ventricular repolarization in the human, canine and porcine heart. *Progress in Biophysics and Molecular Biology*, *120*(1–3), 222–235. http://doi.org/10.1016/j.pbiomolbio.2016.01.007

Otsuji, T. G., Minami, I., Kurose, Y., Yamauchi, K., Tada, M., & Nakatsuji, N. (2010). Progressive maturation in contracting cardiomyocytes derived from human embryonic stem cells: Qualitative effects on electrophysiological responses to drugs. *Stem Cell Research*, *4*(3), 201–213. http://doi.org/10.1016/j.scr.2010.01.002

Paquet, D., Kwart, D., Chen, A., Sproul, A., Jacob, S., Teo, S., … Tessier-Lavigne, M. (2016). Efficient introduction of specific homozygous and heterozygous mutations using CRISPR/Cas9. *Nature*, *533*(7601), 125–129. http://doi.org/10.1038/nature17664

Perry, M. D., Ng, C. A., Phan, K., David, E., Steer, K., Hunter, M. J., … Vandenberg, J. I. (2016). Rescue of protein expression defects may not be enough to abolish the pro-arrhythmic phenotype of long QT type 2 mutations. *The Journal of Physiology*, *594*(14), 4031–4049. http://doi.org/10.1113/JP271805

Perry, M., Sachse, F. B., Abbruzzese, J., & Sanguinetti, M. C. (2009). PD-118057 contacts the pore helix of hERG1 channels to attenuate inactivation and enhance K+ conductance. *Proceedings of the National Academy of Sciences of the United States of America*, *106*(47), 20075–80. http://doi.org/10.1073/pnas.0906597106

Perry, M., Sachse, F. B., & Sanguinetti, M. C. (2007). Structural basis of action for a human ether-a-go-go-related gene 1 potassium channel activator. *Proceedings of the National Academy of Sciences of the United States of America*, *104*(34), 13827–32. http://doi.org/10.1073/pnas.0703934104

Powell, A. C., Garan, H., McGovern, B. A., Fallon, J. T., Krishnan, S. C., & Ruskin, J. N. (1992). Low energy conversion of atrial fibrillation in the sheep. *Journal of the American College of Cardiology*, *20*(3), 707–711. http://doi.org/10.1016/0735-1097(92)90028-L

Powell, T., & Twist, V. W. (1976). A rapid technique for the isolation and purification of adult cardiac muscle cells having respiratory control and a tolerance to calcium. *Biochemical and Biophysical Research Communications*, *72*(1), 327–33. Retrieved from http://www.ncbi.nlm.nih.gov/pubmed/985476

Priori, S. G., Napolitano, C., & Schwartz, P. J. (1999). Low Penetrance in the Long-QT Syndrome. *Circulation*, *99*(4). Retrieved from http://circ.ahajournals.org/content/99/4/529

Qu, Z., & Weiss, J. N. (2015). Mechanisms of ventricular arrhythmias: from molecular fluctuations to electrical turbulence. *Annual Review of Physiology*, *77*, 29–55. http://doi.org/10.1146/annurev-physiol-021014-071622

Ran, F. A., Hsu, P. D. P., Wright, J., Agarwala, V., Scott, D. a, & Zhang, F. (2013). Genome engineering using the CRISPR-Cas9 system. *Nature Protocols*, *8*(11), 2281–2308. http://doi.org/10.1038/nprot.2013.143.Genome

Richardson, C. D., Ray, G. J., DeWitt, M. A., Curie, G. L., & Corn, J. E. (2016). Enhancing homology-directed genome editing by catalytically active and inactive CRISPR-Cas9 using asymmetric donor DNA. *Nature Biotechnology*, *34*(3). http://doi.org/10.1038/nbt.3481

Roti, E. C. R., Myers, C. D., Ayers, R. A., Boatman, D. E., Delfosse, S. A., Chan, E. K. L., … Robertson, G. A. (2002). Interaction with GM130 during HERG ion channel trafficking. Disruption by type 2 congenital long QT syndrome mutations. Human Ether-à-go-go-Related Gene. *The Journal of Biological Chemistry*, *277*(49), 47779–85. http://doi.org/10.1074/jbc.M206638200

Sala, L., Yu, Z., Ward-van Oostwaard, D., van Veldhoven, J. P., Moretti, A., Laugwitz, K.-L., … Bellin, M. (2016). A new hERG allosteric modulator rescues genetic and drug-induced long-QT syndrome phenotypes in cardiomyocytes from isogenic pairs of patient induced pluripotent stem cells. *EMBO Molecular Medicine*, *8*(9), 1065–81. http://doi.org/10.15252/emmm.201606260

Sanguinetti, M. C., Jiang, C., Curran, M. E., & Keating, M. T. (1995). A mechanistic link between an inherited and an acquired cardiac arrhythmia: HERG encodes the IKr potassium channel. *Cell*, *81*(2), 299–307. Retrieved from http://www.ncbi.nlm.nih.gov/pubmed/7736582

Satin, J., Itzhaki, I., Rapoport, S., Schroder, E. A., Izu, L., Arbel, G., … Gepstein, L. (2008). Calcium Handling in Human Embryonic Stem Cell-Derived Cardiomyocytes. *Stem Cells*, *26*(8), 1961–1972. http://doi.org/10.1634/stemcells.2007-0591

Schwartz, P. J., Stramba-Badiale, M., Crotti, L., Pedrazzini, M., Besana, A., Bosi, G., … Spazzolini, C. (2009). Prevalence of the Congenital Long-QT Syndrome. *Circulation*, *120*(18). Retrieved from http://circ.ahajournals.org/content/120/18/1761

Sicouri, S., & Antzelevitch, C. (1991). A subpopulation of cells with unique electrophysiological properties in the deep subepicardium of the canine ventricle. The M cell. *Circulation Research*, *68*(6). Retrieved from http://circres.ahajournals.org/content/68/6/1729

Smith, G. A. M., Tsui, H.-W., Newell, E. W., Jiang, X., Zhu, X.-P., Tsui, F. W. L., & Schlichter, L. C. (2002). Functional Up-regulation of HERG K+ Channels in Neoplastic Hematopoietic Cells. *Journal of Biological Chemistry*, *277*(21), 18528–18534. http://doi.org/10.1074/jbc.M200592200

Smith, J. L., Anderson, C. L., Burgess, D. E., Elayi, C. S., January, C. T., & Delisle, B. P. (2016). Molecular pathogenesis of long QT syndrome type 2. http://doi.org/10.1016/j.joa.2015.11.009

Spencer, C. I., Baba, S., Nakamura, K., Hua, E. A., Sears, M. A. F., Fu, C., … Conklin, B. R. (2014). Calcium Transients Closely Reflect Prolonged Action Potentials in iPSC Models of Inherited Cardiac Arrhythmia. *Stem Cell Reports*, *3*(2), 269–281. http://doi.org/10.1016/j.stemcr.2014.06.003

Sterneckert, J. L., Reinhardt, P., & Scholer, H. R. (2014). Investigating human disease using stem cell models. *Nat Rev Genet*, *15*(9), 625–639. Retrieved from http://dx.doi.org/10.1038/nrg3764

Studenik, C. R., Zhou, Z., & January, C. T. (2001). Differences in action potential and early afterdepolarization properties in LQT2 and LQT3 models of long QT syndrome. *British Journal of Pharmacology*, *132*(1), 85–92. http://doi.org/10.1038/sj.bjp.0703770

Stühmer, W., & Parekh, A. B. (1995). Electrophysiological Recordings from Xenopus Oocytes. In Single-Channel Recording (pp. 341–356). Boston, MA: Springer US. http://doi.org/10.1007/978-1-4419-1229-9_15

Sun, N., Yazawa, M., Liu, J., Han, L., Sanchez-Freire, V., Abilez, O. J., … Wu, J. C. (2012). Patient-Specific Induced Pluripotent Stem Cells as a Model for Familial Dilated Cardiomyopathy. *Science Translational Medicine*, *4*(130), 130ra47-130ra47. http://doi.org/10.1126/scitranslmed.3003552

Takahashi, K., Tanabe, K., Ohnuki, M., Narita, M., Ichisaka, T., Tomoda, K., & Yamanaka, S. (2007). Induction of Pluripotent Stem Cells from Adult Human Fibroblasts by Defined Factors. *Cell*, *131*(5), 861–872. http://doi.org/10.1016/j.cell.2007.11.019

Takahashi, K., & Yamanaka, S. (2006). Induction of Pluripotent Stem Cells from Mouse Embryonic and Adult Fibroblast Cultures by Defined Factors. *Cell*, *126*(4), 663–676. http://doi.org/10.1016/j.cell.2006.07.024

Tan, P. S., Perry, M. D., Ng, C. A., Vandenberg, J. I., & Hill, A. P. (2012). Voltage-sensing domain mode shift is coupled to the activation gate by the N-terminal tail of hERG channels. *The Journal of General Physiology*, *140*(3), 293–306. http://doi.org/10.1085/jgp.201110761

Tanskanen, A. J., Greenstein, J. L., O'Rourke, B., & Winslow, R. L. (2005). The Role of Stochastic and Modal Gating of Cardiac L-Type Ca2+ Channels on Early After-Depolarizations. *Biophysical Journal*, *88*(1), 85–95. http://doi.org/10.1529/biophysj.104.051508

Terrenoire, C., Wang, K., Tung, K. W. C., Chung, W. K., Pass, R. H., Lu, J. T., … Kass, R. S. (2013). Induced pluripotent stem cells used to reveal drug actions in a long QT syndrome family with complex genetics. *The Journal of General Physiology*, *141*(1), 61–72. http://doi.org/10.1085/jgp.201210899

Thouta, S., Hull, C. M., Shi, Y. P., Sergeev, V., Young, J., Cheng, Y. M., & Claydon, T. W. (2017). Stabilization of the Activated hERG Channel Voltage Sensor by Depolarization Involves the S4-S5 Linker. *Biophysical Journal*, *112*(2), 300–312. http://doi.org/10.1016/j.bpj.2016.12.021

Thouta, S., Sokolov, S., Abe, Y., Clark, S. J., Cheng, Y. M., & Claydon, T. W. (2014). Proline Scan of the hERG Channel S6 Helix Reveals the Location of the Intracellular Pore Gate. *Biophysical Journal*, *106*(5), 1057–1069. http://doi.org/10.1016/j.bpj.2014.01.035

Valamehr, B., Abujarour, R., Robinson, M., Le, T., Robbins, D., Shoemaker, D., & Flynn, P. (2012). A novel platform to enable the high-throughput derivation and characterization of feeder-free human iPSCs. *Scientific Reports*, *2*, 213. http://doi.org/10.1038/srep00213

Vandenberg, J. I., Perry, M. D., Perrin, M. J., Mann, S. A., Ke, Y., & Hill, A. P. (2012). hERG K+ Channels: Structure, Function, and Clinical Significance. *Physiological Reviews*, *92*(3).

Vandersickel, N., Kazbanov, I. V., Nuitermans, A., Weise, L. D., Pandit, R., & Panfilov, A. V. (2014). A Study of Early Afterdepolarizations in a Model for Human Ventricular Tissue. *PLoS ONE*, *9*(1), e84595. http://doi.org/10.1371/journal.pone.0084595

Wagner, C. A., Friedrich, B., Setiawan, I., Lang, F., & Bröer, S. (2000). The use of Xenopus laevis oocytes for the functional characterization of heterologously expressed membrane proteins. Cellular Physiology and Biochemistry : International Journal of Experimental Cellular Physiology, Biochemistry, and Pharmacology, 10(1–2), 1–12. http://doi.org/16341

Wang, J., Myers, C. D., & Robertson, G. A. (2000). Dynamic control of deactivation gating by a soluble amino-terminal domain in HERG K(+) channels. *The Journal of General Physiology*, *115*(6), 749–58. Retrieved from http://www.ncbi.nlm.nih.gov/pubmed/10828248

Wang, J., Trudeau, M. C., Zappia, A. M., & Robertson, G. A. (1998). Regulation of deactivation by an amino terminal domain in human ether-à-go-go-related gene potassium channels. *The Journal of General Physiology*, *112*(5), 637–47. Retrieved from http://www.ncbi.nlm.nih.gov/pubmed/9806971

Wang, L., Feng, Z.-P., Kondo, C. S., Sheldon, R. S., & Duff, H. J. (1996). Developmental Changes in the Delayed Rectifier K+ Channels in Mouse Heart. *Circulation Research*, *79*(1). Retrieved from http://circres.ahajournals.org/content/79/1/79.long

Wang, W., & MacKinnon, R. (2017). Cryo-EM Structure of the Open Human Ether-a-go-go -Related K + Channel hERG. *Cell*, *169*(3), 422–430.e10. http://doi.org/10.1016/j.cell.2017.03.048

Watanabe, H., Yang, T., Stroud, D. M., Lowe, J. S., Harris, L., Atack, T. C., … Roden, D. M. (2011). Striking In Vivo Phenotype of a Disease-Associated Human SCN5A Mutation Producing Minimal Changes in VitroClinical Perspective. *Circulation*, *124*(9). Retrieved from http://circ.ahajournals.org/content/124/9/1001.long

Wilde, A. A. M., Jongbloed, R. J. E., Doevendans, P. A., Düren, D. R., Hauer, R. N. W., Van Langen, I. M., … Geelen, J. L. M. C. (1999). Auditory stimuli as a trigger for arrhythmic events differentiate HERG- related (LQTS2) patients from KVLQT1-related patients (LQTS1). Journal of the American College of Cardiology, 33(2), 327–332. http://doi.org/10.1016/S0735-1097(98)00578-6

Wilson, L. D., Jennings, M. M., & Rosenbaum, D. S. (2011a). Point: M cells are present in the ventricular myocardium. *Heart Rhythm*, *8*(6), 930–933. http://doi.org/10.1016/j.hrthm.2011.01.026

Wilson, L. D., Jennings, M. M., & Rosenbaum, D. S. (2011b). Rebuttal to M cells are not present in the ventricular myocardium. *Heart Rhythm*, *8*(7), 1099. http://doi.org/10.1016/j.hrthm.2011.04.029

Wu, R., & Patwardhan, A. (2004). Restitution of Action Potential Duration during Sequential Changes in Diastolic Intervals Shows Multimodal Behavior. *Circulation Research*, *94*(5), 634–641. http://doi.org/10.1161/01.RES.0000119322.87051.A9

Yan, G.-X., & Antzelevitch, C. (1998). Cellular Basis for the Normal T Wave and the Electrocardiographic Manifestations of the Long-QT Syndrome. *Circulation*, *98*(18).

Yan, G.-X., Wu, Y., Liu, T., Wang, J., Marinchak, R. A., & Kowey, P. R. (2001). Phase 2 Early Afterdepolarization as a Trigger of Polymorphic Ventricular Tachycardia in Acquired Long-QT Syndrome. *Circulation*, *103*(23). Retrieved from http://circ.ahajournals.org/content/103/23/2851?ijkey=0fc198c53134e7a711eb0b3003c060d2512c83c4&keytype2=tf_ipsecsha

Yang, X., Pabon, L., & Murry, C. E. (2014). Engineering adolescence: maturation of human pluripotent stem cell-derived cardiomyocytes. *Circulation Research*, *114*(3), 511–23. http://doi.org/10.1161/CIRCRESAHA.114.300558

Yu, Z., Liu, J., van Veldhoven, J. P. D., IJzerman, A. P., Schalij, M. J., Pijnappels, D. A., … de Vries, A. A. F. (2016). Allosteric Modulation of K_v 11.1 (hERG) Channels Protects Against Drug-Induced Ventricular Arrhythmias. *Circulation: Arrhythmia and Electrophysiology*, *9*(4), e003439. http://doi.org/10.1161/CIRCEP.115.003439

Zarraga, I. G., Zhang, L., Stump, M. R., Gong, Q., Vincent, G. M., & Zhou, Z. (2011). Nonsense-mediated mRNA decay caused by a frameshift mutation in a large kindred of type 2 long QT syndrome. *Heart Rhythm*, *8*(8), 1200–1206. http://doi.org/10.1016/j.hrthm.2011.03.039

Zeng, H., Lozinskaya, I. M., Lin, Z., Willette, R. N., Brooks, D. P., & Xu, X. (2006). Mallotoxin Is a Novel Human. *Pharmacology*, *319*(2), 957–962. http://doi.org/10.1124/jpet.106.110593.channel

Zhang, H., Zou, B., Yu, H., Moretti, A., Wang, X., Yan, W., … Li, M. (2012). Modulation of hERG potassium channel gating normalizes action potential duration prolonged by dysfunctional KCNQ1 potassium channel. *Proceedings of the National Academy of Sciences*, *109*(29), 11866–11871. http://doi.org/10.1073/pnas.1205266109

Zhou, J., Augelli-Szafran, C. E., Bradley, J. A., Chen, X., Koci, B. J., Volberg, W. A., … Cordes, J. S. (2005). Novel Potent hERG Potassium Channel Enhancers And Their In Vitro Antiarrhythmic Activity. *Molecular Pharmacology*, *68*(3), 876–884. http://doi.org/10.1124/mol.105.014035

Zhou, Z., Gong, Q., Epstein, M. L., & January, C. T. (1998). HERG channel dysfunction in human long QT syndrome. Intracellular transport and functional defects. *The Journal of Biological Chemistry*, *273*(33), 21061–6. http://doi.org/10.1074/JBC.273.33.21061

Zhou, Z., Gong, Q., & January, C. T. (1999). Correction of defective protein trafficking of a mutant HERG potassium channel in human long QT syndrome. Pharmacological and temperature effects. *The Journal of Biological Chemistry*, *274*(44), 31123–6. Retrieved from http://www.ncbi.nlm.nih.gov/pubmed/10531299

Zimmer, H.-G. (1998). The Isolated Perfused Heart and Its Pioneers. *News in Physiological Sciences : An International Journal of Physiology Produced Jointly by the International Union of Physiological Sciences and the American Physiological Society*, *13*, 203–210. Retrieved from http://www.ncbi.nlm.nih.gov/pubmed/11390791

Appendix A. Supplementary data

Table A1: Mean slope factor (k) values derived from Boltzman fits of conductance-voltage relationships for activation and deactivation of WT and R56Q hERG channels at physiological durations.

Protocol	Genotype	n	Mean	SD	SE	95% CI – lcl,ucl
Activation	R56Q	6	11.8	0.7	0.3	11.1, 12.5
	WT	5	11.9	0.7	0.3	11.0, 12.8
Deactivation	R56Q	6	7.5	1.0	0.4	6.5, 8.5
	WT	5	9.6	1.0	0.4	8.4, 10.8

CI: Confidence Interval; lcl: lower confidence interval; ucl: upper confidence interval

Table A2: Effect of 10 μM RPR on mean $V_{1/2}$ of activation in WT and R56Q hERG channels at physiological durations.

Genotype	Solution	n	Mean (mV)	SD (mV)	SE (mV)	95% CI – lcl,ucl (mV)
WT	ND96	4	-10.0	2.5	1.3	-14.1, -6.0
	RPR	4	-9.0	2.0	1.0	-12.2, -5.7
R56Q	ND96	5	-7.8	3.2	1.4	-11.8, -3.8
	RPR	5	-6.0	4.7	2.1	-11.8, -0.2

CI: Confidence Interval; lcl: lower confidence interval; ucl: upper confidence interval

Table A3: Effect of 10 μM RPR on mean $V_{1/2}$ of deactivation in WT and R56Q hERG channels at physiological durations.

Genotype	Solution	n	Mean (mV)	SD (mV)	SE (mV)	95% CI – lcl,ucl (mV)
WT	ND96	3	-66.6	3.0	1.8	-74.2, -59.1
	RPR	3	-73.7	4.2	2.4	-84.2, -63.3
R56Q	ND96	5	-38.8	2.0	0.9	-41.2, -36.4
	RPR	5	-41.5	1.0	0.4	-42.7, -40.3

CI: Confidence Interval; lcl: lower confidence interval; ucl: upper confidence interval

Table A4: **Effect of 10 μM RPR on mean $V_{1/2}$ of steady-state inactivation in WT and R56Q hERG channels.**

Genotype	Solution	n	Mean (mV)	SD (mV)	SE (mV)	95% CI – lcl,ucl (mV)
WT	ND96	3	-50.2	9.9	5.7	-74.8, -25.5
	RPR	3	-48.7	17.5	10.1	-92.2, -5.2
R56Q	ND96	5	-45.2	18.0	8.0	-67.5, -22.9
	RPR	5	-30.8	12.8	5.7	-46.6, -14.9

CI: Confidence Interval; lcl: lower confidence interval; ucl: upper confidence interval

Appendix B. Supplementary figures

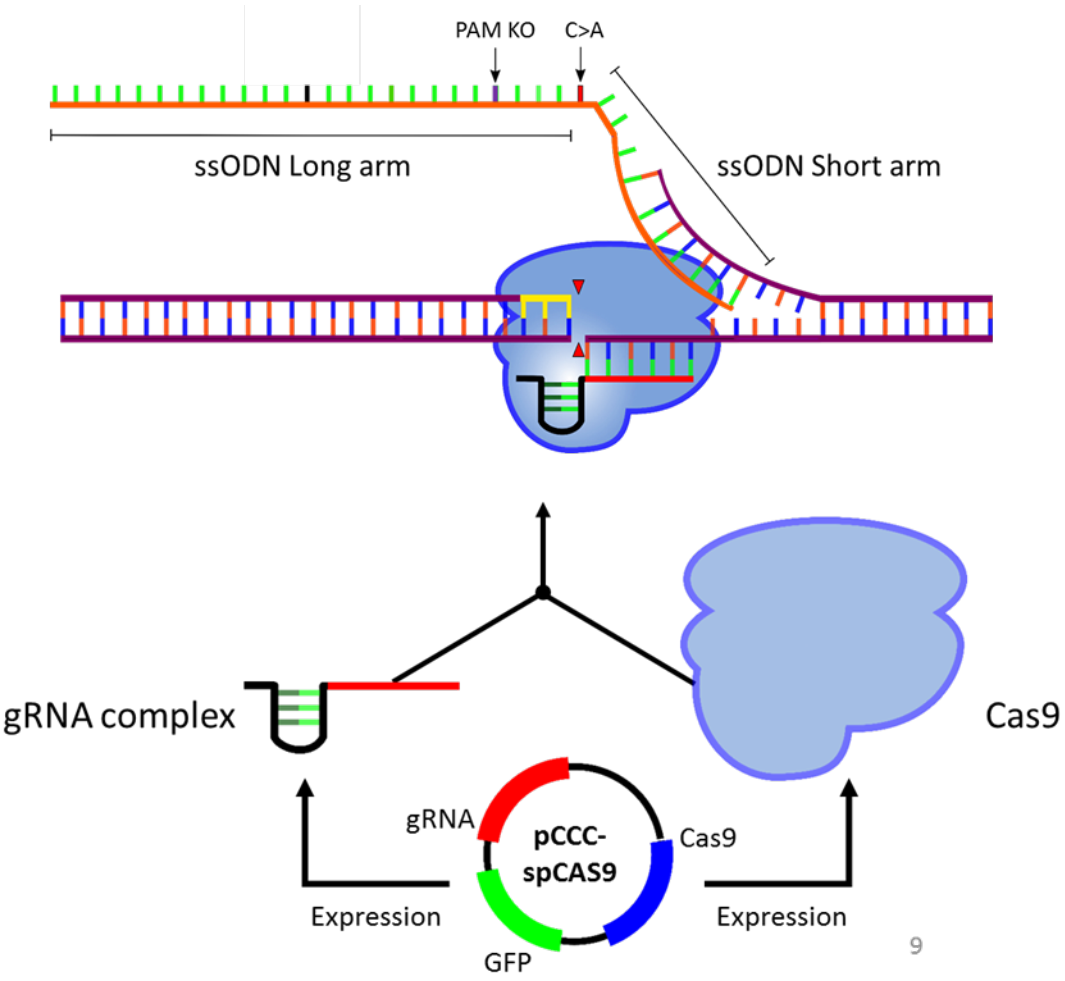

Figure B1: The CRISRP Cas9 genome editing system with donor template to introduce point mutations. The pCCC vector encodes the CAS9 complex (blue) and by site-specific guide RNA (red) and activated by the linked trans-activating CRISPR RNA (black). The gRNA associates with the Cas9 protein and targets its endonuclease activity to a site-specific region in the genome. The endonuclease action of Cas9 introduces a double-stranded break in the genome adjacent to the PAM sequence (yellow). As the strand opposite the PAM is released first, a single stranded oligonucleotide donor (orange) can provide a template for repair. It includes a point mutation that will then be introduced into the genome of the cells

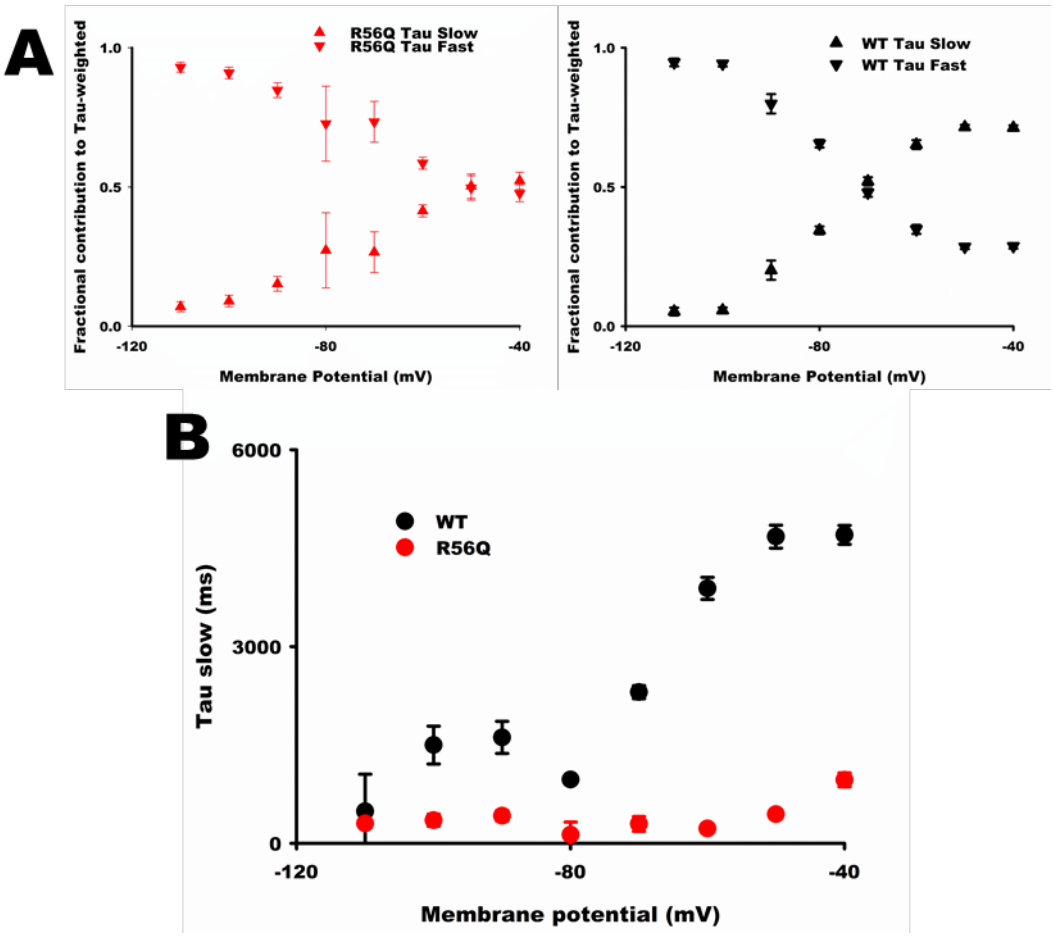

Figure B2: Relative contribution to τ_{fast}. **A)** Relative contribution of slow component, τ_{slow} (▼), and fast component, τ_{fast} (▲), to the aggregate time course of deactivation, $\tau_{weighted}$ for WT (black) and R56Q (red) channels. **B)** Slow component, τ_{slow}, plotted against deactivation potential for WT (black) and R56Q (red) channels.